TEXTURAL AND MICROSTRUCTURAL STUDIES OF ZINC SULFIDE AND ASSOCIATED PHASES IN CERTAIN BASE METAL DEPOSITS.

by

ANDREW PETER MORE

thesis submitted in partial

requirements for the degree of

Doctor of Philosophy

at the

University of Aston in Birmingham

June, 1988

The University of Aston in Birmingham.

TEXTURAL AND MICROSTRUCTURAL STUDIES OF ZINC SULFIDE AND ASSOCIATED PHASES IN CERTAIN BASE METAL DEPOSITS.

by

ANDREW PETER MORE

submitted for the degree of
Doctor of Philosophy
June, 1988

SUMMARY

A textural and microstructural study of a variety of zinc sulfide-containing ores has been undertaken, and the possible depositional and deformational controls of textural and microstructural development considered. Samples for the study were taken from both deformed and undeformed zinc ores of the Central U.S. Appalachians, and deformed zinc ores of the English Pennines.

A variety of mineralogical techniques were employed, including transmitted and reflected light microscopy of etched and unetched material, transmission electron microscopy and electron microprobe analysis. For the Pennine zinc sulfides, spectroscopic, X-ray diffraction and fluid inclusion studies were also undertaken.

Optical and electron optical examination of the Appalachian material confirmed the suitability of zinc sulfide for detailed study with such techniques. Growth and deformation-related microstructures could be distinguished from specimen-preparation induced artifacts. A deformationally-induced lamelliform optical anisotropy was seen to be developed in areas hosting a dense planar microstructure of {111} twin- and slip-planes.

The Pennine zinc sulfide texturally records a changing depositional environment. Thus, for example, delicately growth-zoned crystals are truncated and cross-cut by solution disconformities. Fluid inclusion studies indicate a highly saline (20-25 wt. % equiv. NaCl), low temperature (100-150^{o}C.) fluid. Texturally, two varieties of zinc sulfide can be recognised; a widely developed, iron- banded variety, and a paragenetically early variety, banded due to horizons rich in crystal defects and microscopic inclusions. The zinc sulfide takes the form of a disordered 3C-polytype, with much of the disorder being deformational in origin. Twin- and slip-plane fabrics are developed. A deformation-related optical anisotropy is seen to overprint growth-related anisotropy, along with cuprian alteration of certain {111} deformation planes.

Keywords: zinc sulfide, sphalerite, texture, anisotropy, microstructure.

ACKNOWLEDGEMENTS

Thanks are extended to Professor David Vaughan and Dr. John Ashworth for their initiation and supervision of the project. Samples and support were additionally supplied by Dr Robert Ixer, University of Aston, and Professor James Craig, V.P.I.S.U.; to whom thanks are also given. Financial support for the project was provided by a studentship from the Natural Environment Research Council, who are gratefully acknowledged.

Thanks are due to Mr. E. J. Hartland and the technical staff of the Department of Geological Sciences for their unfailing help and support. The thesis benefitted from numerous discussions with the staff and postgraduate community of the department. Special thanks are extended to Mr. R. Howell of the Dept. of Materials for assistance in maintaining an 'aged' transmission electron microscope.

Many of the microprobe analyses reported in the thesis were obtained at the Dept. of Geology, University of Manchester. Tim Hopkins and Dave Plant are thanked for their assistance. Dr. Andrew Gize, University of Southampton, is thanked for assistance with the U.V. and F.T.I.R. analysis, as is Dr. David Manning, Univ. of Newcastle, for help with the U.V. analysis of material.

Finally thanks are given to my family and friends, both at Aston and elsewhere, for support and encouragement during the course of the thesis.

CONTENTS.

CHAPTER 3: Principal Investigative Techniques.

CHAPTER 6: General Petrography Part One: Growth Related Textures.

CHAPTER 7: Analytical Studies and Copper Related Alteration.

CHAPTER 9: Nenthead Sphalerite: A Textural Discussion.

CHAPTER 10: Conclusions and Suggestions for Future Research.

LIST OF FIGURES

LIST OF PLATES

LIST OF TABLES.

CHAPTER 1: Introduction and Aims of Thesis.

1.1 Introduction.

The relationships between mineral textures, microstructures and mineral deformation mechanisms are well documented for many of the common rock-forming silicates and metallurgically important metal and alloy systems. Previous studies have attempted to to relate textures and associated microstructures to the chemical and mechanical properties of the phases concerned. The textures developed may be related, therefore to deformation conditions or growth conditions of the minerals. Controlled laboratory experiments have been used for the determination of textural origins and their relationship to possible changes in mineral properties (e.g. strength, crystal structure). Many geologically important materials, however, have not been studied in this way. Growth and deformation histories are, at best, partially known. Studies have been undertaken, especially on the common rock-forming silicates, to compare laboratory-induced 'synthetic' textures with those observed in natural rock-forming minerals. Such studies may provide some indication of the processes that have acted on the rock through geological time (Putnis and McConnell, 1980).

The present work is concerned with metal sulfides, in particular zinc sulfide. Textural studies of sulfides tend to be purely petrographic and descriptive. The textures are well described, but less attention is given to their possible origins and the processes (growth or deformational) involved in their development. Textural,

mineral, and compositional studies may yield information about mineral growth and post-formation environments. Aspects of the chemistry and properties of the ore-depositing fluid may often be inferred from such studies. Post-depositional processes, mechanical or chemical, may often be deduced from a detailed mineralogical and textural study of the mineral components of an ore. Such textural studies of sulfide materials tend not to use many of the techniques that have been used in similar studies of metal systems and silicate phases. Where such techniques have been applied to studies of silicates, documentation and explanation of many of the more 'problematical' textures has been possible. Examples of this include the application of transmission electron microscopic techniques to studies of exsolution, replacement and deformation textures. Feldspars (Smith, 1974), pyroxenes (Nord et al., 1976), and olivines (Green, 1976) have all successfully been examined with this technique, as have silicate mineral deformation mechanisms and textures in general (Christie and Ardell, 1976). Such techniques may yield similar information about the textures developed in sulfide phases.

1.2 Aims of Thesis.

The thesis is aimed at the examination and documentation of textures and microstructures developed in one of the more common sulfide minerals (sphalerite), sampled from slightly deformed ores. Material from the zinc deposits of the Appalachian Mountains of the U.S.A. was examined to assess the suitability of the sulfide for

electron-optical examination and the associated specimen preparation techniques involved. Much of the material is too deformed to allow the assessment of growth-related and deformation-related microstructures. One sample, however, was relatively undeformed and this permitted the documentation of growth related phenomena and the assessment of damage induced during specimen preparation. For the only slightly deformed samples, sphalerites from the Alston Block of the North Pennine Orefield were selected. Studies aimed at documenting both growth-related and deformation-related textures and any associated microstructures were successfully undertaken on this material. The use of slightly deformed samples enabled growth-related textures and microstructures to be distinguished from deformationally-induced textures and microstructures. Deformational processes tend to overprint rather than obliterate growth-related phenomena. In addition to using traditional petrographic techniques, techniques that have sucessfully been employed in similar studies of silicate minerals were used. Electron-optical techniques, in particular, were employed to assess their suitability for the textural analysis of growth and deformation textures.

Petrographic studies have been supplemented by fluid inclusion studies in order to provide possible fluid salinities and deposition temperatures for those samples subject to deformation (North Pennine material). Such studies were aimed at evaluating the nature of the deformation-inducing stress; i.e. a thermal origin, a mechanical origin or a combination of both. This approach necessitated the setting-up and calibration of a fluid inclusion heating and freezing microscope stage.

1.3 Thesis Structure.

Chapter 2 outlines common textural and microstructural characteristics seen in many Mississippi-Valley type(henceforward abbreviated M.V.T.) and other hydrothermal, low temperature, sphalerites. Textural descriptions are given along with possible textural origins and microstructural processes operative. Growth-related and deformation-related microstructures are described and possible causes of their formation outlined. Also discussed are the factors governing the choice of sphalerite as the mineral for such a detailed study.

Chapter three details the principal techniques employed in the study. Thesis petrographic and electron-optical techniques, along with sample preparation procedures are detailed. Also outlined are the setting-up and calibration procedures employed for the fluid inclusion microscope stage. Data collection and correction procedures are outlined.

Textural studies were essentially conducted in two parts, with the principal research being concentrated on the North Pennine Ore samples. Prior to this a brief examination of the breccia infilling ores from the Tennessee (Appalachian-type) ore deposits was undertaken. The Appalachian material was used partly to assess the suitability for sphalerite for electron-optical investigation. The material allowed the documentation of possible specimen preparation-induced microstructures. Comparative studies of visibly deformed and undeformed Appalachian samples allowed specimen preparation-induced artifacts to be distinguished from co-existing deformation

microstructures. This distinction proves useful when examining and 'unravelling' the more complex microstructures which are seen developed within the deformed Nenthead sphalerite samples.

The study of the Appalachian Ores formed the basis for the documentation of deformation, growth, and specimen-induced microstructures and anisotropy. Chapter 4 outlines the geology, mineralogy and previous studies (petrographic and analytical) of the sampled ores, along with optical and electron optical studies of the textures and microstructures developed. The textures and their implications regarding growth, deformation and specimen preparation induced-microstructures are discussed.

The chapters (5 to 9) on the North Pennine Ores comprise the bulk of the textural study. Growth and deformation-induced textures, and mineral microstructures are described, along with the effects of a later supergene stage of mineral alteration. Chapter 5 details the geology, mineralogy, and possible ore-fluid origins for the Alston Block ores.

Chapters 6, 7 and 8 describe the range of growth and deformation textures observed. Textural characterisation, possible origins, and implications for the nature of the ore-depositing fluid are all discussed in chapter 9. Possible relationships between the processes involved and the textures developed are also outlined, and finally, textural and microstructural features for future study are proposed. Both the sampled area (Nenthead), and the North Pennine Orefield sphalerites as a whole are considered.

Chapter 2: Outline and Review of Textures Investigated.

2.1 Criteria and Suitability of Sphalerite for Study.

Of the commonly occurring ore and gangue minerals present in both hydrothermal vein ores, and low temperature Mississippi Valley Type ores (henceforth abbreviated M.V.T.), sphalerite may be considered the most suitable for studies aimed at evaluating the conditions of mineralisation (Barton, 1982). Sphalerite is a widespread, sometimes the only, ore mineral in M.V.T. ores and is usually present, even if only in trace amounts, in many hydrothermal vein ores.

Sphalerite may potentially yield information regarding physical and chemical conditions of ore deposition. Such information is gleaned from studies of its chemistry and textures. Fluctuations in the depositional environment are manifest as variations in the composition of the growing sphalerite grain. In particular, variations in the iron content of sphalerite can be used to model the activity of FeS in ZnS, which is known to depend on the sulfur activity of the fluid and to a lesser extent on the temperature of mineralising fluid.

Sphalerite, pyrite, and arsenopyrite are the most frequently deposited refractory ore mineral phases. More resistant to internal homogenisation and the effects of ore deformation than galena, pyrrhotine, and many of the other common sulfides, these phases are better able to preserve any growth-related textures .

Sphalerite's transparency, unlike pyrite and arsenopyrite, enables the simple observation and correlation of growth banding. Careful examination of some of the more delicately banded and complex ores has enabled the setting-up of a 'microstratigraphy' for some ore deposits (McLimans et al., 1980). Transparency also aids observation of subtle variations in crystal composition and microstructure that would remain undetected using conventional analytical techniques (e.g. electron probe micro-analysis and singly-polished thin sections or polished blocks. Craig and Vaughan, 1981). Also possible are thermometric studies of fluid inclusions which may yield information about the temperature and salinity of the mineralising fluids.

Crystal habit may provide some indication about possible rates of precipitation during ore development and about levels of fluid supersaturation with respect to dissolved ZnS. A variety of crystal forms, varying from a gem-like or euhedral through to fibrous and colloidal have been related to the above factors (Barton et al., 1963).

Both types of deposit sampled (North Pennine Fluoritic-M.V.T. and Appalachian Central Tennessee M.V.T.) host significant quantities of sphalerite as relatively large (millimetre sized) grains, which have been subject only to low levels of deformation. Sphalerite sampled from both deposits is well suited to compositional and textural studies.

2.2 Growth Defects.

A wide variety of growth-related crystal microstructures are

reported in the literature. Characterised by transmission electron microscopy, X-ray diffraction, and cross-polarised transmitted light microscopy, the majority of growth-related defects may be assigned to one of two principal classes: non-planar and planar.

2.2.1 Lattice defects (non-planar varieties).

These are due to the laying down of a non-ideal cubic (sphalerite-3C) or non-ideal hexagonal (wurtzite-2H) structure during crystal growth. Included in this group are 'point' (i.e. small localised) defects, and line defects such as screw dislocations.

Both the mineralogical and solid state physics literature detail the presence of a variety of non-planar lattice defects for the various structural varieties of zinc sulfide. Both naturally occurring and synthetic sulfides have been described (e.g. Verma, 1956; Komatsu and Sunagawa, 1965; Barton and Bethke, 1987). Three principal defect types are recognised:

1. 'Point'-defects.
2. Screw dislocations.
3. Other line defects.

Point (Localised) Defects. A high concentration of such defects may locally render sphalerite opaque in a manner similar to that reported for small inclusions (see section 2.3.3). The presence of 'point' defects in a growing crystal may be promoted by, or give rise to, the nucleation of other mineral phases within the zinc sulfide. A degree

of lattice mismatch will usually exist between a second mineral phase and the host zinc sulfide. The precipitation of second phases at defect sites is aided by the release of energy associated with the defect. This energy helps overcome the activation energy required for the nucleation of the second phase. Fluctuations in the chemical nature of the depositing fluid may be responsible for the precipitation of two mineral phases together.

Screw Dislocations. Studies of the two principal zinc sulfide polytypes, 3C-Sphalerite and 2H-Wurtzite, have shown screw dislocation development to be common for both natural and synthetic mineral specimens (Verma, 1956; Aragona and Delavignette, 1966). Screw dislocations may have a role in polytype development and polytype stabilisation (Daniels, 1966; Mardix and Steinberger, 1970; Mardix, Lang and Blech, 1971). The complex mechanisms advocated for these processes are discussed in the solid state physics literature (Mardix, 1984b; 1986).

Line defects. Recently described by Barton and Bethke (1987), the textural features due to high concentrations of such defects are recognised in naturally occurring samples of sphalerite. The texture comprises a rod or chain like defect, possibly derived by a point defect having been "carried" by the crystal surface during growth (Barton, pers. comm, 1986). The possibility of the defect being decorated by other sulfide phases has been suggested (Barton and Bethke, 1987). In particular decoration of the defect by copper-iron sulfides is advocated as a possible mechanism in the development of

the textural phenomenon termed "chalcopyrite disease" (section 2.5).

2.2.2 Polytypism and Planar Defects.

These defect types reflect the ease with which zinc sulfide may be precipitated in a variety of structural forms. Included in this category of crystal defect are growth twins, polytypes, and non-periodic stacking faults. These microstructural and lattice modifications may give rise to a variety of optical effects, the most significant of which are anisotropy and twinning.

The mineralogical and solid state physics literature contains numerous studies of stacking fault development and lattice modifications to the 'end-member' polytypes; i.e. the 3C-sphalerite and 2H-wurtzite lattice structures. Stacking sequences for zinc sulfide are defined along the [00.1] growth axis for 2H-wurtzite and the equivalent [111] growth axis for 3C-sphalerite. A stacking fault occurs when there exists a degree of layer mismatch perpendicular to the [00.1] or [111] growth axis, respectively (see figure 2.2).

Figure 2.1 details the 3C, 2H, and a variety of the more commonly occurring polytypic forms of zinc sulfide. The 3C-sphalerite structure may be seen to comprise a 3 layered cubic structure with close-packed sulfur ions stacked along the [111]-axis, each stacked layer comprising units of hexagonal symmetry. The 2H-wurtzite structure comprises a 2 layer [00.1]-axis stacked sequence of similar hexagonal layer types.

Direct observation of layer mismatch (stacking faults) in zinc sulfide is detailed in a variety of electron optical studies (Aragona

and Delavignette, 1966; Fleet, 1975; Akizuki, 1981). Layer mismatch is indirectly inferred during petrographic examination (transmitted light, crossed polars) of doubly-polished thin sections. The stacking faults give rise to small non-cubic, and hence birefringent, regions within the material.

Ideal 3C-sphalerite (space group $F\bar{4}3m$) is optically isotropic, having 0 percent hexagonal close packing. 2H-wurtzite (space group $P6_3mc$) may be thought of as showing the maximum birefringence (or 100 percent hexagonal close packing) attained by the various polytypes. Pure 2H-wurtzite has a birefringence value of 0.024. Naturally occurring material with its inherent polytypism and lattice disorder will typically display birefringence values between the 3C and 2H end-member values. A linear relationship has been demonstrated between the degree of structural disorder (or degree of hexagonality) and birefringence (Nelkowski and Pfutzenreuter, 1971). This concept has been successfully applied to studies of natural low temperature ores (Fleet, 1977a).

Studies of polytypism in zinc sulfide have been based on two separate aspects of poytypism; the structural sequence i.e. elementary unit comprising a number of layers, which will generate a polytype if periodically repeated, and the polytype periodicity (Mardix, 1986). If the layers have a different lateral sequence (i.e. if periodicity is locally lacking) then a stacking fault is said to exist. However, if some degree of periodicity is apparent for the sequence, then the structure is deemed to be polytypic. The polytype is defined by the number of layers which comprise the repeat unit. Actual

controls of polytype periodicity and stacking fault development for zinc sulfide are uncertain (Scott and Barnes, 1972; Steinberger, 1983; Mardix, 1986; Frey et al., 1986).

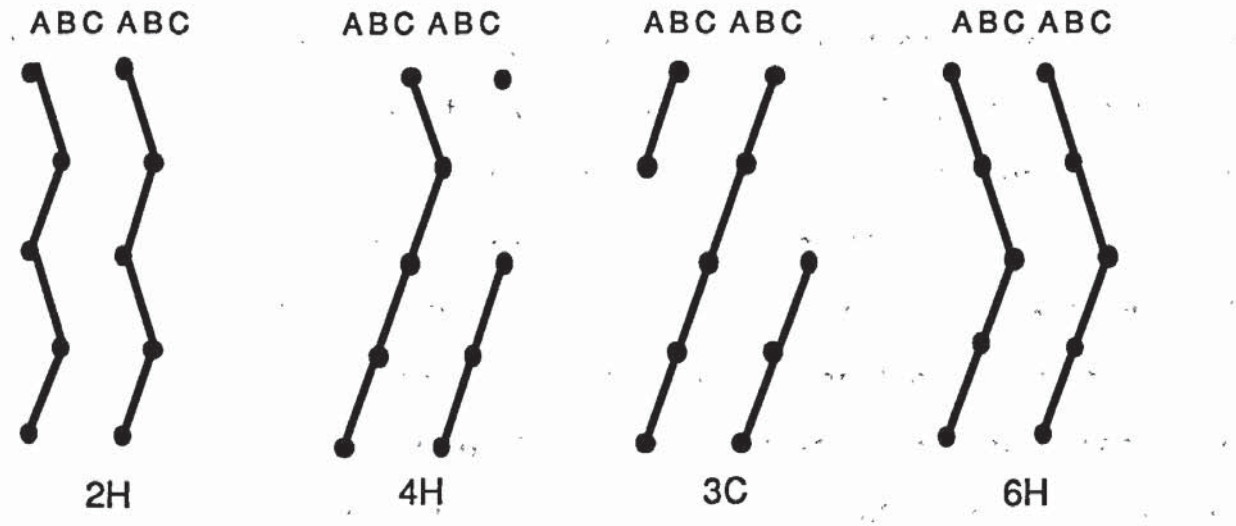

(11.0) Layer projections of various ZnS polytypes, two unit cells wide. Modified from Fleet, 1977b.

FIGURE 2.1

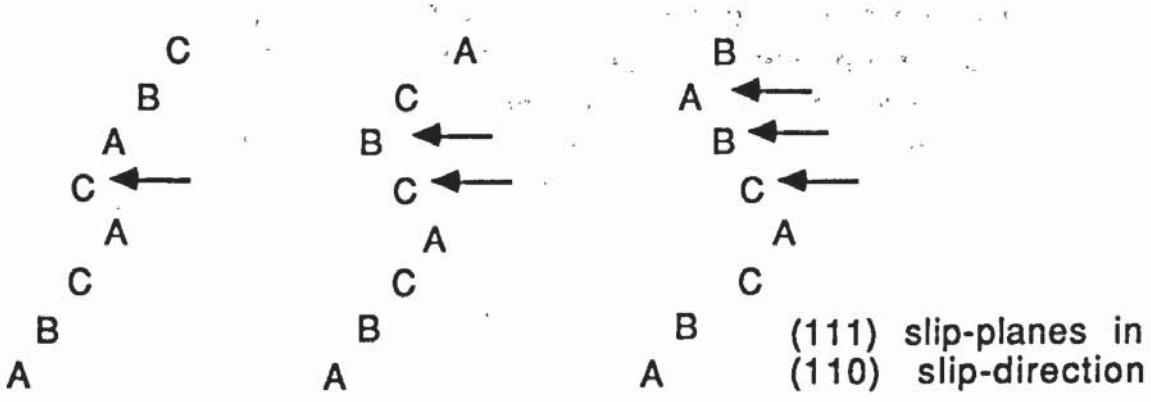

Single, double, and triple deformation fault in cubic ZnS lattice: Triple faulted region is equivalent to twinned 3C region of sphalerite.

FIGURE 2.2

X-ray diffraction studies on naturally occurring hydrothermal zinc sulfides indicate growth-related polytypism to be common. Similar studies on synthetic zinc sulfides have revealed a large number of polytypes (approximately 200; see Mardix, 1986), often several in one crystal (Frondel and Palache, 1950; Jahnke, 1986; Mardix and Kiflawi; 1970). Also reported is the common development of stacking disorder for both natural and synthetic sulfides (Smith, 1955, and Table 2.1). The 3C-cubic polytype would appear to be the best represented in most natural low temperature samples (Smith, 1955).

One type of stacking fault of special note is the growth twin. A twinned region of sphalerite is structurally analogous to a narrow 6H-polytypic region (figure 2.3). Etch studies of natural ores have shown growth twinning to be widespread for undeformed hydrothermal zinc sulfide (e.g. Ramdohr, 1980; Frater, 1985).

Twinned 3C-Sphalerite structure (110) projection. Twinned region of sphalerite has same structure as the region of 6H-Wurtzite in figure 2.1.

FIGURE 2.3.

Twinned region of 3C-Sphalerite illustrating the narrow 6H-Polytypic region generated by the twin plane (after Fleet, 1977b).

Locality	Colour, etc.	% Cubic Packing	Cell edge (Å)
Low (?) temperature zinc sulfide:			
Bautch Mine, Wisconsin	White band	95.8	5.4102
Bautch Mine, Wisconsin	Brown band	92.1	5.4106
Bruce Peninsula, Ontario	Light brown	89.3	5.4106
Clay City, Ohio	Very light brown	84.2	5.4097
De Rocher, Wisconsin	Dark brown	84.8	5.4108
El Potosi Mine, Mexico	Black	89.9	5.4232
Gibsonberg, Ohio	Light brown	89.3	5.4095
Mascot, Tennessee	Light Yellow	91.1	5.4101
North Hunt Mine, Oklahoma	Very light brown	91.2	5.4108
Ottawa Co., Oklahoma	Very light brown	88.4	5.4113
Picher, Oklahoma (M Bed)	Very light brown	78.4	5.4101
Picher, Oklahoma (J Bed)	Very light orange	88.5	5.4113
Pine Point, N. W. T., Canada	Light brown	94.8	5.4106
Pine Point, N. W. T., Canada	Brown banded	86.8	5.4105
Pine Point, N. W. T., Canada	Brown fossil filling	91.1	5.4102
Intermediate (?) temperature zinc sulfide:			
Bleisharley Mine, Germany	Brown banded	90.5	5.4106
Butte, Montana	White band	93.0	5.4902
Butte, Montana	Brown band	90.2	5.4106
Darwin Mine, California	Black	89.3	5.4196
Freiberg, Saxony	Light brown band	95.0	5.4132
Freiberg, Saxony	Light brown band	93.8	5.4128
Gaspe, Quebec	Very light yellow	90.0	5.4106
Leadville, Colorado	Light brown	90.2	5.4111
Moresnet, Belgium	Light brown band	86.0	5.4073
Moresnet, Belgium	Dark brown band	63.0	5.4087
Prizbram, Bohemia	Brown acicular	92.3	5.4133
Prizbram, Bohemia	Brown acicular	60.2	5.4138
Santander, Spain	Light yellow	87.3	5.4019
High (?) temperature zinc sulfide:			
Bachelor Lake, Quebec	Light yellow	96.3	5.4111
Balmet, New York	Brown	99.6	5.4152
Eskaminish, Manitoba	Dark brown	88.8	5.4177
Frontenac Mine, Ontario	Brown	90.6	5.4173
New Calumet Mine, Ontario	Brown	91.3	5.4172
Ogdensburg, New Jersey	Very light yellow	90.0	5.4116
Parry Sound, Ontario	Brown	92.0	5.4166

TABLE 2.1

Examples of natural zinc sulfides with a cubic close packing (3C-Sphalerite structure) dominant. Examples taken from Smith (1955)

2.3 Growth Textures: Optical.

A variety of growth-related textures in ores reflect open-space deposition from a circulating fluid (as outlined in Craig and Vaughan, 1981, and Ramdohr, 1980). Three growth-related textures in particular are important in this study:

1. Regular or rhythmic banding or zoning within one sphalerite grain or cluster of grains.
2. The development of large numbers of solid, liquid, or vapour inclusions.
3. The development of anisotropy .

2.3.1 Band Development in Sphalerite.

The presence of internal banding or zoning is taken as indicative of fluctuating physical or chemical conditions for the depositional environment. Four kinds of banding are recognised:

1. Variations in the crystal composition.
2. Variations in the inclusion content of the crystal.
3. The effects of hydrocarbon contamination of the ore fluid.
4. Variations in defect content of the crystal (see section 2.2 for details).

Many sphalerites exhibit banding that may be attributed to a combination of the above listed causes.

2.3.2 Variations in Chemical Composition.

The development of composition-related banding reflects the ability of other metals to substitute for zinc, the most reported of which are iron and cadmium. Many other metals may substitute in trace amounts giving rise to a range of coloured varieties (Craig and Vaughan, 1981).

Iron may substitute for zinc up to 56 mole percent (Barton and Toulmin, 1966) and a correlation between iron content and crystal colour has been reported (Palache et al., 1944; McLimans et al., 1980; Barton, Bethke and Roedder, 1977). The iron-poor sphalerites are typically pale-coloured, in contrast to iron-rich varieties; the majority of which are strongly coloured. The studies of Craig, Solberg, and Vaughan (1983) showed that for iron concentrations of less than two weight percent there may be little or no correlation between sphalerite colour and iron content, a feature also noted by Roedder and Dwornik (1968). Similarly McLimans et al., (1980) point out that for iron concentrations greater than 8 mole percent (approx. 4.75 wt. percent), changes in body colour may not always be readily apparent due to the mineral being rendered opaque.

Cadmium substitution has little or no effect upon colour. In common with sphalerite, the cadmium sulfide greenockite absorbs little light from the visible spectral range (Boldish, 1973).

Antimony, arsenic, and copper, are often recorded in trace amounts in sphalerite, and may impart a 'tetrahedrite red' colour (Ixer and Pattrick. pers. comm. for Mendips Orefield sphalerites). Ixer et al. (1986) describe a vug-grown sphalerite from the Semail ophiolitic

complex, Oman, where trace levels of copper and arsenic are correlated with a deep red internal banding. However there is debate as to the mechanism; the effects of solid-solution of other metals for zinc, or the presence of sub-microscopic tennantite-tetrahedrite type particles.

2.3.3 Variations in Inclusion Content.

Sphalerite grains often trap solid or fluid phases during crystal growth. High concentrations of trapped inclusions may render the mineral translucent when viewed in thin section. A very high inclusion content may cause the sphalerite to be opaque in thin section. Banding due to such a trapping mechanism is not an uncommon phenomenon, best observed where the trapped particles are either opaque fluids (e.g. hydrocarbons) or solids. Inclusions range in size from optically identifiable phases (tens or hundreds of microns in size) to submicroscopic. Submicroscopic inclusion development in minerals generally may be related to either a solid-solution origin, or a crystal defect origin; i.e. exsolution or primary precipitation on the defect site (White, 1985).

Examples of inclusion-banded sphalerite ores are well documented in the literature. Craig and Vaughan (1986) describe such a texture from the M.V.T. ores of the Central Appalachians. Likewise Foley and co-workers (1981) noted similiar textures in ores from the Ridge and Basin Province.

The association of many Mississippi Valley-type lead-zinc deposits with organic matter or hydrocarbons has been noted by many

workers (e.g. Roedder, 1962; Gize et al., 1981 and 1987). There exists some debate in the literature as to the possible role played by the hydrocarbon material in the mechanism of sulfide precipitation and metal complexing (e.g. Barton, 1967; Barnes,1983; Spirakis, 1983).

Such material, however, is cited as a possible cause of banding in M.V.T. sphalerite grains (Foley, 1980; Craig, Solberg and Vaughan, 1983). The presence of horizons rich in numerous small opaque or translucent hydrocarbon inclusions in growth banded sphalerites is described from the Idol Mine by Craig and Vaughan (1986). They correlate such hydrocarbon-rich horizons over several hundred metres. In addition to the development of inclusion-rich horizons, hydrocarbon contamination may take the form of thin and irregular films that are interstitial to the grains (Craig, Solberg and Vaughan, 1983).

2.3.4 Anisotropy.

The development of anisotropy reflects the presence of non-cubic (wurtzitic) material or the development of non-cubic regions in the lattice. Non-cubic domains principally take the form of stacking faults, especially twin planes.

Fleet (1977a) described the anisotropy in a wurtzite "schalenblende". The "schalenblende" comprised a deformed zinc-bearing ore assemblage containing both banded regions of wurtzite and sphalerite. Birefringent areas take the form of diffuse and patchily developed, broad, wedge-shaped lamellae. Inversion processes acting on the hexagonal sulfides have reduced their degree

of hexagonality and these lamellae may often be observed terminated by stacking faults developed in areas of lower birefringence.

The two principal textural varieties of anisotropic regions in sphalerite are described by Seal, Cooper and Craig (1985). A grid-iron and a lamelliform texture are recognised. The grid-iron texture comprises two sets of diffuse or broad birefringent lamellae perpendicular to each other. The texture is likened in appearance, but not in origin, to that observed in microcline. Seal et al. (1985) attribute the grid-iron texture to a combination of stacking fault development and twin plane development.

Where twinning is strongly developed (as is more typical of deformed sulfides; see section 2.4.3), lamelliform anisotropy is observed. Comprising a series of narrow (typically a few microns in width), sub-parallel, sharply bounded laths, the anisotropic texture may be optically correlated with twin-dominated regions.

The above textures are not restricted to a growth-related origin. Mechanical and thermal stresses may generate a range of similar features (see section 2.4.4).

2.4 Deformation and Inversion Textures.

The mineralogical and solid state physics literature contains few studies, theoretical or descriptive, of naturally occurring low temperature hydrothermal zinc sulfide deposits which have been subject to mild deformation. Studies relating optical fabrics to processes and mechanisms operative during such deformation are especially poorly documented. The majority of studies have been of a

petrographic nature, describing chemically-etched polished sections (for example Ramdohr, 1980; Edwards, 1947; and Richards,1966).

Well documented, high temperature studies (1000 K and above) of zinc sulfides have been undertaken on polytype stability and the mechanisms of polytype transformation, particularly those involving wurtzite to sphalerite and sphalerite to wurtzite inversions (for example, Akizuki, 1970, 1981; Baars and Brandt, 1973; Frey et al., 1986). Two possible factors are cited as controlling textural development; thermally-related processes and mechanically-induced processes.

2.4.1 X-Ray Diffraction and Electron Optical Studies of Thermally Induced Microstructures.

Thermal studies have largely been based on the work of Allen and Crenshaw (1912), who noted that 3C-Sphalerite represents the low-temperature polymorph and 2H-Wurtzite the high temperature form. The actual polytype inversion temperature, initially determined as 1293 K, is uncertain and may depend on a variety of factors (Scott and Barnes, 1972).

Sphalerite to Wurtzite transformation.

Natural samples of sphalerite (and hence impure and defect-containing) have been observed to transform to a faulted wurtzite structure in the region of 1290 K (Akizuki, 1981; Frey et al.,1986). Lower temperature annealing of the material (at approx. 1000 K) generates a range of hexagonal polytypes, principally a mixture of the

2H- and 4H- hexagonal forms. The actual transformation mechanism is said to depend on the degree of structural disorder (Frey et al., 1986).

At considerably lower temperatures, a different response to annealing is noted (Akizuki, 1970). Instead of inverting to a wurtzitic form, the crystal responds to thermal stress by the development of stacking faults and twinning. As the temperature increases, so does the extent of twinning and faulting until a disordered hexagonal structure develops (at approx. 1300 K).

Wurtzite to Sphalerite Transformation.

Low temperature studies have shown that wurtzite responds to thermal stress by the nucleation of stacking faults. As the temperature is increased twinning develops, resulting in a twinned disordered sphalerite structure (Sebastian and Krishna, 1984; Krishna and Sebastian, 1986). The greater the temperature, the more rapid is the transformation; however, above 1320 K the reverse transformation occurs (see above).

2.4.2 X-Ray Diffraction and Electron Optical Studies of Mechanically-Induced Microstructures.

Many hydrothermal zinc ores, M.V.T. ores in particular, have been subject to temperatures of no more than five hundred degrees kelvin. For these ores, ductile and brittle deformational processes are important in textural development. Mild deformation of the sulfides produces deformation textures similar to those promoted by thermal

stressing as outlined in section 2.4.1. The hexagonal polymorphs, in particular, are very sensitive to the effects of stress (Farkas-Jahnke and Gacs, 1979; Clark and Kelly, 1973).

Low levels of stress lead to a loss of hexagonality in the non-cubic polymorphs, and the resultant structure is that of a disordered, twinned sphalerite. Sphalerite, however, does not undergo a polymorphic transition when stressed but becomes twinned (Fleet,1977b).

Stress may also induce translation gliding and slip-plane development in sphalerite (Clark and Kelly, 1973). In an optical study using etched material, twinning and slip were produced experimentally under confining stresses of less than 0.5 kilobars. Clark and Kelly (1973) concluded that both brittle and ductile processes can operate concurrently, a concept borne out in many petrographic studies.

2.4.3 Petrographic Studies of Deformation.

Both brittle and ductile deformational processes are observed to operate in a variety of ore deposits (Lawrence, 1973; Ramdohr, 1980). Brittle processes are principally that of microcrack and fracture development. The {110} cleavage planes do not appear, however, to be activated by these processes.

Ductile deformational processes include twin development, glide plane development, subgrain development, and recrystallisation. Twins tend to be multiple (up to 160 lamellae per millimetre), narrow (often one micron or less in width), and may branch or taper along

their length (Richards, 1966). They may be observed to nucleate from, or terminate at, subgrain boundaries or other twin planes, or in mid-grain. Crystal glide planes are best observed by their offsetting of twin lamellae. Subgrain development and recrystallisation tend to generate equant polygonal mosaics that are characterised by 120 degree junctions (Lawrence, 1973).

Frater (1985) additionally details the development of dislocation networks during recovery, by sub-grain and sub-boundary development. Frater (1985) concluded that the ductile deformation textures progressively develop in a manner analogous to steady-state creep in metals.

2.4.4 Anisotropy.

As outlined in section 2.3.4, twin plane and stacking fault development may generate a range of anisotropic textures. Deformation-related anisotropy, especially for twin-related textures, differs slightly from similar growth-related textures. Deformation twinning, and hence its associated anisotropy, will reflect the stress field, and one twin direction tends to be dominant.

Lamelliform anisotropy is more typical of deformation-related processes. Grid-iron anisotropy is more typical of growth-related mechanisms (Seal, Cooper, and Craig, 1985), but the distinction is not clear-cut.

2.5 "Chalcopyrite Disease" and Related Alteration Processes.

The common occurrence of chalcopyrite within sphalerite in a wide variety of ore deposits has been attributed to exsolution (Ramdohr, 1980, Shimazaki, 1980) or replacive process (Eldridge, Barton, and Ohmoto, 1983; Barton and Bethke, 1987). The texture, distinctive in its appearance, is termed 'chalcopyrite disease' because of the spotted appearance in reflected light (Barton, 1978).

Chalcopyrite may adopt a variety of morphological forms. The more common forms are detailed in figure 2.4 and listed below:

1. As a series of crystallographically oriented rods and lamellae. The direction of rod development or lamellae orientation corresponds to the <111> directions of the hosting sphalerite grain.
2. Apparently randomly distributed, anhedral blebs within the host grain. Bleb size may vary in size within any one host grain.
3. A fine dusting of micron-sized anhedra or rods randomly distributed throughout the host crystal.

Petrographic studies of the Japanese Kuroko ores contain descriptions of textures that are incompatible with an exsolution origin (Eldridge, Barton, and Ohmoto, 1983; Barton and Bethke, 1987). More than one generation of sphalerite mineralisation was in existence when some of the earlier generation became 'diseased'. Individual grains show irregular development of chalcopyrite, with the texture developed along certain horizons or bands. Barton (1978) concluded that much of the fine chalcopyrite dusting has developed

subsequent to sphalerite growth and that the texture has a replacement rather than an exsolution origin.

Phase equilibria studies of the Cu-Fe-Zn-S system provide further evidence for a replacement origin from the stability fields of sphalerite and chalcopyrite under geological and ore-forming conditions (Wiggins and Craig, 1980; Hutchison and Scott, 1981; Kojima and Sugaki, 1984, 1985). Figure 2.5 outlines the solubility field of CuS in sphalerite. At ore-forming temperatures of less than 300 degrees C the solubility limit is less than 0.5 mole percent. This contrasts sharply with observed levels of chalcopyrite in "diseased" sphalerite. Bulk CuS concentrations often exceed 10 mole percent (e.g. Sugaki et al., 1987).

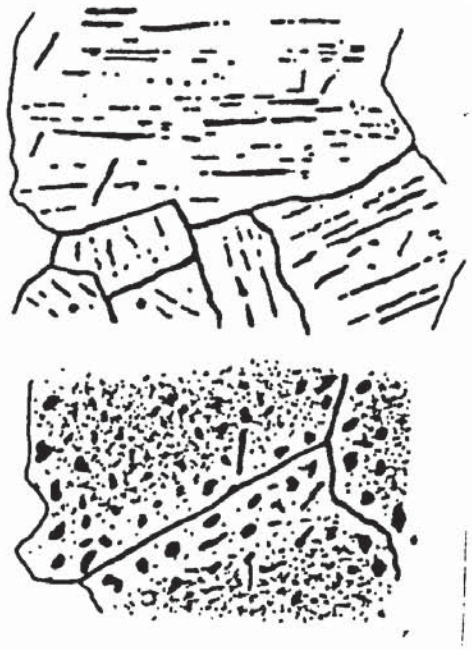

Crystallographically oriented rods and lamellae of chalcopyrite

centimetres

0 1

Bimodal size distribution for anhedral blebs of chalcopyrite. The larger blebs tend to be near to the sphalerite grain boundaries.

FIGURE 2.4

Typical textural examples of "chalcopyrite disease" developed in sphalerite.

The experimental work of Bourcier et al. (1984) has demonstrated the possibility of cultivating the texture in natural "undiseased" sphalerite samples. They found that for high levels of copper supersaturation in the experimental fluid, the sphalerite was replaced wholesale by chalcocine (Cu_2S). Chalcopyrite development took place only at lower levels of copper supersaturation.

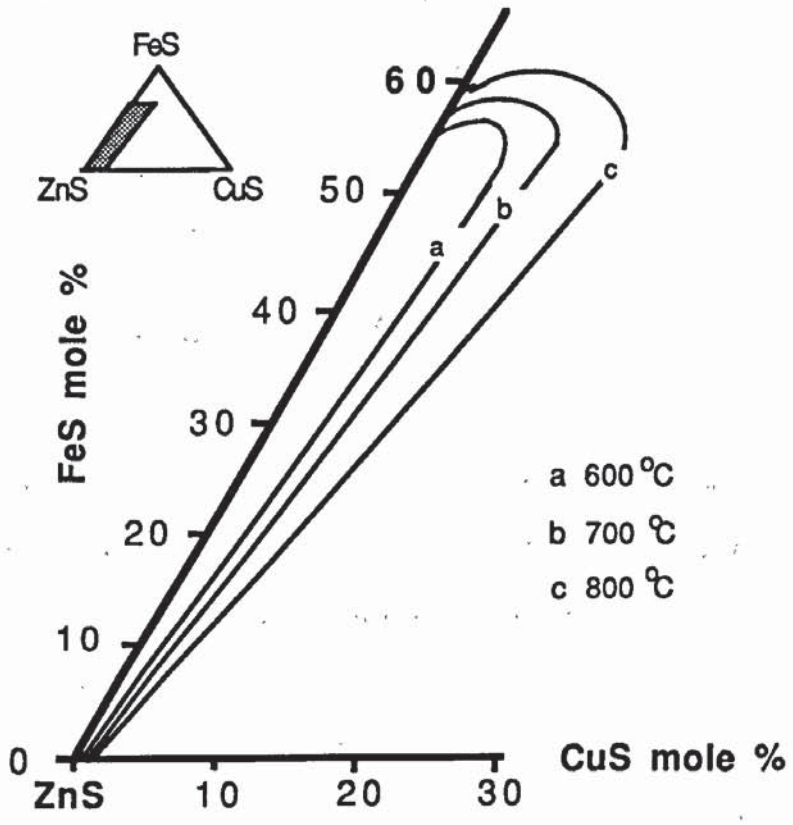

FIGURE 2.5 Solubility field for CuS in sphalerite (after Sugaki et al., 1987).

2.5.1 Supergene Copper-Related Alteration of Sphalerite.

De Waal and Johnson (1981) describe the development of chalcopyrite and chalcopyrite-like phases in the supergene environment. They distinguish an iron-rich, copper-poor sphalerite termed 'primary', from two varieties of secondary sphalerite; a chemically altered, copper-rich variety (up to 10 mole percent copper), and a variety termed 'neoform' (1.6 to 2.4 mole percent copper). The copper-rich variety is characteristically developed close to, or just below, the water table and is observed to contain a chalcopyrite-like phase which has been tentatively identified as talnakhite ($Cu_9Fe_8S_{16}$). They postulated that chalcopyrite developed in the supergene environment by a copper enrichment process i.e.:

$$yCu^{+n} + Zn_xFe_{1-x}S =$$

$$Zn_xFe_{1-x-2y}S_{1-2y} + yCuFeS_2 + yFe^{2+} + (2-n)ye \qquad (2.1)$$

Where n = 1 or 2, and x and y are variables. If n = 1, an oxidation-reduction step is involved and , if n = 2, the reaction is a cation exchange. Primary sphalerite is depleted in iron for either of the two possible processes.

Supergene alteration processes will be assisted by any deformation of the sphalerite grains, which will generate crystal defects and open up the crystal to copper-bearing pore fluids (De Waal and Johnson, 1981).

The supergene environment may be regarded as a proton-

producing one. A reduced pH value will increase the solubility of any metal ions in pore-filling solutions. Such a mechanism, capable of generating copper ions in solution, tends to yield ions in the cuprous state (Cotton and Wilkinson, 1972). The migration of cuprian pore-fluids into a more reducing environment may generate a range of 'blue sulfides' (esp. covelline) and react with any iron-bearing sphalerite present.

The actual mechanisms involved in the replacement of sphalerite are poorly understood. The possibility of 'intermediate' Cu-Fe sulfides forming as a precursor to chalcopyrite cannot be ruled out. Bornite and similar Cu-Fe sulfides are known to develop in 'diseased' sphalerite on a sub-microscopic scale. They have been successfully imaged electron-optically (Dickinson, pers. comm., Dickinson and Pattrick, 1986).

CHAPTER 3: Principal Investigative Techniques.

3.1 Petrographic Studies.

The zinc-bearing ores were examined in both reflected light and transmitted light with a dual purpose polarising petrographic microscope. The majority of the samples took the form of doubly-polished thin sections rather than polished blocks or conventional covered thin sections. The use of doubly-polished thin sections enables both a transmitted and a reflected light examination of the same specimen, in addition to permitting etch and fluid inclusion studies of the sample. Doubly-polished thin sections are preferred to conventional thin sections when studying translucent ore minerals (e.g. cassiterite and sphalerite). The diffuse scattering of the transmitted light by an unpolished surface (as is the case for a singly polished thin section) can make the recognition of many internal textures impossible. The studies of Barton (1978), and Eldridge, Barton, and Ohmoto (1983), on the Kuroko volcanogenic massive sulfide ores of Japan illustrate clearly the wealth of fine detail and information that may remain undetected when examining the ores as either polished blocks or as unpolished thin sections.

The doubly-polished thin sections were prepared from 3 millimetre thick wafers of ore material. The wafers were cut using a fine-blade slow-speed diamond saw. The use of a slow-speed saw reduces fracturing and deformation of the ore material to a minimum (see section 3.7.2). However, the friable nature of many ore samples necessitates vacuum impregnation of the samples with a cold-setting resin prior to sample cutting and sectioning. The majority of the

samples were impregnated with cold setting Araldite, dissolved in an acetone medium.

One side of the wafer was carefully ground by hand and polished in the manner outlined by Craig and Vaughan (1981, Ch. 2). After cutting and polishing one side of the wafer, the polished side was mounted on to a 28 by 48 millimetre glass slide using a low temperature soluble adhesive. Lakeside 30C, Canada Balsam, and dental wax were all used in sample preparation and Canada Balsam was found to be the best suited for the majority of the materials sampled. After mounting the wafer on the glass slide, the section was machine ground on a Logitech automated sectioning machine to a thickness of approximately 0.5 millimetres.The section was then hand ground and lap polished. Hand grinding of the sample is preferred to the automated thinning of the section. Both surface damage due to mechanical machining, and any variations in sphalerite body colour or transparency may be compensated for by periodic thinning and inspection. A standard 30 micrometres thick, machine prepared section reveals few, if any, of the variations developed in the body colour of the sphalerite or associated textural variations in microstructure. Sections ranging in thickness from 100 to 150 micrometres were commonly employed throughout the study except for transmission electron microscopic purposes (see section 3.7.1).

3.2 Etch Studies.

In addition to reflected light examination of untreated surfaces, many of the polished sections were chemically etched and

the etched surfaces re-examined in reflected light. The etched surfaces revealed a variety of growth- and deformation-related textures. Extreme care was taken when polishing and grinding the samples before etching, in order to try and minimise any possible surface damage to the sample. Any such damage is clearly visible in the etched sections and may obscure the finer textural features revealed in the etching process . The etchant used was 53 percent hydriodic acid with an etch time of three to four minutes, following one of the methods most commonly used (Richards, 1966., Ramdohr, 1980).

The etch rate is sensitive to the crystallographic orientation of the surfaces, the composition of the etched surface, and the presence of small inclusions, or particles, which preferentially etch out. If the surface being etched hosts a high concentration of crystal defects or dislocations then they may be apparent as numerous small pits on the etched surface (Akizuki, 1970).

3.3 Electron Probe Micro-Analysis.

Electron probe microanalysis (E.P.M.A.) of the ore minerals was undertaken at the Department of Geology, University of Manchester, on a joint University and Natural Environment Research Council (N.E.R.C.) owned microprobe. The machine used for the duration of the investigation was a C.A.M.E.C.A. Camebax probe which was equipped with two wavelength dispersive spectrometers (W.D.S.) and a Link Systems 860-500 energy dispersive spectrometer (E.D.S.).

Sulfide analysis was undertaken with an accelerating potential

of 20 kilovolts and a beam current in the range of 14 nanoamps. An X-ray take-off angle of 40 degrees was employed throughout the study. The software packages permitted the automated operation of the machine overnight for elemental profiling and zone analysis. A 12 hour run enabled up to 100 points to be analysed for up to 10 elements, most of them at trace or minor levels. A range of natural and synthetic sulfides were employed as standards.

Samples for probe analysis took the form of polished thin sections, 26 millimetres by 48 millimetres in size. Prior to analysis a full petrographic examination of the mineralisation was undertaken. Transmitted-light and reflected-light photomicrographs were made of the areas and textures of interest. The photomicrographs are necessary for the location and recording of analysed areas.

Before micro-probe analysis, a 20 nanometre layer of conductive carbon was deposited on the sample to prevent specimen charging. Carbon coating was done by resistively heating two pointed carbon rods held in contact under vacuum (see Reed, 1975, for details).

For major element analysis, count times of 60 seconds per element were used. For minor and trace level elements, the count time was extended to 100 seconds to improve analysis accuracy. Raw count data collected were computer corrected using standard procedures (Reed, 1975) for the effects of atomic number, absorption, and fluorescence. ZAF 4/FLS software, along with a 'SPECTRA' software package was employed for the correction procedures. Detection limits for the elements are better than 0.02 wt %.

3.4 Organic Analysis.

Ultra-violet fluorescence microscopy (U.V. microscopy) and Fourier Transform Infra-Red spectroscopy (F.T.I.R.) were two specialised techniques used to check for the presence of any organic material in the ores (in particular, in samples from the North Pennine Orefield). Both techniques detect both liquid and solid phases. U.V. microscopy represents a relatively simple and widely available technique which may be used for routine examination of ore material. F.T.I.R. microscopy represents a relatively more specialised technique not readily available. It complements the U.V. technique in that it is less sensitive to the effects of any thermal maturation of organic matter, and may be used to semi-quantitatively define the nature of any such matter present.

3.4.1 Ultra-Violet Fluorescence Microscopy.

Organic matter is observed to fluoresce when irradiated with U.V. radiation (wavelength 350 to 410 nanometres). The intensity of fluorescence is a function of the thermal maturity of the organic matter, and of the type of organic matter present.

Specimen preparation is the same as that used for conventional reflected light microscopy with two additional modifications. The intensity of fluorescence for organic matter is observed to fall with increasing grade of thermal maturation. Cold-setting impregnating resins were used to avoid 'baking' the samples. Also necessary during specimen preparation, especially during polishing, is the avoidance of

any oil-based lubricants. Any oil or grease contamination of the specimen produces a spurious fluorescence during irradiation. Prior to examination, the specimens were cleaned in an acetone bath to remove any fingerprints, dirt, or dust, which would also fluoresce. After washing in acetone the sample was placed under vacuum for ten days to ensure complete evaporation of the solvent. All samples were stored in grease-free and air-tight containers prior to examination.

Examination of the material was undertaken at the Department of Organic Geochemistry, University of Newcastle, and at the Department of Geology, University of Southampton, using a Zeiss ultra-violet photomicroscope. Similiar in design to a conventional photomicroscope, the ultra-violet light microscope uses a high pressure mercury vapour lamp with special filters fitted to prevent the microscope user suffering ultra-violet light damage to the eye. Both polished blocks and doubly-polished thin sections were examined for luminescent phases within the sphalerite.

3.4.2 Fourier Transform Infra-Red Spectroscopy.

This recently developed technique makes use of a spectrometer coupled to a dedicated computer. The spectrometer records spectra in the infra-red range of 400 cm^{-1} to 20 cm^{-1} transmitted by the specimen under investigation. From the spectra recorded, it is possible to compute any absorption spectra developed which will characterise any organic phases present.

The use of a dedicated, computer-aided spectrometer enables spectral profiles to be collected and analysed in a matter of seconds.

Upwards of 3000 spectral sweeps per hour may be obtained and summed, as opposed to 5 sweeps per hour using conventional spectral techniques. A high number of spectral sweeps reduces background noise to negligible levels, thus enhancing any absorption spectra present. F.T.I.R. has successfully been applied to small sample areas (e.g. fluid inclusions) and apparently optically opaque sample areas (Gize, pers. comm., 1986).

Samples for investigation were prepared in the form of 30-micron thick wafers that were doubly-polished to enhance spectral transmission. Similiar precautions regarding contamination by oils during polishing were followed as detailed in section 3.4.1.

The samples were analysed by Dr. A. Gize at the Geophysical Laboratory, Carnegie Institute of Washington. For the North Pennine samples both banded and unbanded *type-two* areas were scanned and the spectral profiles obtained were ratioed to contrast the banded and unbanded material.

3.5 Thermometric Analysis of Fluid Inclusions.

Thermometric studies were undertaken on a wide variety of two phase inclusions in the sphalerite and accompanying gangue quartz. Thermometric analysis is another technique that necessitates the use of doubly-polished wafers. Wafer thickness may vary according to sphalerite body colour. Dark banded sphalerite wafers were occasionally less than 0.1 millimetre in thickness. The quartz gangue wafers were typically 0.1 to 0.2 millimetres in thickness. Wafer fabrication is the same as that outlined in section 3.1, with

one major exception; wherever possible, samples were left unimpregnated due to the possibility of resin breakdown occurring during the heating runs on the inclusion stage.

REAGENT	Melting Point.
ACETANILIDE	114 deg. C.
ANILINE	-6.5 deg. C.
BENZOIC ACID	112.13 deg. C.
CALCIUM NITRATE	42.7 deg. C.
CARBON TETRACHLORIDE	-22.99 deg. C.
CHLOROBENZINE	-45.6 deg. C.
PHENYL BENZOATE	69.0 deg. C.
WATER [a]	0.0 deg. C.

a - Double distilled.

TABLE 3.1

Chemicals employed as standards for calibration of fluid inclusion stage. All chemicals are of 'Analar' grade unless otherwise indicated.

Prior to inclusion analysis, a full petrographic and photographic study was made of the inclusion-bearing areas of interest. The preparation of a photographic map greatly facilitated relocation of areas and inclusions of interest.

A Linkam T.H.600 combined heating and freezing stage was employed for the purpose of this study, mounted on a metallurgical microscope. Necessary modifications of the microscope included the

fitting of an X-Y stage, long working-distance sub-stage condenser lens, and long working-distance 20x and 40x objective lenses.

All heating and freezing runs were made with the Linkam stage purged by a gentle flow of dry nitrogen gas, the rate of the gas flow being dependent on the required temperature in the case of the freezing runs. Separate nitrogen gas lines were employed for the freezing and heating gas flows. The freezing line was obtained by passing the gas line (in the form of a copper coil) through a Dewar of liquid nitrogen. The stage and gas-line layout is illustrated in figure 3.1. Before the stage was used to generate homogenisation and freezing data, it was necessary to calibrate the stage for horizontal and vertical temperature gradients, and check the platinum resistance thermometer for accuracy over the temperature range of interest (Shepherd et al.,1985).

3.5.1 Stage Calibration.

The stage accuracy was checked using a reference set of compounds (herein called standards) of high purity and known melting point. A list of the standards used is given in table 3.1. Slightly different procedures were adopted for standards that melted above and below room temperature.

For compounds that melted above room temperature, a few grains of the compound were placed between a pair of thin glass cover slips and the Linkam stage then purged of air with a gentle flow of nitrogen gas. The temperature of the stage was raised to ten degrees below the specified melting point of the compound and held at this

temperature for a period of at least fifteen minutes to allow a state of thermal equilibrium to be attained. A heating rate of 10 degrees per minute was used for this stage of the operation. The stage was then raised at a rate of 1 degree per minute until first melting of the standard was observed. The temperature of the stage was then held constant at this point to compensate for the latent heat of melting of the standard. The temperature was then increased by intervals of 0.1 degree per minute until final melting occurred. The temperature recorded was that of final melting. This procedure was repeated 3 or 4 times.

For compounds that are volatile at room temperature, a small amount of the liquid standard was sealed in a 1 centimetre length of thin-walled, narrow bore, silica glass capillary tubing which was sealed at either end with a plug of cold wax. As for the non-volatile standards, a slow heating rate was used. The sample was frozen to about 40 degrees C. below the specified compounds' freezing point to allow for supercooling effects. The same heating procedure as that for the non-volatile compounds was adopted.

During the above calibration runs any discrepancy between the true (i.e. specified) and the actual (i.e. observed) values for melting point temperatures never exceeded more than a couple of degrees, and this only for the higher temperature runs (those greater than 150 degrees). A graph was constructed of true values against actual values to provide a calibration curve for the correction of experimental data.

Vertical and horizontal thermal gradients across the stage were assessed. For the horizontal gradients, portions of the standard

were placed at different locations on the sapphire window (see figure 3.2) and the melting temperatures recorded. On following the heating and freezing procedures outlined above, no horizontal thermal gradient was discernible. The presence of any vertical gradients, ie. variations of temperature with inclusion height relative to the base of the stage, was checked for by placing grains of the standard on a stack of glass cover slips of known thickness, and then determining the melting point of the standard.

This procedure was repeated for sample heights that varied from 0.03 millimetres to 0.2 millimetres. The standard or reference height was taken as 0.1 millimetres. By heating the stage gradually, punctuated with periods of constant temperature, it was possible to minimise vertical thermal gradients across the sample and stage. For the duration of the study, provided care and time were taken during analysis, it was found to be unnecessary to correct for horizontal and vertical thermal gradients across the Linkham stage.

3.5.2 Data Collection.

As for the stage calibration heating and freezing runs, sample runs were undertaken with slow, controlled heating and cooling rates. During the heating and freezing runs the stage was periodically held at a constant temperature to allow a state of thermal equilibrium to develop across the stage.

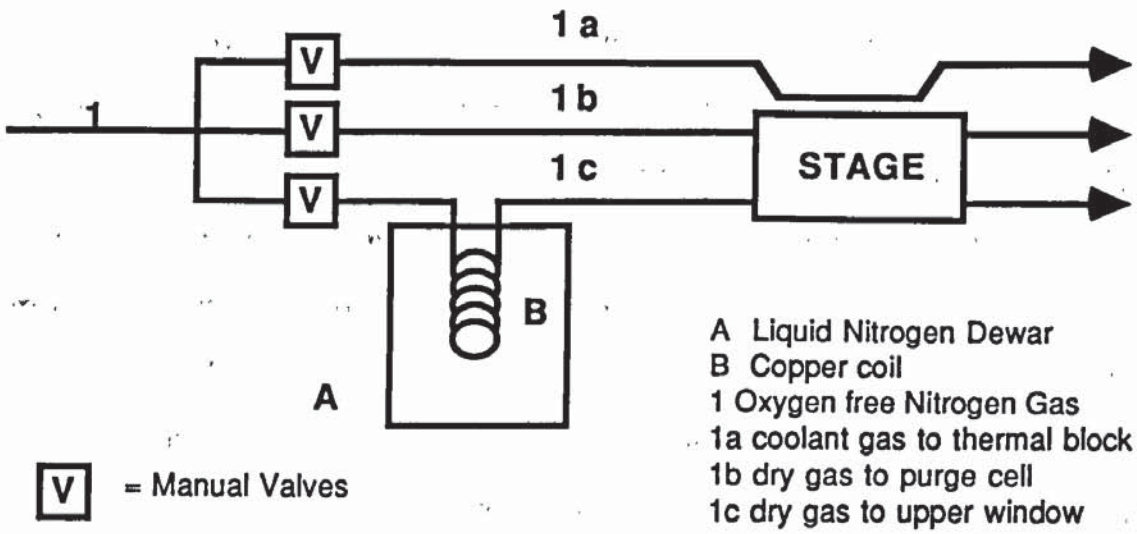

FIGURE 3.1

Stage and gas line layout for the Linkam TH 600 thermometric microscope stage (adapted from Shepherd et al., 1985).

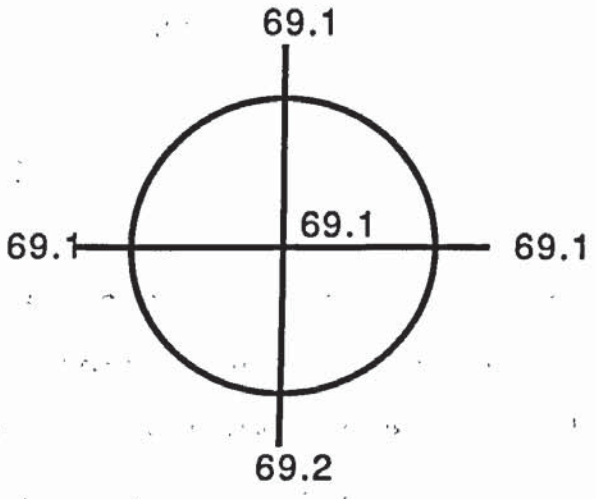

FIGURE 3.2.

Typical thermal gradient developed across the sapphire window for a registered (i.e. uncorrected) temperature of 69.1 deg. C., for phenyl benzoate.

In addition to producing accurate data, a slow heating rate prevents the possibility of severe overheating of the inclusions. This phenomenon may produce reproducible but erroneous data due to stretching of the inclusion walls (Roedder, 1984). The possibility of inclusion stretching is more of a problem for sphalerite than for, for example, quartz. Freezing runs may also be a possible cause of inclusion stretching. Ice has a much lower density than water, hence water-rich inclusions, i.e. those low temperature inclusions with only a very small vapour bubble, may yield erroneous homogenisation data. Homogenisation data should be collected prior to salinity data if it is suspected the inclusions are liable to stretch. The bulk of the inclusions subject to analysis do not fall into this class of inclusion. It should be noted, however, that all inclusion data for a sample must be obtained prior to any cathodo-luminescence studies of the sample because luminescence studies may cause stretching of many inclusion types (Barker and Halley, 1986).

3.5.3 Data correction.

The homogenisation and freezing temperatures obtained on the Linkham stage were corrected using the calibration curve derived in section 3.5.1. The experimental data were corrected using a modified curve-fitting correction program as outlined in appendix 1. The program, initially developed by staff at the B. P. Research Centre, Sunbury on Thames, was modified to run on a B.B.C. model B microcomputer.

3.6 X-Ray Diffraction Studies.

X-ray diffraction studies were undertaken on a variety of samples to enable polytype identification (for the North Pennine zinc sulfides) and the identification of unknown minerals; principally carbonates, sulfates, and hydroxides. Both a Debye-Scherrer Camera and a scanning goniometer were employed during the study. A cobalt K-alpha source was used, operating at 30 kilovolts with a beam current of 30 milliamps and an Fe filter. Both techniques are more fully outlined in McKie and McKie (1974) and Zussman (1977).

3.6.1 Debye-Scherrer Technique.

The Debye-Scherrer camera was used for identifying unknown phases. A Philips camera of 57.3 millimetres radius was used. Samples of interest were obtained by digging grains out of a polished section or block with a steel needle. Ground between two glass slides, the powdered mineral sample was carefully introduced into a short length of capillary tubing.

The capillary tubing used was made of a boro-silicate glass with a low X-ray absorption coefficient. Sealed at one end and drawn out to an internal diameter of less than 0.25 millimetres, the tubing was centred in the camera prior to darkroom loading of the X-ray sensitive film. Run times varied between 2.5 and 4.5 hours.

When using the Debye-Scherrer technique, traces of powdered silica were occasionally mixed with the ground sample to provide an internal calibration standard. The diffraction lines due to silica

enabled checks to be carried out for film shrinkage. Processing of the X-ray film can give rise to shrinkage of up to 5 percent. Shrinkage was kept to a minimum, however, by allowing the film to dry overnight at room temperature, and away from any direct heat source. For the films processed, the worst case of shrinkage was 1.5 millimetres in 200 millimetres. Shrinkage was typically less than 0.5 millimetres in 200 millimetres.

3.6.2 Powder-Goniometric Technique.

The goniometric technique was employed chiefly for polytype detection. Samples were first ground under acetone using an agate mortar and pestle, and the resultant sulfide slurry was then floated on to a 28 by 48 millimetre glass slide and allowed to dry. A slow scanning speed of 1 degree 2Ø per minute was employed for the detector.

3.7 Transmission Electron Microscopy.

Transmission electron microscopy (TEM) permits a high magnification investigation of material previously examined with the petrographic microscope and yields information about the crystalline state of the material from electron diffraction patterns. A fuller account of the theoy of transmission electron microscopy is outlined in Champness (1977), and Hirsch et al. (1965).

3.7.1 Specimen Preparation.

In sample preparation, the technique of ion sputtering or ion-beam thinning was utilised. Pioneered by Barber (1970) and Heuer et al. (1971) it involves the use of a beam of high energy argon ions to bombard the specimen until a region thin enough to transmit electrons is obtained. For ion-thinning, demountable doubly-polished thin sections (30 microns thick) were used. Lakeside 30C adhesive was used for section mounting.

A complete petrographic and photographic record was made of the areas of interest prior to ion-thinning. A thin copper disc, 3 millimetres in diameter, was glued on to the section with an insoluble adhesive (usually araldite). The copper disc contains a 2 by 1 millimetre aperture that is sited over the area of interest. One thin section would typically be used to prepare several discs of material.

The margin of the disc was carefully scored with a razor blade to aid solvent-demounting of the disc. The solvent used for Lakeside 30C was a mixture of one part acetone with one part ethanol. The demounted discs then had a second disc glued to the other side. The second disc comprised a fine titanium or nickel support mesh to help to prevent sample disintegration during, and after, the ion-thinning stage. An Ion Tech thinning machine was used with a 30 degree angle of incidence.

3.7.2 Damage to Sample during Specimen Preparation.

Damage may occur during wafer production and ion beam

thinning. Three main areas of damage are recognised:

1. Mechanical damage during wafer production.
2. Thermal and mechanical damage during ion-thinning.
3. Contamination of the sample during ion-thinning.

The cutting and polishing stages in specimen preparation may cause twinning and fracturing of the sphalerite. Stress and pressure-induced microstructures have been reported for sphalerite (Clark and Kelly, 1973). For the sphalerite samples studied, deformation-induced microstructures, twinning in particular, are widely developed. This made the identification and documentation of specimen preparation-induced damage difficult. However, studies undertaken on an undeformed vug-filling sphalerite from the Appalachians revealed a largely twin- and slip- free microstructure when examined with the TEM (see chapter 4 for discussion). It was apparent that careful polishing and the use of a slow speed saw for sample cutting kept mechanical damage to a low level.

3.7.3 Thermal and Mechanical Damage due to Ion-Thinning.

During the ion-thinning processes an ion-damaged layer is produced due to the argon ions impinging on the foil surface (Barber 1972). This damaged layer, several Ångstrom units thick, is amorphous and does not affect either image contrast or electron diffraction. The layer is visible as an amorphous margin to the foil.

The use of a 3 to 5 kilovolt accelerating potential for the

ion-beam may cause a significant rise in temperature of the specimen. A reduction in the operating voltage is not possible as the argon ions would then have insufficient kinetic energy to cause specimen sputtering. Temperatures of several hundred degrees centigrade have been reported (McConnell, 1977). Thermally-induced microstructures have been reported for zinc sulfide (e.g. Akizuki, 1970), but for temperatures several hundreds of degrees higher than those attained during the sputtering process. Temperatures reached during ion-beam thinning of the zinc-sulfide samples is probably much less than that reported by McConnell (1977) as a water cooled stage was employed in the ion-beam thinning machine, and the high thermal conductivity of zinc sulfide aids heat dissipation.

Checks for thermally-induced damage, polytype formation in particular, were undertaken using a suspension of finely powdered zinc sulfide rather than ion-beam thinned wafers. A suspension of finely powdered material was floated on to a carbon film supported by a titanium grid. Some of the smaller grains were found to be suitable for imaging. The non-ion-thinned, crushed material appeared similar to the ion-thinned material except for the presence of mechanically-induced defects (e.g. fracturing). No thermally-induced damage would appear to have developed in the ion-thinned material.

Ion-beam thinning, in addition to sputtering a hole in the specimen, may cause some etching of the specimen in a manner similar to that of chemical etchants. This process has proved useful during electron optical examination of banded material and material dominated by slip- and twin-plane development.

3.7.4 Contamination during Ion Thinning.

Specimen contamination was detected during analytical electron microscopy, undertaken at the Department of Metallurgy and Materials, University of Birmingham. Argon and tantalum peaks were observed in spectral profiles of copper-bearing sphalerites (figure 3.3). Neither element was detected in electron microprobe studies of the same material. The argon may be assumed to have been implanted during ion-beam thinning of the material. Tantalum contamination may arise due to sputtering of the tantalum specimen holder during ion-beam thinning and its subsequent deposition on the sample. Accompanying such contamination was the development of dendritic overgrowths at the foil margin (plate 3.1).

3.7.5 Specimen Observation and Associated Beam Damage.

Samples were examined using a JEOL JM100B transmission electron microscope with an accelerating potential of 100 kilovolts. A double tilt goniometric sample holder was employed for the study to enable selected crystallographic orientations to be identified from diffraction information. Prior to microscopy, it is necessary to carbon-coat the thinned samples to prevent their charging in the electron beam (Kay, 1965).

Beam damage, either as loss of crystallinity or ion damage (defect introduction), has been reported in studies of many silicate minerals (White, 1985). Similar damage to sulfides has not been widely reported, probably due to their simpler structure and

delocalised bonding (Ashworth, pers. comm.). However examination of some sphalerite samples, after a period of prolonged exposure in the electron beam, sees the development of damage, initially seen as spotting of the sphalerite. By focusing the beam on the affected area and increasing the rate of damage, observation of the diffracton pattern suggests a loss in crystallinity. The spots were observed to broaden, decrease in intensity, and take on a more diffuse appearance.

Accompanying this form of damage was the occasional 'burning up' of secondary phases. Small areas were seen to vaporise under the electron beam, leaving behind clusters of negative crystal voids ranging in size from 2 to 0.2 micrometres. The voids are taken as representative of less stable, possibly fluid, inclusions in the sphalerite (see section 6.7 for a fuller discussion).

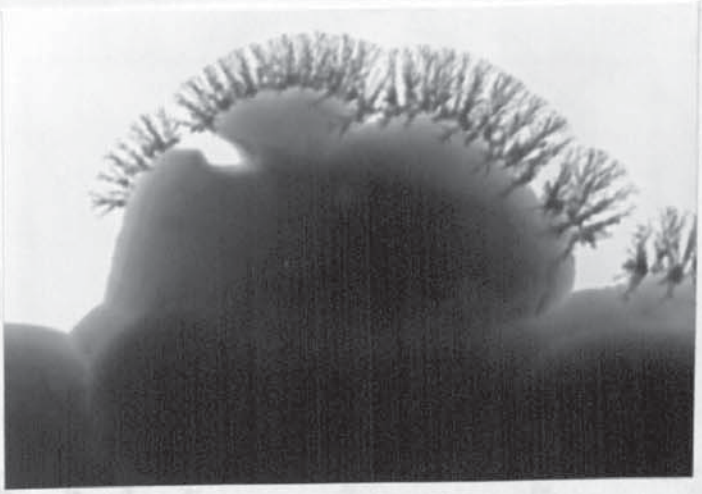

PLATE 3.1

Photomicrograph of dendritic growths produced during ion-beam thinning of sphalerite. Field of view ~ 7.2 microns.

3.7.6 Analytical Transmission Electron Microscopy.

Analytical transmission electron microscopy (ATEM) on the samples was undertaken at the Department of Metallurgy and Materials, University of Birmingham. A Philips E.M. 400 microscope was used, at an operating potential of 100 kilovolts. The microscope is fitted with an energy dispersive detector to enable semiquantitative analysis to be performed. To reduce background radiation a beryllium specimen holder was used.

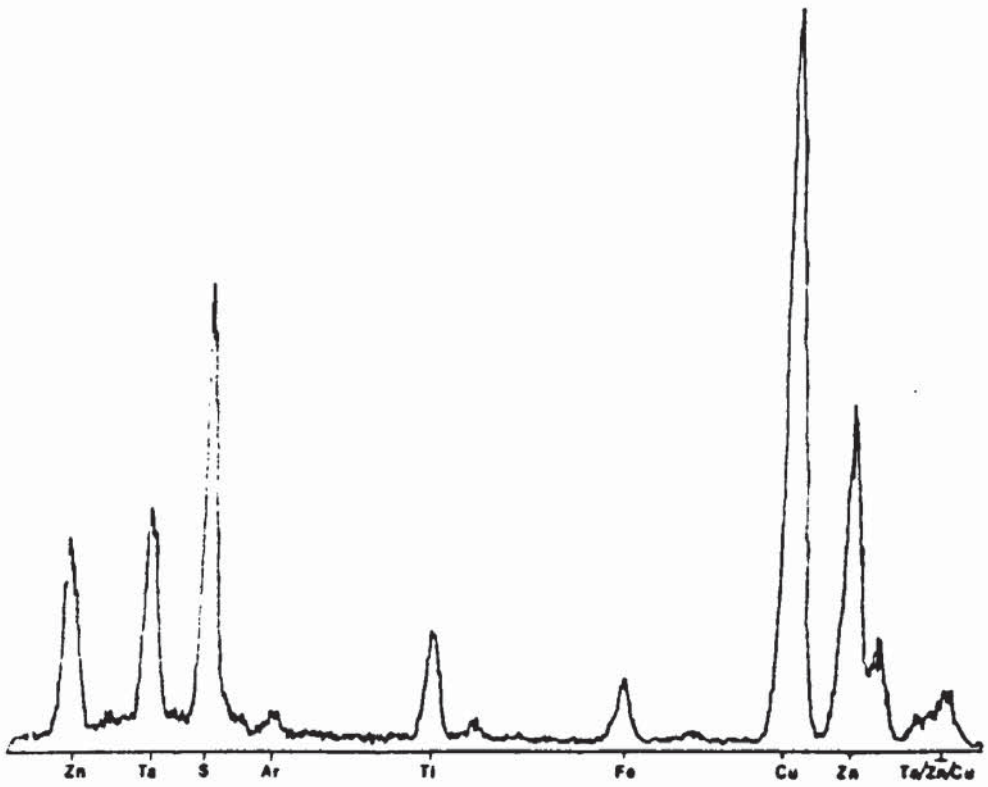

FIGURE 3.3

Spectral profile of a cuprian region of *type-one* sphalerite contaminated during ion-beam thinning. Tantalum (Ta) is derived from the specimen holder, titanium (Ti) is from the sample support grid and argon (Ar) is due to implantation of the ion-beam. Philips EM 400 A.T.E.M. operating at 100 kV with a 100 second count time.

The microscope was principally used for analysis of altered regions of sphalerite, cuprian regions in particular. To prevent any possibile grid-related copper contamination of the samples occuring during ion beam thinning, nickel and titanium grids were used. One hundred second count times and a beam width of less than 100 nanometres were employed throughout the study. Semiquantitative analyses of altered regions, composed of particles set in a sphalerite matrix, were obtained by following the procedures outlined by Lorimer and Cliff (1984). A fuller treatment of both the theory and practice of analytical electron microscopy is provided by Williams (1984).

CHAPTER 4: Anisotropic Sphalerite from the East Tennessee Zinc District.

4.1 Introduction.

The samples used for the present study were those used in the textural studies of Craig and co-workers (Craig, Solberg and Vaughan, 1983a and 1983b; Craig and Vaughan, 1986). Textural studies were undertaken to document optical anisotropy in the sphalerite and a preliminary electron optical study was undertaken to assess the suitability of the material for T. E. M. examination. This material had also been used in the petrographic, analytical, and fluid inclusion studies of Craig and co-workers (1983a, 1983b, and 1986). The material consists of samples taken from breccia-infilling mineralisation from a variety of mine localities in the Mascot-Jefferson City district, East Tennessee.

4.2 The Appalachian Orefield.

Three main ore-associations are recognised for the Central Appalachian Province. They are;

1. The Great Gossan Lead District (metamorphosed Pb-Zn ores).
2. The 'Mineral' District (Massive and disseminated pyrite and metalliferous ores.
3. Disseminated Pb-Zn carbonate hosted ores.

Samples used for study are from the third class of ore deposit. The disseminated lead-zinc ores are hosted in the carbonates of the Valley and Ridge Province. Ranging from Pennsylvania to Tennessee, the principal deposits are hosted in East and Central Tennessee, Virginia, and Pennsylvania (figure 4.1). Zinc-lead mineralisation takes the form of M.V.T. ore-bodies set in shallow marine carbonate strata of Cambro-Ordovician age. The host carbonate strata underwent a phase of westwards thrusting during the Appalachian Orogeny (mid to late Palaeozoic Era).

Appalachian zinc deposits comprise an ore and gangue mineralogy which may be considered typical of carbonate-hosted M. V. T. deposits world-wide. Sphalerite comprises the dominant ore mineral. Pyrite varies in quantity throughout the ores; galena is a minor ore component, and only a trace of chalcopyrite typically is present. The gangue mineralogy comprises dolomite with subordinate calcite. Minor fluorite, quartz and barite are locally present. Fluid inclusion analyses indicate highly saline mineralising fluids with a moderately low temperature (90° to 160° C.).

The degree of post-ore deformation and recrystallisation varies. The Friedensville, Austinville, and East Tennessee ores all locally exhibit deformation textures. Ore-brecciation, offset growth-banding, and curved deformation twin lamellae developed in gangue calcite and dolomite are observed. Some ores, e.g. the Elmwood-Gordonsville ores of Central Tennessee, show textural evidence of minor recrystallisation.

4.3 Mineralisation in the Mascot-Jefferson City District.

Zinc mineralisation in the Mascot-Jefferson City district orebodies is hosted in lower Ordovician carbonate strata; the Knox Group. The principal mines of the Mascot-Jefferson City District are located in figure 4.2. The Ordovician Knox Group comprises, in part, a thick sequence of epicontinental basin sediments which accumulated as a series of basin infill deposits sandwiched between the N. American Craton and the Appalachian Orogenic Belt (Shanmugam and Lash, 1982).

In East Tennessee, the Upper Knox Group is divided into the Kingsport and Mascot formations. Sediments comprise marine peritidal carbonates. Stratigraphic nomenclature for the Ordovician strata of East Tennessee is given in figure 4.3. The Kingsport formation is conformably overlain by the Mascot formation. However, both of these formations are overlain by a major extensive erosional unconformity with erosion being attributed to a phase of platform uplift (Shanmugam and Lash, 1982).

Both the Mascot and Kingsport carbonates host solution breccias. The lower 25 metres of the Mascot formation and approximately 35 metres of the Kingsport formation contain breccias of a probable Mid-Ordovician age. The nature, origin and age of these solution breccias is discussed fully in Hill and Weddow (1971). Five ore horizons are recognised by mine geologists (the U, T, S, R, and Mascot of figure 4.3).

Sphalerite mineralisation is episodic and accompanied by a white sparry dolomite gangue. Mineralisation is developed as a series

of coatings on and around breccia fragments. Minor mineralisation is additionally developed along bedding planes and tensional fractures. Mineralisation is concentrated in areas of carbonate that are subject to solution collapse (Fulweiler and McDougal, 1971).

FIGURE 4.1

Location map of the Mascot-Jefferson City district relative to other carbonate-hosted zinc-lead districts in the S. E. United States. Districts represented by solid black occur in the Lower Ordovician upper Knox Group. Figure adapted from figure 1 of Kyle (1976).

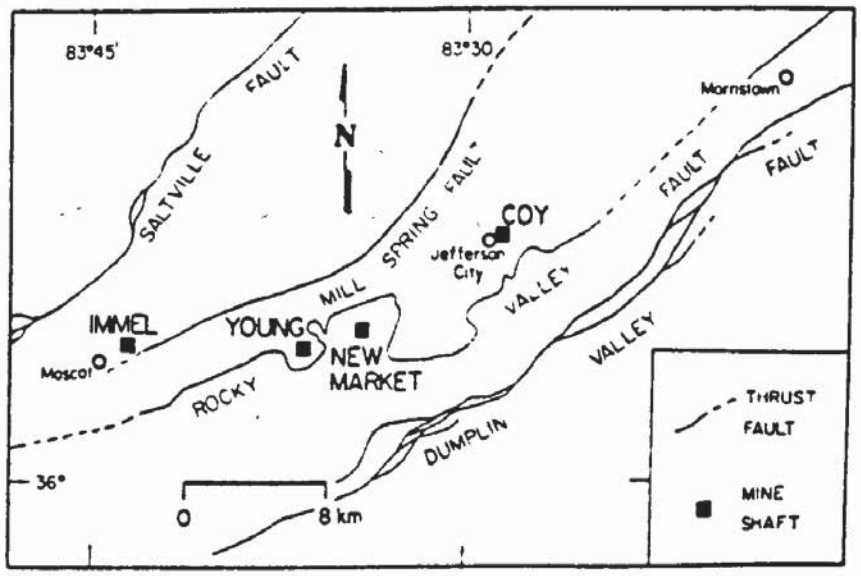

FIGURE 4.2

Principal mines of the Mascot-Jefferson City Zinc District (adapted from figure 1 of Taylor et al., 1983a).

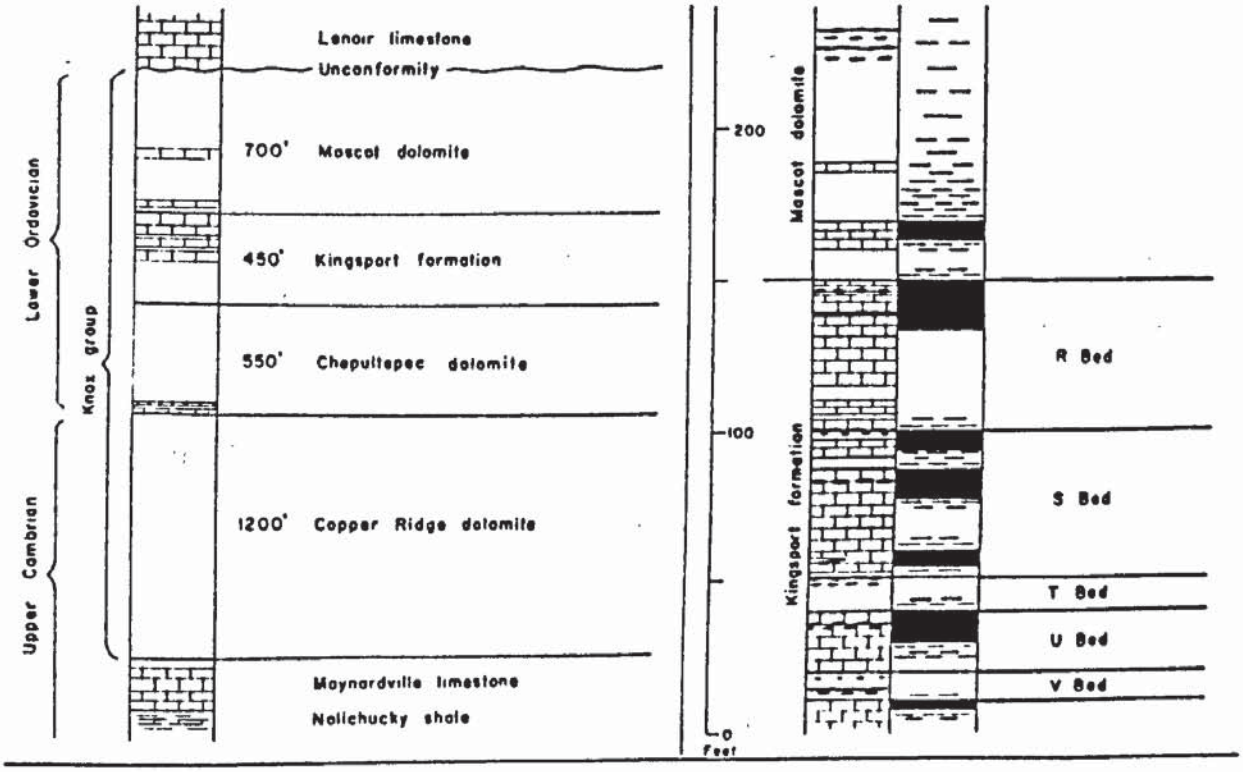

FIGURE 4.3

Generalised stratigraphic sequence and principal ore zones for the Mascot-Jefferson City District Cambro-Ordovician strata (after Crawford et al., 1969).

4.4 Sphalerite Mineralisation.

Several stages of sphalerite mineralisation are recognised on the basis of textural differences: degree of deformation and opacity, abundance and type of solid inclusions, and colour of the sphalerite crystal or layer (Taylor et al., 1983a). Four principal stages of mineralisation are recognised, stages 2, 3 and possibly 4 of which were sampled. The four stages are:

Early Stage Sphalerite.

Cloudy and translucent with abundant solid and fluid inclusions. Twins are deformational and numerous. Solid inclusions include pyrite and organic phases, along with minor dolomite and quartz. Mechanical deformation of the ore is common and may be intense locally.

Intermediate Stage Sphalerite.

Translucent with a range of organic and pyrite inclusons. Etch studies reveal growth twins with subordinate and patchy deformation twins.

Late Stage Sphalerite.

Thin curved {111} polysynthetic deformation twins developed. Solid inclusions are principally dolomite euhedra. Pyrite and organic material is scarce. Sphalerite tends to occur as honey yellow rims on, or interstitial to, earlier stage 1 and 2 sphalerite aggregates.

Vug-Filling Sphalerite.

This represents the final stage of mineralisation. Sphalerite tends to

occur as rosettes nucleated on breccia fragments or sparry dolomite. It may occur as euhedral terminations perched on earlier sphalerite, sparry dolomite or breccia fragments. Thick growth twins are seen.

No evidence is seen for the relative timing of deposition of type 4 relative to the other three. It has been proposed that stages 2 to 3 occur towards the end of the Appalachian orogeny (Alleghenian episode); i.e. of late Carboniferous to early Permian age. Stage 4 probably post-dates the Appalachian orogeny (Hatcher and Odom, 1980).

The temperature of ore deposition fluctuated from approximately 90° to 200° C., with a saline mineralising fluid containing calcium and possibly magnesium chlorides in addition to sodium chloride (Roedder, 1971). Statistical analysis of fluid inclusion data implies more than one mineralising fluid. A high temperature (160° C.), low salinity fluid along with a low temperature (110° C.), high salinity fluid has been recognised (Taylor et al., 1983b). A fluid mixing model for ore body development has been proposed for other East and Central Tennessee zinc deposits on the basis of inclusion and isotopic measurements (Foley et al., 1981; Grant and Bliss, 1983).

4.5 Previous Textural Studies.

The textural studies of Craig, Solberg, and Vaughan (1983a and b) and Craig and Vaughan (1986), recognise a variety of growth-banded textures in the sphalerite. The varieties of banding

recognised are due to variations in crystal colour and inclusion content. Three principal varieties are recognised:

Sharply Bound Banding.

Both fine and coarsely banded varieties are recognised. This texture comprises thin, sharply defined, alternate light and dark laminar bands. Fine banding ranges from 1 millimetre to less than 5 microns in thickness; coarse banding ranges from 5 millimetres to 1 millimetre in thickness. Growth developed from a series of nuclei (nodes) on the host fragments and progressed as a series of concentric bands. Carbonaceous horizons are commonly developed within the material. Examples include deposits from Austinville, Virginia and Friedensville, Pennsylvania.

Diffuse Banding.

Banding is relatively broad (greater than 5 millimetres, and due to variations in the inclusion content of the grain. Bands do not have well-defined margins and contain numerous irregular and lath-like carbonaceous inclusions. Such ores are common throughout the Mascot-Jefferson City district (intermediate and late stages of mineralisation of Taylor et al., 1983a).

Single Crystal Banding.

Growth banding is due to fluctuations in the body colour of the mineral grain. Colour varies from pale-yellow to red-brown. Such sphalerite is best developed in the ores of Timberville, Virginia.

E.P.M.A. analysis of the East Tennessee ores indicate a low iron and high cadmium content for the sphalerite (table 4.1). Other metals are virtually absent. Banding is not reflected by the mineral chemistry except in the dark organic-rich horizons which are observed to be cadmium-enriched. A negative correlation between iron and cadmium levels is apparent.

Craig et al. (1983a and b, 1986) briefly note the sphalerite as being optically anisotropic with lamellar, blotchy, and cross-hatch or microcline-like varieties present (lamelliform, undulose, and grid-iron of this thesis nomenclature). Anisotropy is described in more detail in section 4.6.

Deposit	Iron Range	Cadmium Range	Iron Ave.	Cadmium Ave.
Friedensville	0.11-0.51	0.04-0.49	0.36	0.09
Friedensville	0.08-0.73	0.03-0.75	0.39	0.16
Timberville	1.25-4.40	0.04-1.10	2.70	0.45
Austinville	0.38-1.46	0.01-0.28	1.00	0.13
Austinville	0.24-3.05	0.03-0.64	0.70	0.25
Jefferson-City	0.06-0.41	0.17-0.64	0.22	0.35
Jefferson-City	0.03-0.45	0.10-0.60	0.20	0.30
Jefferson-City	0.08-0.34	0.16-0.54	0.15	0.36
U. S. Steel-Zinc	0.03-0.48	0.13-0.56	0.25	0.34
New Market	0.03-0.34	0.14-0.79	0.12	0.36
Young	0.04-0.37	0.21-0.64	0.19	0.37
Young	0.04-0.31	0.21-0.54	0.14	0.37
Immel	0.05-0.41	0.23-0.73	0.17	0.53
Idol	0.03-1.57	0.00-0.99	0.37	0.32
Idol	0.06-1.60	0.00-2.84	0.70	0.70

TABLE 4.1

Electron microprobe analyses of representative sphalerites from The East Tennessee Zinc District Ore Deposits (from Craig, Solberg, and Vaughan, 1983a). Analysis in wt. %.

4.6 Deformation Petrography and Anisotropy.

Approximately 90 % of the Mascot-Jefferson City district material examined is extensively deformed. Samples are of the 2 and 3 stages (intermediate and late) of Taylor et al (1983a). The remaining 10 % of the sphalerite sampled is relatively undeformed and differs both in texture and colour from the bulk of the mineralisation. Coarsely crystalline and transparent (sample 1433; Immel Mine), this phase probably represents the vug-filling episode of mineralisation of Taylor et al (1983a). For the bulk of the mineralisation no difference between the different mine samples is apparent.

4.6.1 Intermediate and Late Stage Sphalerite.

Material was sampled from the Coy (sample no.1441), Immel, (1446-7) and U. S. Steel (1412) zinc mines. Sphalerite is developed as a series of concentrically banded rosettes and bands. Set in a white sparry dolomite gangue, rosettes tend to occur as coatings perched on silicified carbonate breccia fragments. Pyrite-rich and organic-rich horizons are locally developed. These horizons are concentric with sphalerite banding. Rosettes vary from approximately 0.5 to 1.5 millimetres in diameter. Banded sphalerite typically occurs in units up to 10 millimetres thick. Figure 4.4 illustrates breccia fragments coated with rosettes and banded sphalerite. Fracturing of both the gangue and the sphalerite mineralisation is common.

Viewed in doubly-polished thin section, sphalerite varies from

translucent to opaque. Colourless in thin-section, the sphalerite has banding which is principally due to variations in inclusion content. Bands tend to be diffuse with a band-width of between 1 and 5 millimetres.

Inclusions are lath-like opaque hydrocarbons. Sub-micron to micron wide, they vary in length up to a few hundred microns (plate 4.1). Inclusions are often associated with purple hydrocarbon-stained patches up to 75 microns across. Such inclusions are the organic inclusions described and analysed by Craig, Solberg and Vaughan (1983a). Rod direction corresponds to the principal growth directions of the sphalerite (namely {111} and {111}). Aqueous inclusions, liquid or two-phase, are scarce and only observed in relatively undeformed sphalerite.

Pyrite inclusions enclosed within a sphalerite matrix are subhedral to anhedral and usually heavily fractured. Grain size varies from less than 20 microns to greater than 150 microns.

Etching of the sphalerite confirms the material as being extensively deformed. Both growth and deformation twinning are revealed. Growth-twins comprise simple broad twin lamellae (plate 4.4). Lamella width varies and is typically greater than 40 microns. In transmitted light primary growth-twins are recognised on the basis of reflection effects observed across the composition plane (plate 4.5; twin A). Deformation of growth-twinning is common with curvature of the twins seen (plate 4.4).

Deformation-twins are distinguished from growth-twins by their complex twin morphology. Thin, typically less than 40 microns in width, deformation twins often divide or coalesce along their

length. Such twins are locally abundant, with wedging of twin lamellae common (plate 4.3; 'A' group of twins). Twin plane development is often seen to be coincident with the direction of the rod-like hydrocarbons; namely {111} (see plates 4.1 and 4.2). Fracturing of the material is common and may affect twin morphology. Curvature of twins towards fractures is often developed (plate 4.3; twin group B).

Anisotropy is observed throughout the mineralisation. Both undulose, or patchy, anisotropy and lamelliform anisotropy are seen. Anisotropy may be correlated with degree of deformation. In areas hosting numerous deformation twins, lamelliform anisotropy is observed (plate 4.2). Developed as sharp wedging lamellae, anisotropic regions vary in width from one micron to greater than 20 microns, and may extend for many tens of microns in length. For those lamellae greater than 20 microns wide, regions of undulose or diffuse anisotropy are seen within the lamellae. Such areas of diffuse anisotropy either represent a growth-related anisotropy (see Seal, Cooper, and Craig, 1985) or, more likely, reflect straining of the sphalerite lattice during deformation.

Etching of the sphalerite reveals subgrains developed within the deformed material. Subgrains range in size from 60 to 100 microns. Many such areas have a patchy rather than a lamelliform anisotropy. Anisotropy occasionally may take a cross-hatch form with mutually perpendicular, poorly developed, laths.

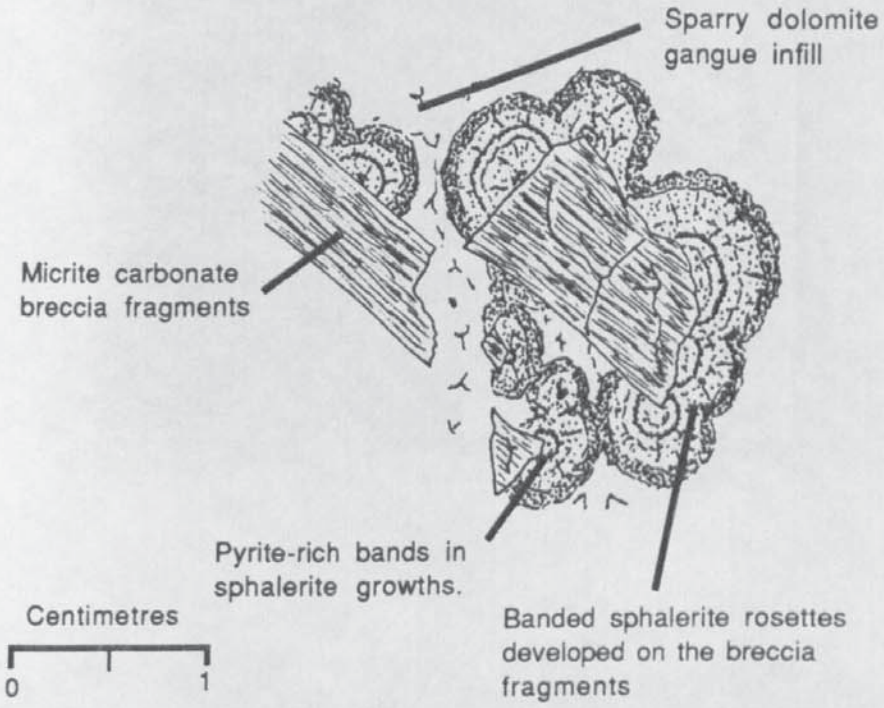

FIGURE 4.4

Diagram illustrating rosette and band morphology for sphalerite mineralisation developed as a coating on carbonate breccia fragments.

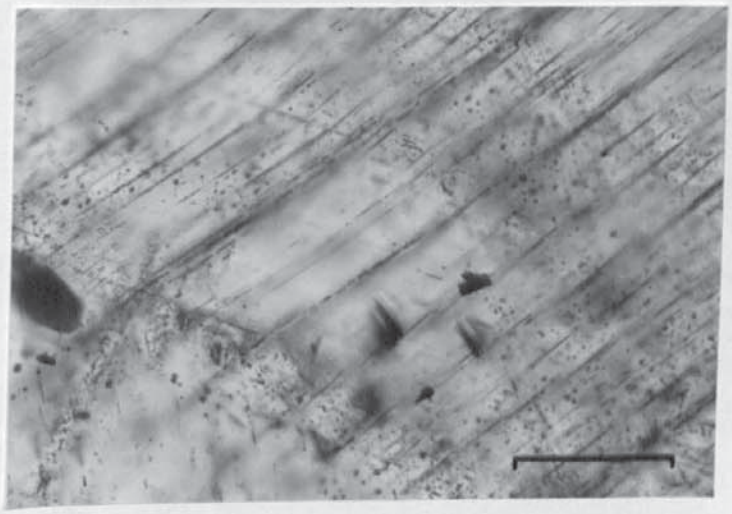

PLATE 4.1

Late to intermediate stage sphalerite, hosting numerous lath-like hydrocarbon inclusions. Bending of the inclusion-hosting planes due to deformation is apparent. Scale bar 60 microns. PPL transmitted light.

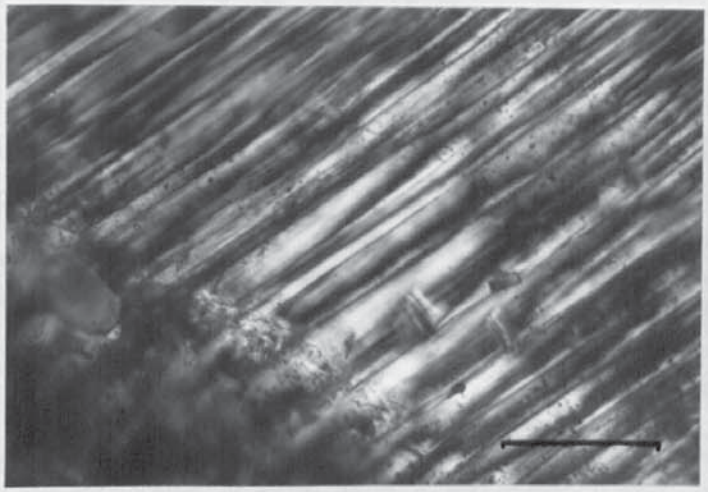

PLATE 4.2

Region of lamelliform anisotropy developed in intermediate to late stage sphalerite. Principal lamellae direction corresponds to direction of hydrocarbon laths and planar fabric of plate 4.1. XPL transmitted light photomicrograph of plate 4.1. Scale bar 60 microns.

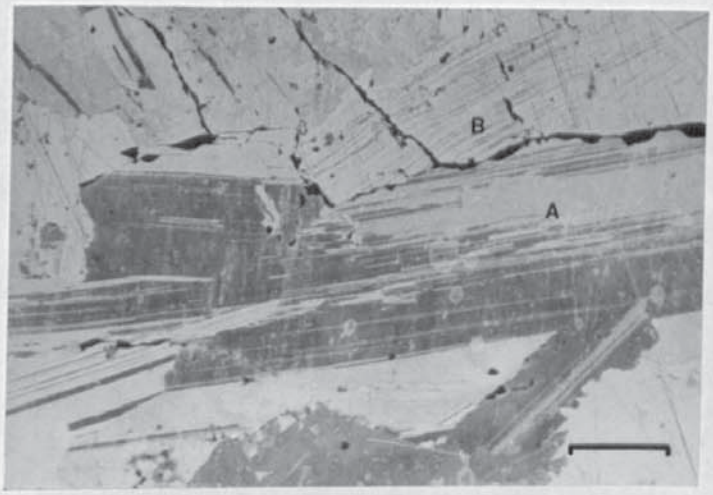

PLATE 4.3

HI etched intermediate to late stage sphalerite showing complex deformation twinning with numerous wedging-out lamellae. Fracturing of the sphalerite has deformed the twins in region B. PPL transmitted light. Scale bar 200 microns.

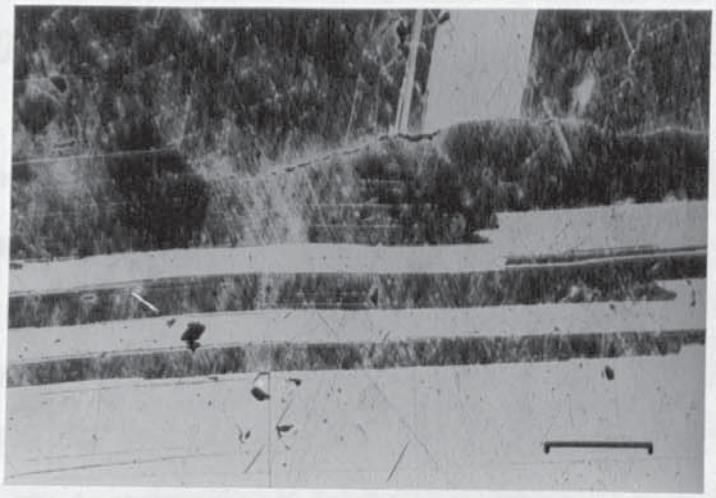

PLATE 4.4

HI etched intermediate to late stage sphalerite illustrating simple lameilliform growth twinning. Curvature of the twins indicates some post-twin deformation. PPL reflected light. Scale bar 200 microns.

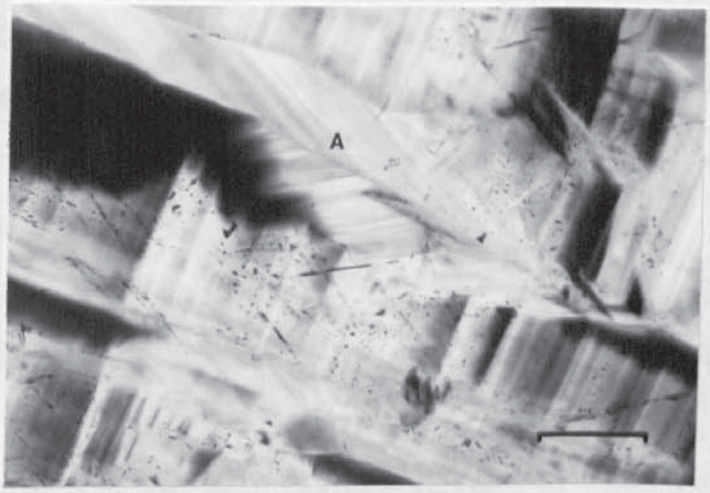

PLATE 4.5

Intermediate to late stage sphalerite with growth twinning developed. An apparent reflection of banding is seen with the twin composition plane (plane A) acting as a mirror plane. PPL transmitted light. Scale bar 200 microns.

4.6.2 Vug-Infilling Sphalerite.

Sample 1435 comprises a coarse-grained sphalerite with individual grains up to 1 centimetre across. The mineralisation differs both optically and texturally from the bulk of the East Tennessee mineralisation sampled. Orange to red-brown in thin section, the sphalerite is commonly fractured with some of the wider fractures (up to 1 millimetre) hosting a dolomitic infill.

Transparent to translucent in thin section (doubly-polished) the mineralisation hosts fewer organic inclusions than the intermediate to late stage samples, and virtually no pyrite. Aqueous liquid and two-phase inclusions are developed. Twin-related textures (reflection effects) are not observed in this sample. The low density of twinning is apparent from the optical anisotropy.

The majority of the sphalerite exhibits undulose or patchy anisotropy. Regions several hundreds of microns across are developed (plate 4.6). Where undulose regions intersect fractures they may be sharply bounded.

Patchy anisotropy often adopts a cross-hatch appearance. Poorly developed laths, mutually perpendicular, are developed. The laths tend to be diffuse with a typical size of 100 by 40 microns (plate 4.7). Laths are equally developed for the two directions.

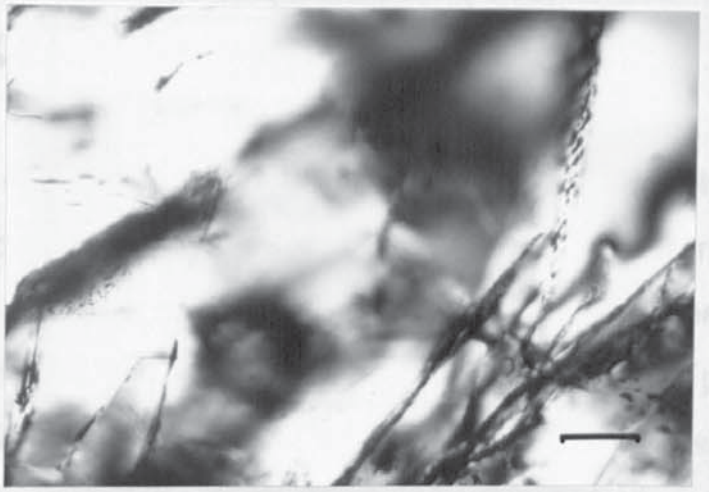

PLATE 4.6

Possible vug-stage sphalerite (sample 1435) illustrating region of undulose anisotropy. Some anisotropic regions are seen sharply bounded by fractures. XPL transmitted light. Scale bar 100 microns.

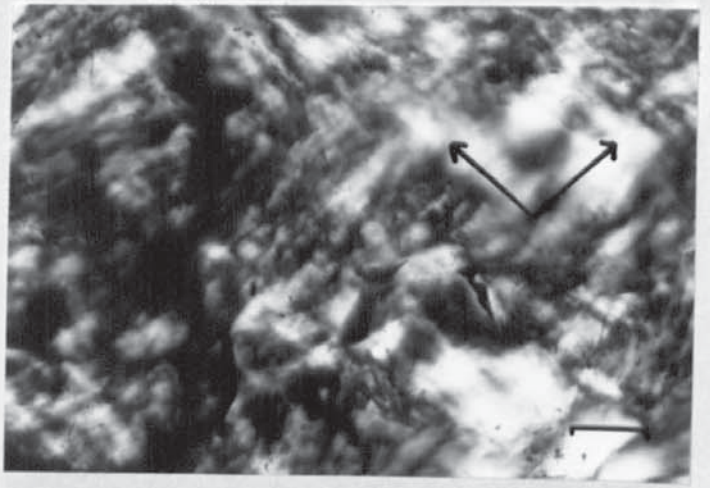

PLATE 4.7

Possible vug-stage sphalerite (sample 1435) illustrating region of patchy cross-hatch anisotropy. Two equally developed, poorly defined, lath directions are apparent (arrowed). XPL transmitted light. Scale bar 100 microns.

4.6.3 Electron Optical Observations.

Electron optical studies of deformed and relatively undeformed Appalachian sphalerite reveal a simple microstructure developed. Throughout the samples examined a planar fabric is seen (plates 4.8 and 4.9). The fabric comprises parallel to subparallel planes with a micron to submicron spacing. Planar density is seen to vary from 'low' in undeformed material to 'high' in deformed material typically showing lamelliform anisotropy. Typically for relatively undeformed material the planar density varies up to 2000 lamellae per millimetre. For the more deformed sphalerite planar density may exceed 4500 lamellae per millimetre. The planar fabric runs subparallel to optical lamellae boundaries where developed. Plates 4.8 and 4.9 illustrate regions of low (1000 lamellae per millimetre) and high (4700 lamellae per millimetre) planar density respectively.

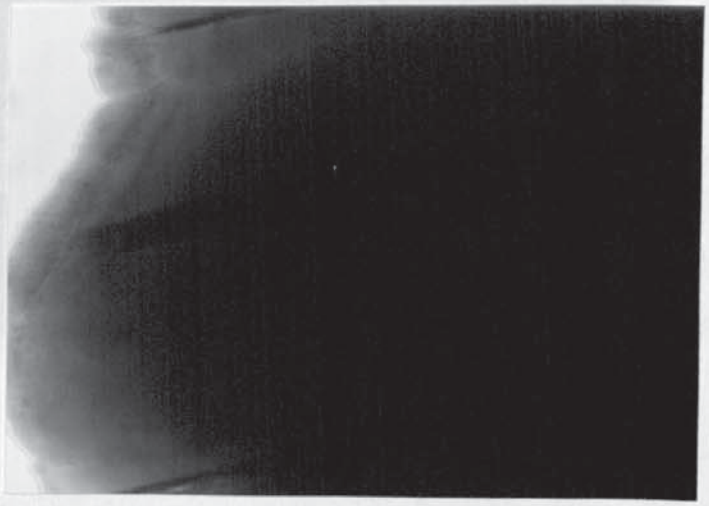

PLATE 4.8

Electron micrograph showing a region of Appalachian sphalerite with a relatively low planar density (approx. 1000 lamellae per millimetre). Field of view 2.5 microns.

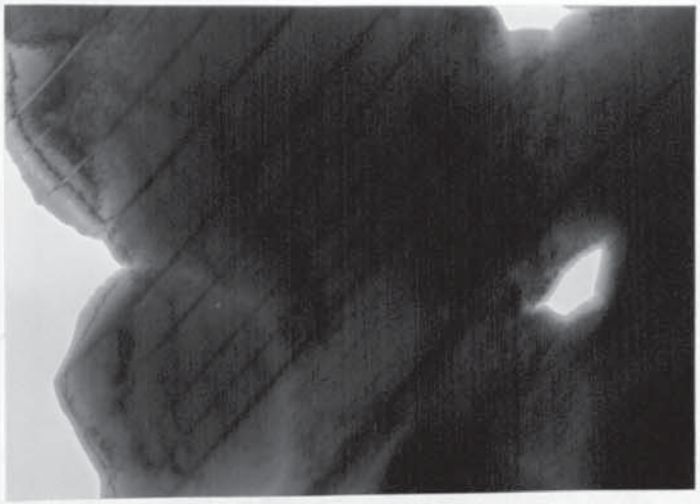

PLATE 4.9

Electron micrograph showing a region of Appalachian sphalerite with a relatvely high planar density (approx. 4700 lamellae per millimetre). Planes are seen to be subparallel. Sphalerite region is taken from a relatively deformed sample. Field of view 5.2 microns.

PLATE 4.10

Electron diffraction pattern taken from a region of sphalerite with a planar density greater than 4000 lamellae per millimetre. Twinning is apparent from the doubling of certain spots, and stacking faults apparent from the streaking of certain spots. The diffraction pattern is interpreted in figure 4.5. [$\bar{1}$11] Beam direction.

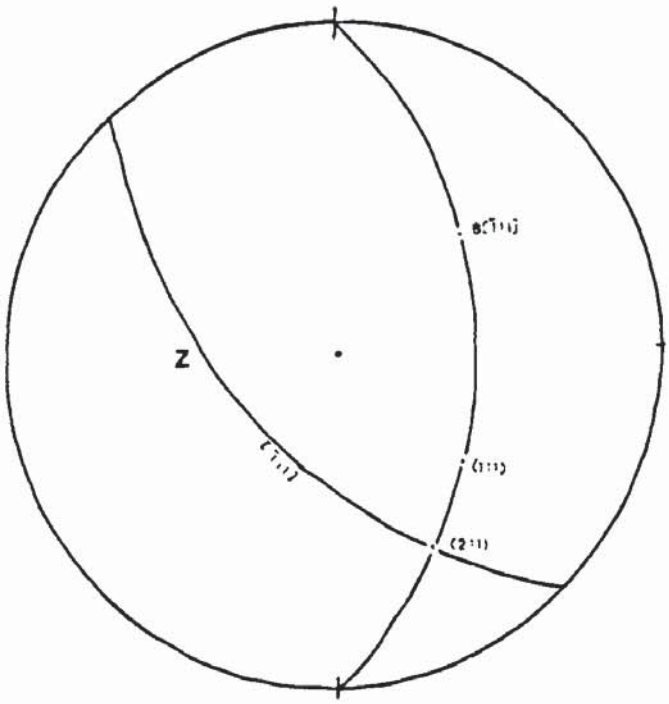

FIGURE 4.5

Streographic trace analysis of streak directions from plate 4.10. The stereogram indicates that a streak trace direction of {211} for a [$\bar{1}$11] projection is consistent with a {111} plane (stacking fault) responsible for streaking. Z represents the zonal plane [$\bar{1}$11], and B the diffraction vector [$\bar{1}$11].

Electron diffraction studies of areas containing the planar fabric imply a {111}-twin and {111}-stacking fault origin for the planes. Plate 4.10 and figure 4.5 illustrates a typical diffraction pattern.

Apart from variations in the planar density few other microstructural features are observed (in contrast to the Pennine material of chapters 6 to 9).

From the above observations two conclusions are drawn:

1. The planar microstructure is not a consequence of the specimen preparation methods (i.e. ion beam thinning). If the planar microstructure were to be related to preparation methods then a more uniform occurrence (i.e. less variation in planar density) would be expected.

2. The variation in planar density (less than 2000 planes per millimetre for relatively undeformed sphalerite, to greater than 5000 planes per millimetre for deformed sphalerite) is related to the degree of crystal deformation. Anisotropy arising from deformation is attributed to the planar features resolved in T.E.M.

4.6.4 Anisotropy: conclusions and discussion.

Lamelliform Anisotropy: This form of anisotropy is principally associated with deformationally-induced microstructures. Cleavage planes, twin-planes and slip-planes are all observed to correlate both in location and direction with the anisotropy. This anisotropy is not observed in undeformed material.

Undulose Anisotropy: Undulose anisotropy is observed in both deformed and undeformed sphalerite. Anisotropy may be associated with deformationally-induced and growth related microstructures. Growth-related microstructures (stacking faults; Seal, Cooper, and

Craig, 1985) are probably operative for the relatively undeformed 'vug stage' sphalerite (sample 1435: Immel). However, for the majority of the deformed sphalerite, narrow regions of undulose anisotropy, especially regions associated with lamelliform anisotropy, reflect straining of the lattice with strain insufficient to induce twin or slip-plane development.

Grid-Iron Anisotropy: Poorly developed and patchy, this anisotropy is problematical in origin. It is attributed to the development of stacking disorder during crystal growth in undeformed ores (cf. Central Tennessee Sphalerite of Seal, Cooper, and Craig., 1985), but in the heavily deformed ores of East Tennessee deformational overprinting of the sphalerite precludes a simple growth-related origin. The grid-iron anisotropy probably represents a relict growth-related anisotropy with a deformation microstructural overprint. Deformationally-induced microstructures may develop by modifying pre-existing stacking faults.

In assigning a textural origin to anisotropy in sphalerite, other textural and microstructural features must also be considered to assess the nature and degree of any post-ore deformational processess that may have been operative. For much of the East Tennessee sphalerite, the extent of post-ore deformation makes the identification of growth-related anisotropy at best speculative.

CHAPTER 5: GEOLOGY OF THE NORTH PENNINE OREFIELD.

5.1 GEOLOGICAL SETTING.

The North Pennine Orefield has traditionally been divided into two distinct regions, the Alston Block in the North and the Askrigg Block in the South. The northern limit of the Orefield extends from the Whin Sill escarpment, running north of the Tyne Valley, to the Craven Uplands of the Settle region.

Both blocks of the Orefield represent structural highs bounded on at least three sides by fold or fault systems. The region sampled for the purpose of this study is situated in the Alston Block. The Alston Block is bounded by the Stublick fault system to the north, the Pennine fault system to the west, and the Lunedale-Stainmore fault system to the south. The block is separated from its southerly neighbour, the Askrigg block, by a broad structural depression; the Stainmore Trough (see fig. 5.1).

Both blocks of the Orefield comprise a series of flat-lying Carboniferous strata lying on stable blocks of Lower Palaeozoic folded strata. Gravity surveys (Bott, 1967; Bott and Masson-Smith, 1957) of both blocks indicate the possible presence of granitic material beneath the orefields. Subsequent drilling of the strata in the Rookhope and Raydale boreholes (Bott and Masson-Smith, 1953) proved the presence of large Caledonian granite batholiths under both the Alston Block (Rookhope borehole) and the Askrigg block (Raydale borehole). These batholiths, known as the Weardale and Wensleydale

granites respectively, have been subject to much debate as regards their possible roles in the origins of the Pennine mineralization. To the east of the orefield the sediments dip under the Durham coalfield (Upper Carboniferous Coal Measures) and Permo-Triassic sediments of the North Sea Basins.

The Carboniferous strata of the Alston and Askrigg blocks comprise three major stratigraphic sequences, each characterised by a rhythmic sequence of limestones passing into calcareous shales which pass into non-marine shales, sandy shales, and finally into a series of sands, often capped by ganisters or coals (figure 5.2). The lithologies are best developed in the middle of the three sequences (the Middle Limestone Group of Visean age). This sequence of alternating carbonates and soft shales is thought to be an influencing factor as to the form and disposition of the ore shoots (Ineson, 1976).

Superimposed on the sequence of flat lying strata of the Alston block are two geological features of note: a major structural disturbance, the Burtreeford Disturbance, and a complex intrusive, the Great Whin Sill. The Burtreeford Disturbance comprises an east-facing monocline which divides the Alston field into an eastern half and a western half. The Great Whin Sill comprises a late Carboniferous to early Permian quartz dolerite intrusion. The sill, actually a series of interconnecting sills and dykes,is observed to outcrop at numerous levels. Accompanying the sill there may be extensive alteration and mineralisation along with some host-rock metasomatism (Young et al., 1985; Ineson, 1976).

Concomitant with the sill's intrusion were a series of earth movements which were responsible for the present day dome-like

structure of the orefield. Accompanying this phase of tectonism was widespread thrusting and faulting of the strata. These thrust and fault planes exert a strong structural control as to the pattern of orefield mineralisation.

5.2 Orefield Mineralisation: Mineral Zoning and Variation.

Mineralisation is developed throughout the stratigraphic successsion; i.e. Basement Ordovician and Silurian slates and shales, through Carboniferous carbonates and siliclastics, into the Permian magnesian limestones. Mineralisation, however, is best developed in the lower, middle, and upper limestone groups of the Visean (Dunham, 1948) with the once-economic deposits concentrated within the Great Limestone strata.

The orefield has been divided into a series of concentric zones. Each zone is defined by the presence of, or absence of, specific mineral components (Dunham, 1948). The central zone, dominated by fluorite, is observed to overlie the granite cupolas. In addition to fluorite, quartz and chalcopyrite are common throughout this central zone. The outermost zone is dominated by barite and calcite, with fluorite absent. Between these two zones, a zone containing both fluorite and barite may be observed.

Also apparent in the orefield is some degree of vertical variation in the mineral assemblages. Quartz with chalcopyrite and pyrrhotine-bearing mineral assemblages are observed to pass up into sphalerite with galena and chalcopyrite-bearing assemblages. Gangue fluorite is seen to pass vertically into gangue barite.

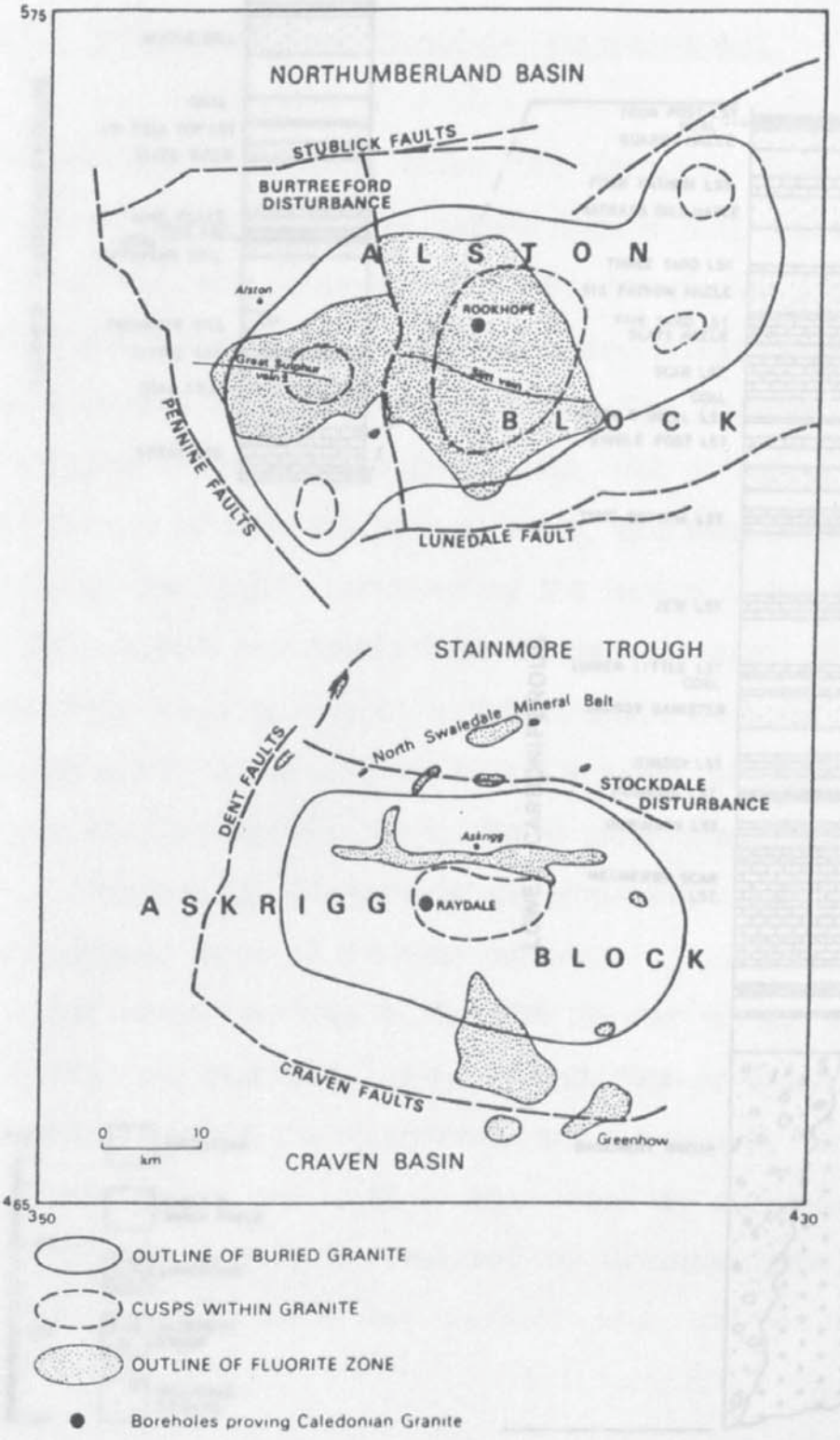

FIGURE 5.1

Schematic map of the North Pennine Orefield showing mineral zonation, adapted from Brown et al. (1987).

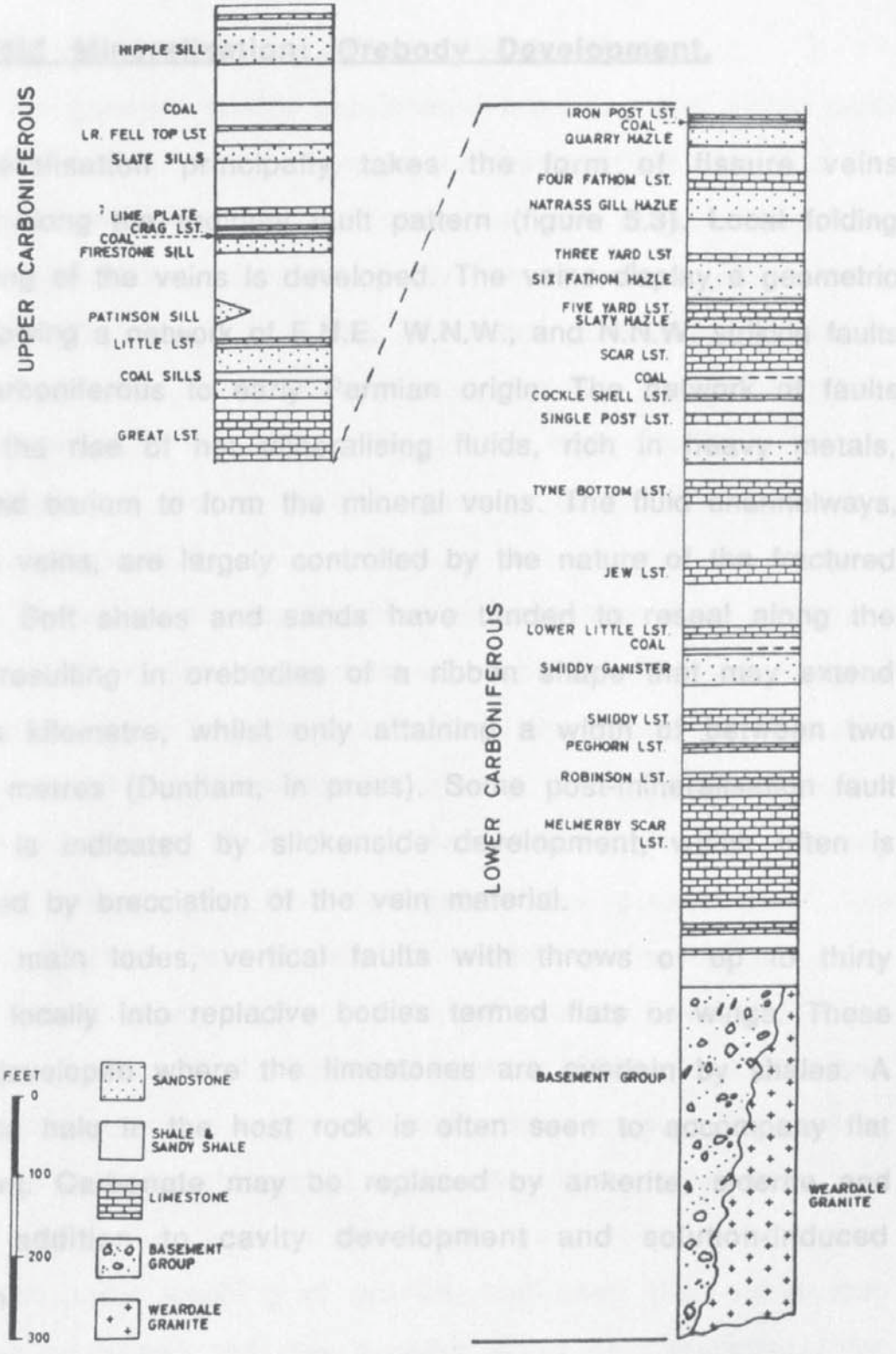

FIGURE 5.2

Generalised stratigraphic sequence for the Alston Block, North Pennine Orefield, adapted from Sawkins (1966).

5.3 Orefield Mineralisation; Orebody Development.

Mineralisation principally takes the form of fissure veins developed along the regional fault pattern (figure 5.3). Local folding and shearing of the veins is developed. The veins display a geometric pattern following a network of E.N.E., W.N.W., and N.N.W. striking faults of late Carboniferous to early Permian origin. The network of faults permitted the rise of hot mineralising fluids, rich in heavy metals, fluorine, and barium to form the mineral veins. The fluid channelways, and hence veins, are largely controlled by the nature of the fractured lithologies. Soft shales and sands have tended to reseal along the fractures, resulting in orebodies of a ribbon shape that may extend for over a kilometre, whilst only attaining a width of between two and three metres (Dunham, in press). Some post-mineralisation fault movement is indicated by slickenside development, which often is accompanied by brecciation of the vein material.

The main lodes, vertical faults with throws of up to thirty feet, pass locally into replacive bodies termed flats or wings. These are best developed where the limestones are overlain by shales. A metasomatic halo in the host rock is often seen to accompany flat development. Carbonate may be replaced by ankerite, siderite and silica, in addition to cavity development and solution-induced brecciation.

5.4 Genesis of the Mineralisation; Alston Block.

Current genetic models put forward regarding the Alston block mineralisation involve speculation as to the possible role that the deep-seated Caledonian batholith underlying the orefield may have had in the mineralising processes. Early genetic models such as that of Wallace (1861), advocating the downward percolation of surface waters, have since been either discounted or greatly modified. Instead, a composite model involving locally high thermal gradients, basin dewatering, and a granitic mineral component has been suggested (Ineson, 1976).

A granite-related mineralisation process was first advocated by Dunham (1934) who, by comparison with the Cornwall vein-ore deposits, suggested a possible link between the zoned Pennine style mineralisation and hot fluids derived from a hidden granitic source. The geophysical work of Bott and Masson-Smith (1957), and the subsequent drilling program, delineated the presence of the deep-seated Weardale granite batholith underlying the Alston mineral field. Radiometric dating of the granite indicated a Devonian/Silurian age (Holland and Lambert, 1970) of between 390 and 410 million years, i.e. of Caledonian origin. Mineralisation, however, is seen to post-date granite emplacement with the vein ores observed cross-cutting both the overlying strata and the granite. A supergene origin, or origin by leaching of granite, has been discounted and, instead, the hypothesis that the cupolas acted as channelways for upwelling fluids from depth has been put forward (Dunham et al., 1965).

Sawkins (1966), on the basis of salinity measurements derived

from fluid inclusion studies, advocated a dual origin for the mineralisation. The lead-zinc and fluorine-bearing minerals were assigned to a fluid of mantle origin that was channelled by the granite. The barium-bearing mineral (barite) was assigned to fluids derived by the dewatering of shale bands situated in nearby sedimentary basins. The model represented an attempt to explain the fluorite-barite zoning seen in the Alston block ores.

Sawkins' model was further modified in view of the sulfur and oxygen isotope studies undertaken by Solomon et al. (1971). The data suggested a connate origin for the sulfate species (barite) but discounted a magmatic origin for the sulfide species. Solomon et al. (1971) suggested the sulfide-sulfur may have originated from connate waters modified by membrane filtration. The granite is regarded as having provided the neccessary thermal gradient required to set up the convection system.

Recent mineralogical and geochemical studies have demonstrated a definite granite-related influence on the orefield mineralogy. Also advocated is a probable granite-related spatial control of the mineralisation (Brown et al., 1987). These authors suggest that localisation of the mineralisation over the granite cupolas results from a Variscan-related regeneration of an earlier developed fracture system, with reactivation related to hydrothermal alteration of the Weardale granite. The Weardale granite, a highly peraluminous granite, hosts a relatively high concentration of heat-producing radiogenic minerals, as do many of the Caledonian granites in the Northern British Isles (Webb et al., 1985). On the basis of theoretical heat-flow calculations, the granite

is regarded as being capable of providing sufficient heat to promote and focus an upward flow of metalliferous fluids into the overlying Carboniferous strata (Fehn et al., 1978).

Sulfide and oxide phases (minor and trace levels):	Reference:
Stanniferous Chalcopyrite	b
Cassiterite	b
Cloanthite	b
Rammelsbergite	b
Safflorite	b
Skutterudite	b
Niccolline	a
Cobaltite	a
Gerdsorffite	c
Loellingite	b
Ullmanite	b
Bismuthinite	b
Molybdenite	b
Bournonite	e
Tetrahedrite	e
Argentopentlandite	a
Sternbergite	a
Pyrargyrite	a
Stephanite	a
Acanthite	a

Rare Earth Bearing Phases (trace levels).	Reference:
Monazite	d
Xenotime	d
Synchysite	d

a Ixer and Stanley, 1987. b Ixer, 1986. c Ixer et al., 1979.
d Brown et al., 1987. e Vaughan and Ixer, 1980.

TABLE 5.1

Non-typical M.V.T. lead-zinc ore mineral phases recorded from the Rookhope-Tynebottom Quartz-Pyrite-Sulfide assemblages, Alston Block (based on a review by Ixer, 1986).

Brown et al. (1987) outline a suite of granitic minerals found in the ore assemblages which are atypical of base metal mineralisation, especially "Mississippi Valley Type" lead-zinc mineralisation. The high temperature cupolas of Rookhope and Tynebottom host early quartz, pyrrhotine, sulfide assemblages containing traces of non-typical M.V.T. mineral phases. These mineral phases are possibly due to a granitic related component developed in the ore fluids (see table 5.1, Ixer (1986), and Brown et al. (1987) for a fuller account).

FIGURE 5.3

Map illustrating the principal mineral veins for the Alston Block. The veins follow the regional pattern of E.N.E., W.N.W., and N.N.W. striking faults.

5.5 Geological and Mining History of the Sample Area; Nenthead, Alston Moor.

The Nenthead area of the Alston Moor was one of the most productive areas of lead-zinc mineralisaton in the North Pennines Orefield.

Figure 5.4 shows the geological structure of the Nenthead Valley region of the orefield. The valley is dominated by a series of ramifying N.W. trending faults and mineral veins which strike parallel to the valley floor. The valley sides host a network of north-east trending veins, many of which yielded rich workable deposits. Mineralisation in these veins tends to be best developed where they cut a north-west trending synclinal structure lying between the Nent and West Allen Valleys.

Initially the veins were worked for lead ore, and then for zinc ore, but Wallace (in Dunham 1948) reports that by 1735 many of the early lead trials had been exhausted. Shortly after 1735, exploration and development of the metalliferous strata of the Great Limestone Series commenced following the discovery of very rich deposits in West Allendale. This discovery (the High Coalcleugh Vein) in Great Limestone strata prompted the London Lead Company to commence mining in the Nent Valley.

The period of maximum lead production for the Nent and West Allen Valleys was the period 1820 to 1880. Following the slump in base metal prices in the 1880's, the mining industry contracted, with the major mining companies pulling out of the region. Lead and zinc mining on a greatly reduced scale continued first through the

Nenthead and Tynedale Zinc Company and then through the Vieille Montagne Zinc Company. Mining continued until the early 1920s, after which lead-zinc extraction was virtually non-existent.

The decline in the lead-zinc mining industry was followed by a rise and growth in the extraction of fluorite and, on a lesser scale, barite. Fluorite was extensively mined in the 1960s and 1970s, with the bulk of the ore bought by British Steel. However, a decline in the steel industry, and resultant drop in the demand for fluorite, has led to the cessation of fluorspar mining in the Alston Block region. Should the fluorspar market ever pick up in the U.K. there are large deposits of fluorite awaiting extraction.

FIGURE 5.4

Structural and contour map of the Nenthead region showing mineral veining (adapted from Dunham, 1948).

CHAPTER 6: General Petrography Part One: Growth Related Textures.

6.1 Introduction.

Sampling of material for the purpose of this study was undertaken both *in situ* (underground) and from mine waste dumps (surface). Underground sampling was undertaken in the lower levels of the Smallcleugh Vein and Handsome Mea Flats, Nenthead. Surface samples consisted of tailings and mine dump material taken from a variety of localities along the Nenthead valley.

Coarsely crystalline, much of the sampled ore comprises a banded vein ore with alternating layers of sphalerite and gangue. In addition to banded vein ore, sphalerite was sampled from fracture infilling assemblages. One to ten centimetres wide, the fractures are best developed in the micritic carbonate wall rock, the bulk of which has been extensively silicified .

Petrographic studies of the ore material (transmitted light, doubly-polished thin sections) define two principal textural varieties of sphalerite. A widely developed form referred to as *type-two* sphalerite is recognised, along with a very patchily and locally observed variety, termed *type-one* sphalerite. Observed to accompany both textural forms of sphalerite are a variety of other ore, and gangue, phases.

6.2 General Petrography: Non Zinc-Bearing Phases.

6.2.1 Gangue Mineralogy.

Gangue mineralisation is best developed in the larger vein ores of sphalerite where an alternation between gangue and ore deposition may be observed. The gangue chiefly comprises quartz and iron carbonate. Together they volumetrically account for greater than 90 percent of the gangue. The other 10 percent comprises dolomite and rare traces of purple fluorite. Gangue minerals may host a suite of non-zinc bearing sulfides in small quantities. The more common of these are galena, marcasite and chalcopyrite. Pyrite, gersdorffite and bismuthinite may locally be present.

Quartz:

Quartz represents the most abundant gangue phase, and volumetrically accounts for greater than 75 percent of the total mineral content. Comprising subhedral to euhedral grains, grain size is generally large (greater than 1000 microns) and individual crystals may reach several millimetres in length. Texturally, quartz is indicative of open space deposition. Well developed comb structures are observed (see Craig and Vaughan, 1981, p113). Individual grains may exhibit a range of features, the most notable of which are:

1. The development of internal zoning (only apparent when viewed using cathodo-luminescence techniques).
2. Fracture and micro-crack development.

3. The development of fluid inclusions (both primary and secondary types).

Fracturing of the quartz is pervasive with anastomosing cracks and fractures observed throughout the gangue mineralisation. Many of the fractures show healing with the resultant development of planes of secondary fluid inclusions. In addition to secondary fluid inclusion development, numerous 10 to 100 micron sized primary inclusions are observed randomly distributed throughout the host grains.

Cathodo-luminescence petrography of gangue quartz associated with well banded sphalerite (both types) reveals a fine scale, well developed, growth banding. Many of the growth bands traced out by the luminescent quartz are coincident with growth bands developed in adjacent sphalerite. Optically, no correlation between the luminescent zoning and any internal textures is apparent.

A variety of primary and secondary fluid inclusions are observed throughout the gangue quartz. Primary inclusions occur as scattered liquid with vapour inclusions ranging in size from 5 microns to 60 microns (see plate 6.1). Some of the smaller, 10 microns and less in diameter, inclusions appear to represent monophase liquid-bearing inclusions. Secondary inclusions are fracture and microcrack related. Healing of the fractures and cracks generates planes of liquid, or liquid-plus-vapour, inclusions (see plate 6.2). The inclusions are typically anhedral and range in size from less than 5 microns to greater than 70 microns. Only monophase or two-phase inclusions are observed. No solid-bearing, or multi-liquid-bearing, inclusions are observed.

The inclusion-bearing quartz grains form the basis for thermometric analysis of the ore material. Primary and secondary inclusion types are easily recognised and are commoner in quartz than in the ductile deformed co-existing sphalerite.

Iron Carbonate (Siderite and Ankeritic Dolomite).

Iron carbonate is widely developed throughout the mineralisation. The carbonate is developed as a fracture infill with quartz, and in association with the alteration of marcasite. Where the carbonate is developed in association with marcasite, the marcasite is seen to be embayed, corroded and often rimmed by goethite. Much of the carbonate mineralisation is characterised by a well developed rhombohedral cleavage. The $\{10\bar{1}1\}$ cleavages commonly show alteration to goethite. Also present is some textural evidence for mild post-ore deformation. Plate 6.3 illustrates such a region of iron carbonate, with curved cleavage traces developed in response to deformation. Plate 6.4 details the textural association of iron carbonate associated with relict marcasite.

6.2.2 Sulfide Mineralogy.

The non zinc-bearing sulfides rarely exceed 1 to 2 percent by volume of the total ore. Marcasite is the only phase locally developed in significant quantities. In the vicinity of the silicified wall rock marcasite may account for more than 30 percent by volume of the ore. Gangue hosted phases differ slightly from those hosted by sphalerite. Both gangue and sphalerite are seen to host marcasite, galena and

chalcopyrite. The gangue also hosts gersdorffite, pyrite and traces of bismuthinite in chalcopyrite. Marcasite development in sphalerite is not widespread.

Pyrite:

For the samples examined, pyrite is not a commonly developed phase. Observed as small anhedral grains up to 10 microns in size, many of the grains have a framboidal habit with little evidence for alteration (cf. marcasite). Pyrite development is associated with quartz gangue, and represents a paragenetically early phase.

Marcasite:

Marcasite represents the common form of iron sulfide developed. Much of the marcasite shows textural evidence for replacement. Pitted and embayed with well-developed careous margins, many of the grains show alteration to goethite (FeO.OH), and replacement by iron carbonate (see plates 6.3 and 6.4).

Twinning is commonly developed in fractured grains. Marcasite is not commonly hosted by sphalerite but by the quartz-carbonate gangue.

Galena:

Galena is observed in both the gangue and sphalerite mineralisation. Anhedral in habit, grain sizes range from less than 20 microns to greater than 200 microns. Characterised by the development of triangular cleavage pits, some deformation of the sulfide is apparent. Many of the cleavage traces are curved in a manner similar to those

described for the iron carbonates.

Chalcopyrite:

Developed both in sphalerite and in the gangue two generations of chalcopyrite are recognised. Much of the chalcopyrite appears to represent a paragenetically late phase. Subhedral to anhedral in form, grains are typically 60 to 90 microns in diameter. For fracture associated chalcopyrite, the grains tend to be smaller, with a grain size of less than 40 microns being typical.

Chalcopyrite is most commonly developed along fractures that cross-cut both the sphalerite mineralisation and the gangue phases. Some of the chalcopyrite hosting fractures cross-cut an earlier generation of quartz-carbonate filled fractures. Reflected light studies of chalcopyrite suggest a random distribution for the grains. However, when viewed in transmitted light, these apparently randomly distributed grains are seen associated with healed microcracks and fractures.

Plate 6.6 illustrates a region of sphalerite with chalcopyrite developed along a healed crack. Grain size is observed to be relatively small (40 microns to less than 10 microns). Associated with the chalcopyrite-hosting fracture are secondary fluid-filled inclusons. Some chalcopyrite anhedra within both sphalerite and associated quartz gangue are not associated with fracturing or sphalerite alteration (see section 7.4). These grains probably precipitated along with the co-existing sphalerite (see plate 6.5).

Gersdorffite:

Gersdorffite represents a paragenetically early phase, best developed between the banded *type-one* and *type-two* sphalerite generations. Set in a quartz-carbonate gangue, the mineralisation comprises a series of small (10 to 40 microns across) euhedral grains. The grains are strongly zoned, with the zoning picked out during polishing (see plate 6.7). Many of the zoned gersdorffite grains are observed to host anhedral grains of sphalerite, often close to the core of the grain.

Bismuthinite:

This phase, identified optically, is present as rare inclusions in chalcopyrite. Comprising small anhedra of less than 5 microns in grain size, this mineral represents only a very minor component of the total sulfide present.

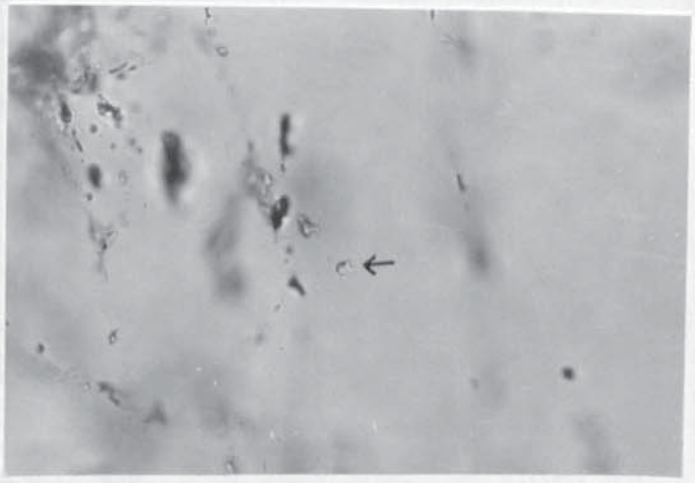

PLATE 6.1

Small primary two-phase inclusion (arrowed) set in gangue quartz. Also developed are numerous secondary fracture-associated fluid inclusions. PPL transmitted light. Field of view 350 microns.

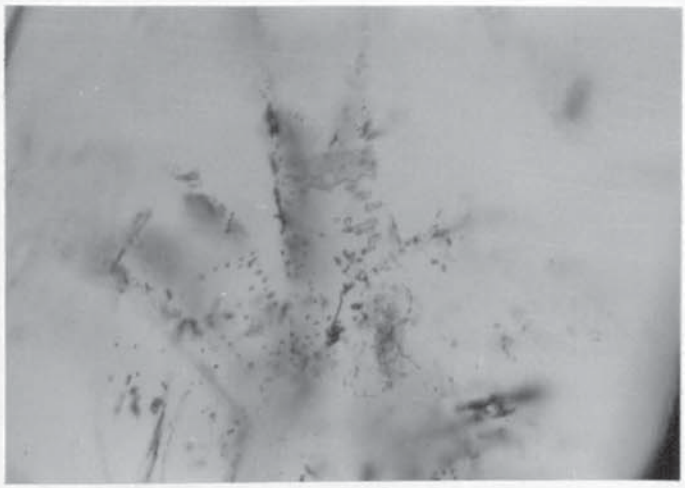

PLATE 6.2

Plane of secondary two-phase saline inclusions set in quartz gangue. Inclusions are developed along healed fractures. PPL Transmitted light. Field of view 560 microns.

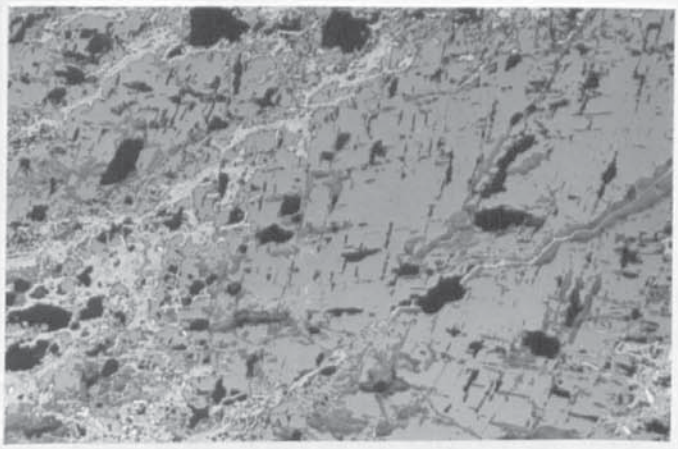

PLATE 6.3

Iron carbonate gangue (mid-grey) with well developed rhombohedral cleavage. Goethite (light-grey) is seen developed along some of the cleavages. Relict marcasite (white) is present in some of the goethite patches. PPL Reflected light. Field of view 2220 microns.

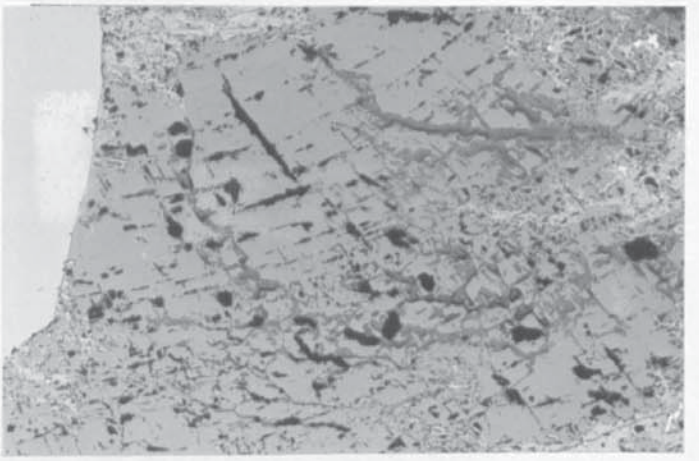

PLATE 6.4

Iron carbonate gangue (mid-grey) with deformation curvature of the $\{10\bar{1}1\}$ cleavages apparent. Goethite (light-grey) is developed as a replacive phase along many of the cleavages. PPL Reflected light. Field of view 2220 microns.

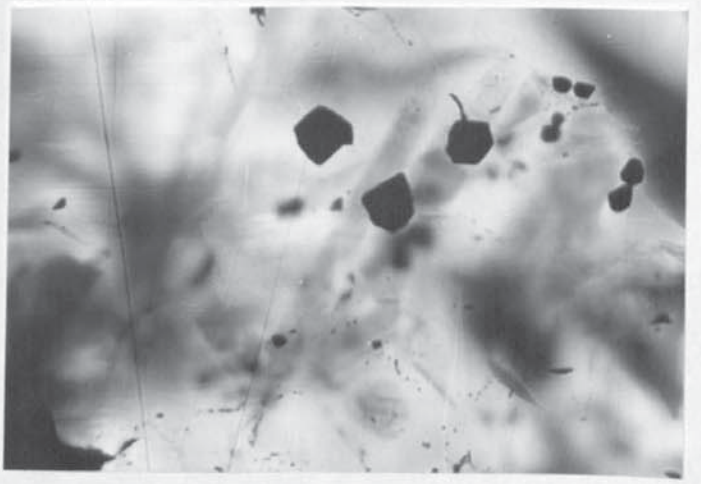

PLATE 6.5

Chalcopyrite euhedra developed as a paragenetically early phase of mineralisation in a sphalerite host. Chalcopyrite mineralisation is not fracture associated. PPL Transmitted light. Field of view 560 microns.

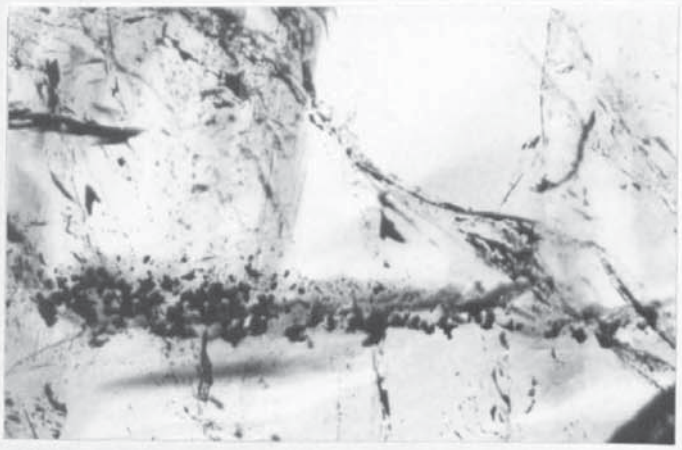

PLATE 6.6

Fracture associated chalcopyrite subhedra in sphalerite. Fracture associated chalcopyrite represents a paragenetically late phase of mineralisation. PPL Transmitted light. Field of view 2220 microns.

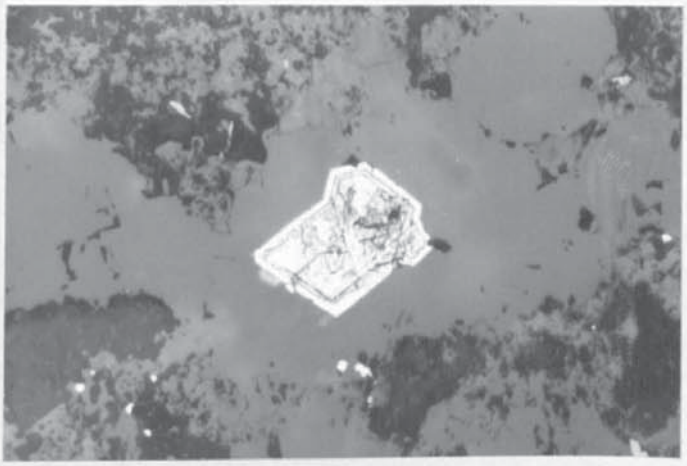

PLATE 6.7

Photomicrograph of a euhedral growth-zoned gersdorffite grain. Gersdorffite grain is set in a quartz gangue (mid-grey). PPl Reflected light. Field of view 350 microns.

6.3 *Type-One* Sphalerite: Textural Description.

Banded *type-one* sphalerite is the term used in this thesis to refer to a textural variety seen in only some of the samples from the Nenthead area. This textural variety is not widely developed, and is observed as isolated regions within the dominant variety which is referred to in this thesis as *type-two*. It is best developed as a separate well-banded episode prior to *type-two* precipitation, in which case it is always bound by a prominent surface. This surface, careous and irregular in outline, represents a major period of sphalerite dissolution. The dissolution surface may often host minor quantities of gangue phases and other sulfides.

Banded *type-one* mineralisation takes the form of a thin crustiform coating on the silicified micritic wall rock, varying in thickness from a few millimetres to two or three centimetres. Individual grains tend to be subhedral to euhedral. {111} and $\{1\bar{1}1\}$ forms are developed, often in combination.

In the banded *type-one* variety, banding comprises numerous sub-parallel black 'lines' or bands of up to one millimetre thickness (typically 200 to 400 microns) which continue into adjacent sphalerite grains and may often be traced laterally for several centimetres. They trace out the crystal growth front (plates 6.8 and 6.9). Some variation in band width is due to to variations in the angle of band intersection with the plane of thin-section.

Separation between individual bands varies from less than 50 microns to greater than 1000 microns. For the majority of the banded samples, the more prominent and well-developed bands may be

recognised and correlated throughout sections of any one sample.

6.3.1 *Type-One* Sphalerite Growth Banding.

Textural studies were undertaken using doubly-polished thin sections. Reflected light examination revealed a uniform grey, apparently unbanded, sphalerite containing traces of gangue and other sulfides.

Transmitted light studies revealed between three and eight prominent bands running throughout the grains (plates 6.8 and 6.9). In between these prominent, or 'marker', bands, other less well-developed, and laterally less extensive, bands are observed. Examination of the latter provided much of the information about the internal characteristics of the bands. Unlike the opaque marker bands, they are translucent, enabling them to be optically studied. The unbanded sphalerite comprises a pale yellow to honey brown sphalerite.

A high magnification (40 x oil immersion) examination is neccessary to document internal banded textures. The majority of the bands are bounded by two differing margins; one sharp and one diffuse (plates 6.11 and 6.10). The sharp margin corresponds to the initial growth front for the band. This margin may be decorated by numerous small irregular opaque inclusions ranging in size from less than one micron to approximately 10 microns. The sharp nature of the margin suggests an abrupt change to the nature of the sphalerite-depositing ore fluid. The diffuse margin represents a return to sphalerite depositing conditions more typical of M.V.T. ores. The diffuse margin

often extends over several microns in width.

Many of the bands are composite in texture. One large band may comprise several small and laterally discontinuous bands of a few microns separation. Typically between twenty and two hundred microns in width, these bands are translucent with a distinct internal texture developed. The bands host numerous black 'lineations' or rods, fractions of a micron in width. These lineations often extend the whole length or width of the band. Three classes of rods are optically apparent:

1. A set parallel to the growth front.
2. A set parallel to the growth direction (i.e. normal to the growth front).
3. A set inclined to the growth front at an angle varying between thirty and sixty degrees.

The rods or lineations present are irregularly shaped. They are observed to vary along their length and often display what is termed a 'blotch-like' texture. Patches or blotches, sub-micron to micron in width are seen decorating the rod (plate 6.10). Due to their sub-micron size, it is not possible optically to resolve the morphology of blotch-like areas. 'Plate-like' particles as described by Barton and Bethke (1987) are not observed decorating rods in the Nenthead material.

The rods, typically sub-parallel to parallel, occasionally divide or coalesce along their length. They tend to group, and often nucleate from the initial sharp growth margin (plate 6.11). Other commonly

observed nucleation points for the rods are small inclusions trapped within the sphalerite.

Where the rods intersect the polished surface no other mineral phase is optically discernible. However, the surface is often seen to be pitted. This pitting may reflect either a void- or defect-like nature for the 'blotched rods' or simply the plucking out of a second phase during sample polishing.

Optically the fabric bears a similiarity to the 'bead chains' developed in other sphalerite deposits, as described by Barton and Bethke (1987). The 'bead chain' texture observed for the Pennine mineralisation, however, is finer and smaller both in width and length compared to those of Barton and Bethke (1987). The 'blotched-rod' texture is poorly developed in the paler yellow unbanded *type-one* sphalerite, and is best developed in the darker banded regions instead. Some rods and beads are seen in the unbanded material but their low intensity imparts only an irregular patchy translucency to the sphalerite rather than a banded texture (as is the case for some *type-two* iron banded sphalerites).

Of the three growth-related varieties, the second class of rods (i.e. those rods which run parallel to growth direction) account for approximately three quarters of all the 'rods' observed. The remaining quarter fall into the third class of lineations, with the majority of these rods angled acutely to the growth direction (30 to 40 degrees). Only a few rods are observed to run sub-parallel the growth banding.

Plates 6.11 and 6.12 illustrate the typical textural morphology developed in *type-one* sphalerite. The individual bands, composite in structure, have well-developed sharp leading, and diffuse trailing,

margins. Also faintly apparent are the rods that comprise much of the banded structure. The majority of these rods are observed to run parallel to the growth direction, although some are inclined to the growth direction.

In addition to the rod-like fabric developed in the banded regions, many of the poorly-developed bands host a dust-like or 'peppered' texture. This texture comprises numerous micron to sub-micron sized particles (or possibly crystal defects) randomly distributed throughout the sphalerite. Unlike the blotched rods, these particles are smaller in size and appear to be distributed without any apparent crystallographic control; i.e. they are not observed aligned in rod-like forms or chains.

Throughout the *type-one* sphalerite, large (up to several hundreds of microns across) aqueous and solid inclusions are seen. A variety of primary, secondary and pseudo-secondary inclusions are observed. These are more fully described in section 6.7.

PLATE 6.8

Micrograph of banded *type-one* sphalerite with well defined 'marker' bands seen tracing out the crystal growth front. PPL Transmitted light. Field of view 6600 microns.

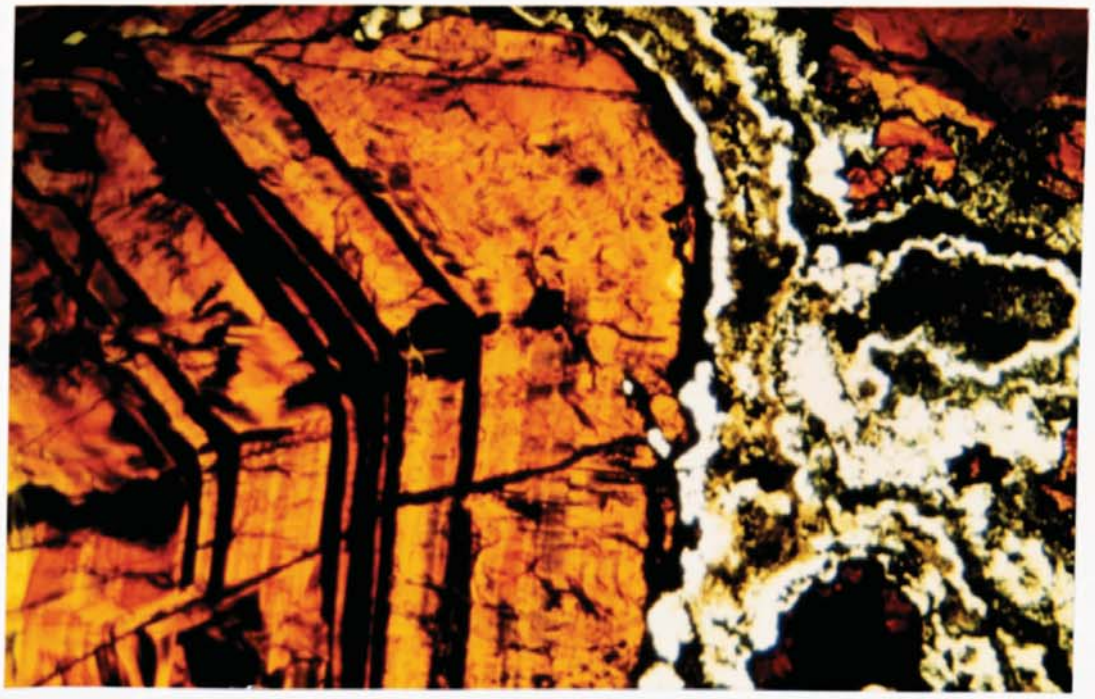

PLATE 6.9

Micrograph of growth banded *type-one* sphalerite. Opaque well developed marker bands may be seen tracing out the crystal growth direction. PPL Transmitted light. Field of view 6600 microns.

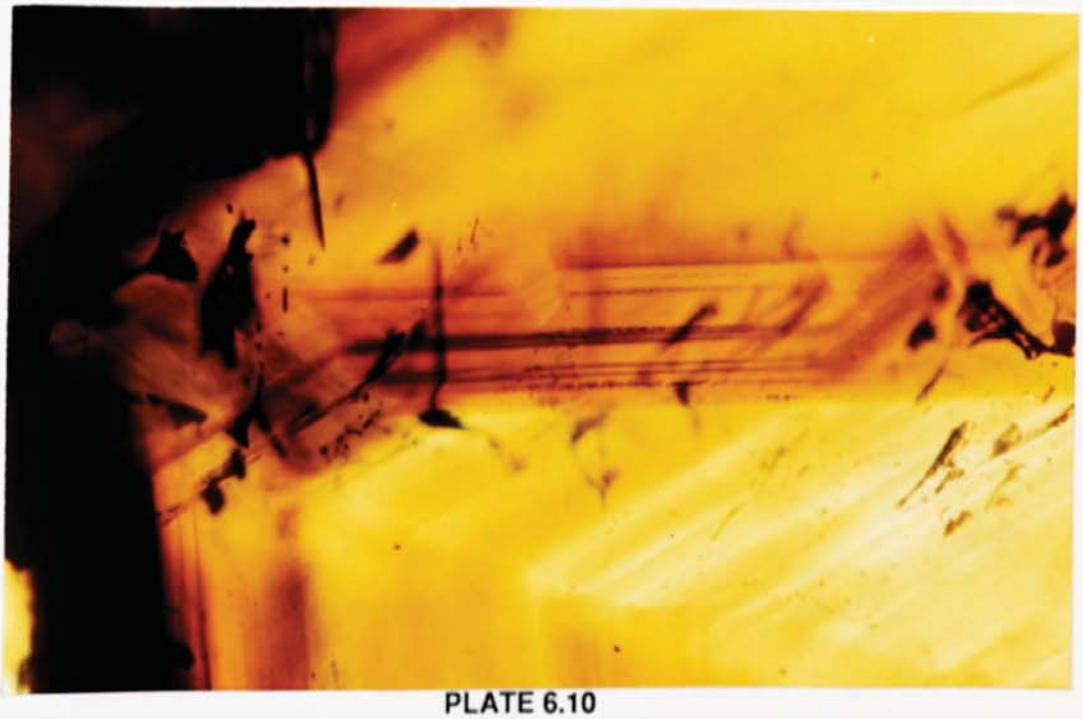

PLATE 6.10

Colour micrograph of growth banded *type-one* sphalerite. Blotching of the bands is developed. Also apparent are the reflection effects due to growth twinning. PPL Transmitted light. Field of view 560 microns.

PLATE 6.11

Micrograph of banded *type-one* sphalerite. Sharp leading and diffuse trailing edges are well developed. Direction of crystal growth is arrowed. PPL Transmitted light. Field of view 890 microns.

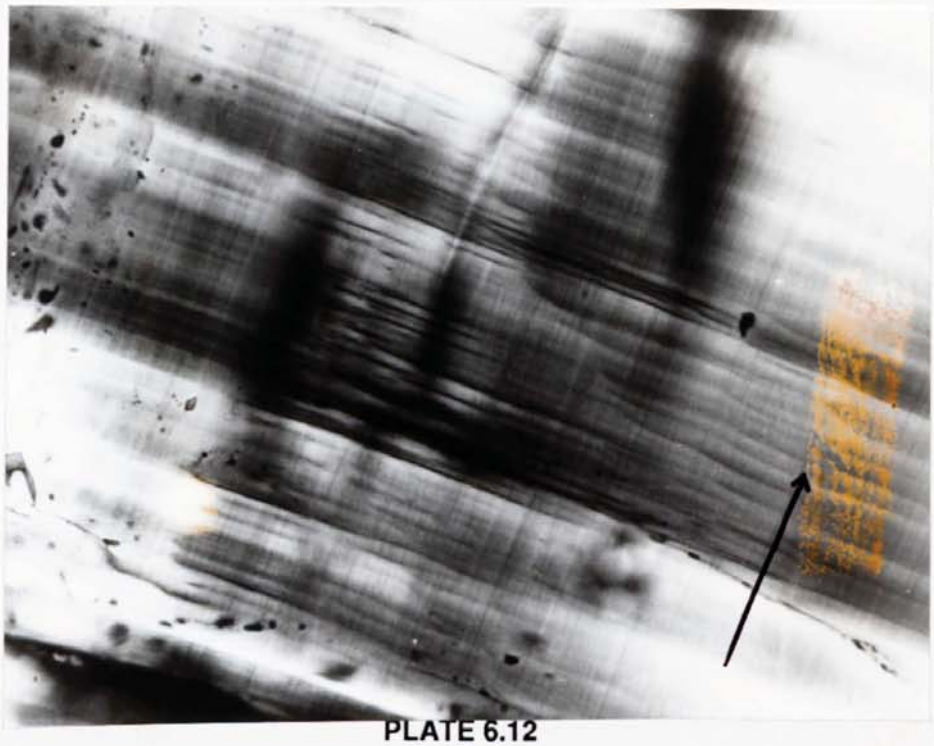

PLATE 6.12

MIcrograph of banded region of *type-one* sphalerite. Banded regions host a growth-related fabric sub-parallel to growth direction (arrowed). Laterally bands are discontinuous and may overlap. PPL Transmitted light. Field of view 350 microns.

6.4 *Type-Two* Banded Sphalerite: Textural Description.

Type-two sphalerite accounts for more than eighty percent of the sphalerite examined from the Nenthead samples. Typically comprising large fractured crystalline masses of subhedral to euhedral grains, both rhythmic-vein and fracture-infill deposits are sampled. Texturally, *type-two* sphalerite is distinguished on the basis of the internal banding developed.

Many of the smaller (approx. 1000 microns) isolated grains contain a dark red-brown core which is surrounded by a pale-brown to yellow sphalerite (plate 6.13). Both the core to rim boundary and banding in the rim are sharply bounded. The colour banding is irregular and varies in thickness along its length. Occasionally the thinner bands may wedge out altogether.

Two main phases of mineralisation are developed with the dark red-brown core representing a particularly early and iron-rich episode of mineralisation (see section 7.1 for analytical data). The two phases are separated by a depositional hiatus with limited sphalerite dissolution having occurred. Bands present in the pale coloured overgrowths are developed in continuity with the dark red-brown banded core. Only a small degree of growth band mismatch due to sphalerite dissolution is apparent (plate 6.14).

6.4.1 *Type-Two* Sphalerite Growth Banding.

Type-two sphalerite banding is characterised by variations in sphalerite body colour. Sphalerite sampled from many of the larger

veins and fractures is often only partially banded. For the purposes of this study, the unbanded regions associated with *type-two* banded material are classed as being of *type-two* origin. Banding apart, they are texturally identical.

Sphalerite body colour is observed to fluctuate from a pale yellow, or honey yellow, variety to a deep red-brown variety with many shades of orange and brown also present. The banding, as for *type-one* sphalerite, traces out the mineralisation growth front, and is ascribed to fluctuations in the composition of the mineralising fluids.

Band width varies from a hundred microns to greater than three millimetres. The vast majority of the bands are between 750 and 1250 microns in width. Gradual colour changes, rather than sharp abrupt colour boundaries are observed for the majority of the bands. Where a sharp colour change is observed, it may usually be correlated with either a dissolution surface or separate phase of sphalerite deposition.

The bulk of the sphalerite mineralisation is observed to be very episodic with repeated intervals of precipitation and dissolution widespread. Careous grain boundary contacts and dissolution surfaces are seen cross-cutting much of the mineralisation. Sphalerite colour and texture may dramatically change across some dissolution surfaces (plate 6.13). As was observed for *type-one* mineralisation, the dissolution surfaces host a variety of gangue and other sulfide phases.

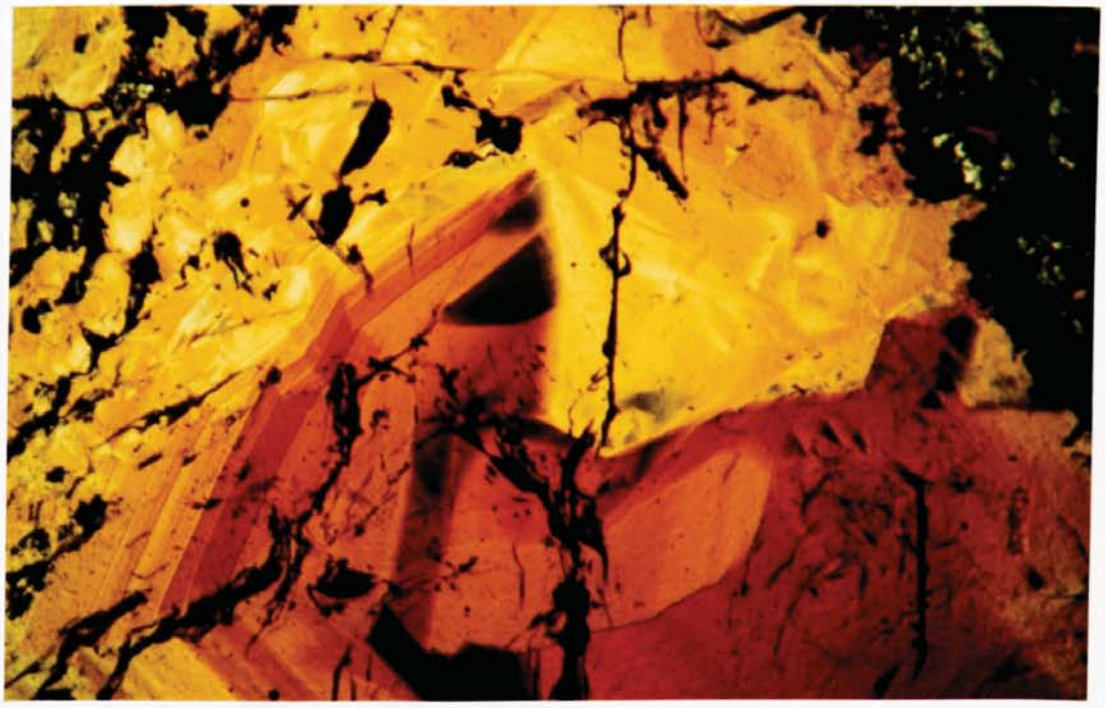

PLATE 6.13

Colour micrograph of banded *type-two* sphalerite. Sphalerite colour is seen to change dramatically across a major dissolution surface. The dissolution surface cross cuts the growth banding. PPL Transmitted light. Field of view 2200 microns.

PLATE 6.14

Colour micrograph of *type-two* banded sphalerite containing numerous minor dissolution surfaces. Dissolution surfaces are sub-parallel to growth banding, and laterally may merge. PPL Transmitted light. Field of view 560 microns.

6.5 Sphalerite Petrography: General.

Of the two types of sphalerite distinguished (*type-one* and *type-two*) *type-one* sphalerite accounts for between 10 and 15 percent of the total material examined. For the *type-one* variety, only 5 percent occurs as a separate episode of mineralisation, the remaining 10 percent is hosted by the *type-two* variety.

Type-one sphalerite is developed only patchily in the *type-two* variety. When developed as a separate episode, it occurs as a well banded, paragenetically early, phase of mineralisation.

Where *type-one* sphalerite is developed in *type-two* sphalerite, a variety of textures are recognised, some of which are attributed to repeated phases of mineralisation and dissolution. *Type-one* is typically present as regions several hundreds of microns in width throughout the *type-two* variety. Two principal textural occurrences of *one* in *two* are noted.

1. Patches or areas of *type-one* in *type-two* that show no apparent discontinuity separating the two types. The *type-two* region passes into the *type-one* region over a width of several tens of microns, with no apparent dissolution surface or grain boundary developed. The *type-one* sphalerite developed shows most of the textures outlined in section 6.3. Banded regions of *type-one* material often coincide with banding developed for the *type-two* material. In particular, the *type-one* banding corresponds to the darker red-brown bands present in the hosting grain.

2. Patches of type-one sphalerite present as a relict texture in type-two material. The type-one material is present as small regions, up to 100 microns in size, set in a matrix of dark red-brown sphalerite. The dark red-brown sphalerite is seen to be colour banded and texturally very similar to the *type-two* variety. The red-brown patches of sphalerite are taken to represent an early, iron-rich, (see section 7.1.2) phase of *type-two* development. The red-brown regions display sharp irregular margins. They occur as isolated remnants of an earlier phase, now set in a matrix of pale coloured *type-two* sphalerite (see plate 6.15).

Type-one sphalerite developed within *type-two* regions is not observed bound by a dissolution surface or other sharp boundary. *Type-one* sphalerite would appear to have developed simultaneously with the *type-two* variety, and may often be seen to overprint the *type-two* colour banding. *Type-one* sphalerite developed in *type-two* sphalerite volumetrically accounts for approximately 10 percent of the sphalerite present. Locally such sphalerite may exceed 30 percent by volume of the sample.

6.6 Dissolution Textures.

Textural evidence for repeated phases of sphalerite deposition, and dissolution, are seen throughout the mineralisation examined. Best observed in *type-two* sphalerite, textures indicate widely varying degrees of dissolution. Minor dissolution is implied for much of the growth banding that characterises *type-two* sphalerite. Many

growth bands, especially the early iron-rich, red-brown bands, are seen to vary in thickness. The bands tend to be sub-parallel rather than parallel: parallel consecutive bands would be expected in the absence of dissolution. The sharp margins and slight mismatch between successive bands indicate minor dissolution (see plate 6.14).

Substantial periods of dissolution are apparent from the presence of relict red-brown patches of *type-one* material set in a later matrix of pale *type-two*, material (plate 6.15). *Type-one* banding in many of these dark red-brown regions shows no continuity with banding in the *type-two* host. For regions subject to prolonged periods of dissolution, correlation of the various generations of sphalerite becomes impossible.

PLATE 6.15

Colour micrograph of a region of *type-one* sphalerite set in a matrix of *type-two* sphalerite. A major dissolution surface separates the two sphalerite types. PPL Transmitted light. Field of view 560 microns.

6.7 Inclusion Petrography.

A wide variety of inclusion morphologies and types are seen. Opaque, translucent and transparent inclusions may be either primary or secondary in origin. A range of monophase (liquid-only and vapour-only) and two phase (liquid with vapour) inclusions are developed. Three-phase inclusions are not seen.

6.7.1 Opaque and Translucent Inclusions.

Euhedral and anhedral opaque inclusions, along with anhedral translucent inclusions, are developed in both sphalerite varieties. Euhedral inclusions are often sulfides. Anhedral inclusions may have more than one origin.

Euhedral inclusions typically range in size from 5 microns to greater than 75 microns. Reflected light microscopy of selected inclusions (revealed by alternate periods of sample grinding and polishing) indicates more than one sulfide present. Chalcopyrite, marcasite, and gersdorffite are all seen to be enclosed within the sphalerite. Plate 6.5 details such inclusions of chalcopyrite.

Anhedral inclusions have an irregular, lobate, or sub-spherical morphology. Ranging in size from less than one micron to greater than 100 microns, many of the larger anhedral inclusions represent sporadically developed galena. Occasionally, carbonate inclusions may develop. The majority of the irregular inclusions, however, are vapour or liquid-filled inclusions that reflect the illuminating light beam. Such inclusions tend to be steeply inclined to the plane of the thin

section. The same origin is apparent for the translucent inclusions occasionally observed.

6.7.2 Aqueous and Vapour-Bearing Inclusions.

Aqueous and vapour-bearing inclusions are numerous in all material examined. They have highly variable morphology and mode of occurrence. Two classes are recognised; primary and secondary. Secondary inclusions predominate throughout the sphalerite mineralisation.

Primary Inclusions.

Primary inclusions tend to be small (5 to 15 microns) and proved unsuitable for thermometric analysis. Large (40 microns and greater) inclusions are scarce and best developed in undeformed *type-two* grains that have not undergone multiple phase dissolution and precipitation.

Small inclusions are randomly scattered throughout the material. In addition, inclusions are observed developed in bands. These tend to be monophase (liquid only), only a few of the larger inclusions containing a vapour phase in addition to a liquid phase. The inclusion-rich zones are parallel to growth banding, be it *type-one* or *type-two* (plate 6.16).

Large primary inclusions suitable for thermometric studies show a subhedral to anhedral form. Up to 75 microns in size, they are liquid-rich two phase (L + V). They are best developed in undeformed regions of *type-two* sphalerite.

Some primary inclusions show textural evidence for post-depositional modification. The necking-down of narrow or elongate inclusions is common, as is inclusion deformation. Many inclusions show a twin-plane or glide-plane control to morphology (plate 6.17).

Secondary Inclusions.

Liquid, vapour, and liquid with vapour secondary inclusions are developed in abundance in both varieties of sphalerite. The majority are related to healing of numerous fractures throughout the mineralisation. Healing of the fractures generates planes of small anhedral liquid, or two-phase, inclusions. In addition to crack-related inclusions, cleavage and slip plane-related inclusions are apparent. Many of the slip plane-related inclusions probably represent altered primary inclusions.

Geometrically the most complex inclusions are those developed along cleavage planes. Inclusion morphology reflects the cubic symmetry of the host phase. Inclusions may have either a liquid, or two-phase, infill. Plate 6.18 illustrates a typical cleavage plane fluid inclusion.

Tubular inclusions.

In addition to primary and secondary fluid-bearing inclusions, a range of 'tubular' inclusions are observed throughout the samples. They vary in length from a few tens to many hundreds of microns, and in width from a few microns to sub-micron.

Many tubular inclusions show textural evidence for post-depositional modification. The necking down of narrow elongate

inclusions is common and produces a chain of small secondary liquid, and two-phase inclusions (plate 6.19). The majority of apparently unaltered tubular inclusions are liquid-only Such inclusions are considered unsuitable for thermometric analysis.

Monophase (liquid) tubular inclusions typically develop in clusters. Inclusion orientation is usually parallel to growth direction (plate 6.20). Some of the inclusions display a complex geometric morphology with 'tubes' or 'arms' along three mutually perpendicular directions (plate 6.21). One, or occasionally two, of the 'arms' may be greater than 100 microns long. The remaining 'arms' are typically less than 25 microns in length.

Some of the thinnest inclusions take on the form of a thick 'rod' similar in appearance to those contained in the opaque banded regions of *type-one* sphalerite (plate 6.22). Some inclusions with more than one 'arm' bear a similarity to the growth defects described by Barton and Bethke (1987). In areas hosting both rods and a range of narrow tubular inclusions, the distinction between rod and inclusion is often uncertain.

PLATE 6.16

Micrograph of inclusion rich *type-two* sphalerite. The inclusions are concentrated as a series of sub parallel bands which parallel growth banding. PPL Transmitted light. Field of view 280 microns.

PLATE 6.17

MIcrograph of inclusions developed in *type-two* sphalerite. Many of the inclusions show a twin or glide plane control to inclusion morphology. PPL Transmitted light. Field of view 350 microns.

PLATE 6.18

Micrograph of *type-one* banded sphalerite with secondary fluid inclusions. Inclusions are due to partial healing along cleavage planes with a resultant complex geometric inclusion morphology. PPL Transmitted light. Field of view 1100 microns.

PLATE 6.19

Micrograph of *type-one* sphalerite with narrow elongate fluid inclusions developed. Inclusions modified by necking down are considered unsuitable for thermometric analysis. PPL Transmitted light. Field of view 350 microns.

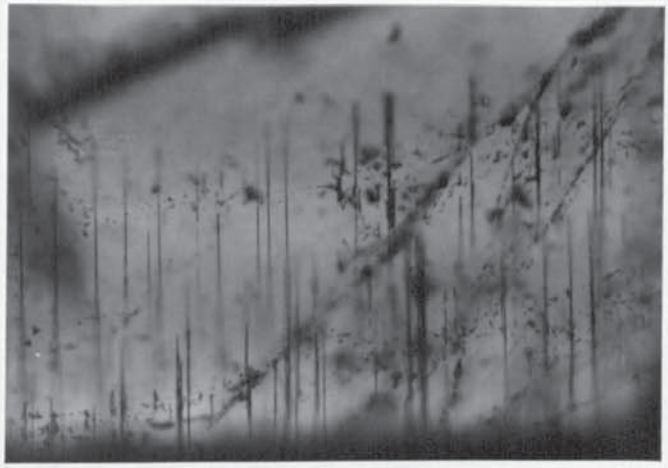

PLATE 6.20

Micrograph of *type-two* sphalerite with numerous tubular inclusions developed. Tube direction corresponds to crystal growth direction, namely [111] or equivalent. PPL Transmitted light. Field of view 560 microns.

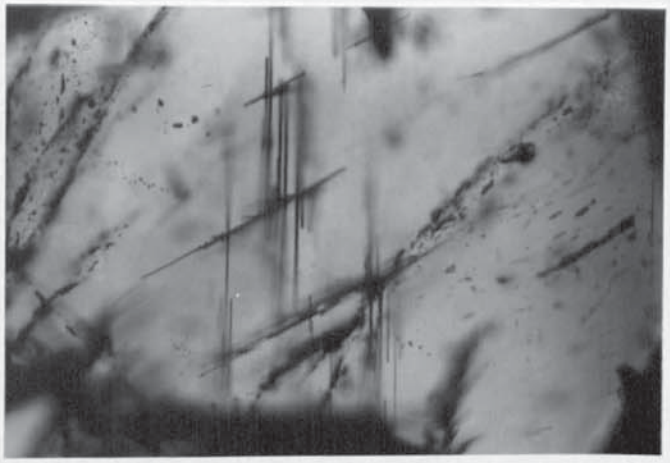

PLATE 6.21

Micrograph of *type-two* sphalerite containing numerous tubular inclusions. Three mutually perpendicular directions are apparent for tube development, with two of the three directions well developed. PPL Transmitted light. Field of view 560 microns.

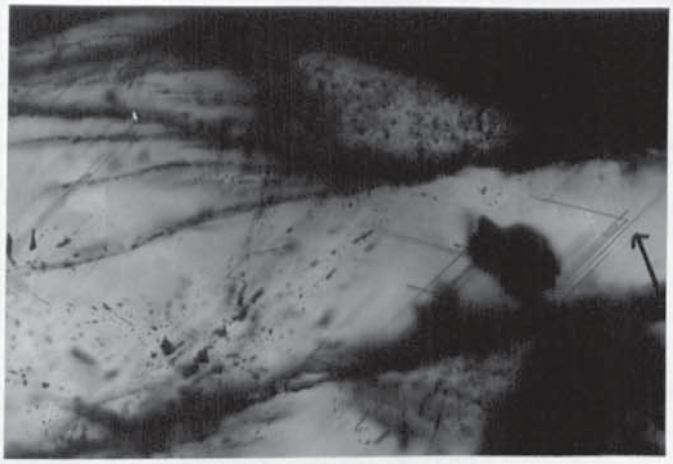

PLATE 6.22

Micrograph of *type-two* sphalerite with thin rod-like inclusions developed. Inclusions may change direction (arrowed) and thin to defect-like proportions (see text for discussion). PPL Transmitted light. Field of view 225 microns.

6.8. Electron Optically Observed Growth-Related Microstructures.

Electron optical studies of banded *type-one* material revealed a number of growth related microstructures. The majority of these microstructures may be related to band structure. In particular the development of numerous inclusions, localised (i.e. 'point') and planar defects is noted, within banded regions of sphalerite. Inclusions are observed to be both solid (stable under the electron beam) and volatile, i.e. liquid.

Solid inclusions are not widely developed. Recognised as areas of increased diffraction contrast, such inclusions vary in form from euhedral to subhedral or anhedral (plate 6.23). No relation between particle development and later, deformation-related, microstructures is apparent.

Certain regions of banded *type-one* sphalerite host numerous volatile inclusions, along with voids after the inclusions have vaporised out of the material. Voids range in size from 0.2 microns to 1.0 microns width, and from 0.6 to 3.0 microns in length. Plates 6.24 and 6.25 illustrate typical inclusion and void morphology. The majority of these inclusions develop a euhedral rectangular habit. Poorly developed corner facets are often present. The volatile inclusions probably represent sub-micron vapour-filled or fluid-filled inclusions. Associated with the inclusion-rich areas are 'ribbon-like' faults similar in appearance to stacking faults generated during crystal growth (Aragona and Delavignette, 1966). Such stacking faults are also apparent in regions rich in localised defects (see plate 6.26).

'Planar' and localised defects are seen throughout the banded *type-one* material. Localised defects are often accompanied by a pair of semi-circular strain fields, and regions of enhanced diffraction contrast (see plate 6.27). Regions characterised by localised defects are often associated with apparently planar defects (plate 6.27). These may represent sections lengthwise along the rod-like structures that comprise much of the banded material. They are observed to have a common strike across any one region imaged.

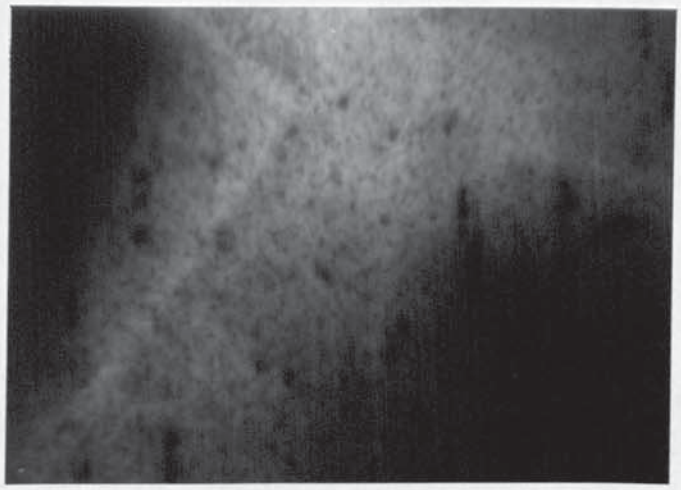

PLATE 6.23

Transmission electron micrograph of type-one sphalerite containing small unidentified particles (regions of enhanced diffraction contrast). No strain field is seen between the particles and the matrix. Field of view ~ 2 microns.

PLATE 6.24

Transmission electron micrograph of *type-one* sphalerite with voids developed after volatile inclusions. Sphalerite contains numerous ribbon-like stacking faults. Field of view ~ 2.6 microns.

PLATE 6.25

Transmission electron micrograph of voids in *type-one* sphalerite left by volatile, possibly aqueous, inclusions. A chain of dislocations may be seen between two of the voids (arrowed). Field of view ~ 4.3 microns.

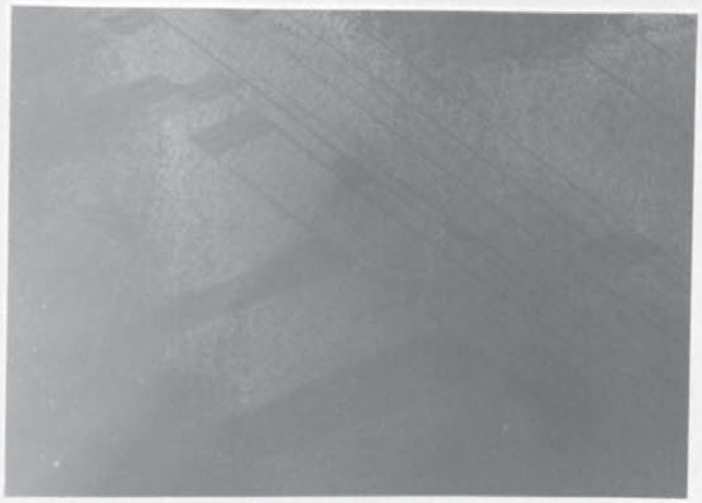

PLATE 6.26

Transmission electron micrograph of growth faults (stacking) in *type-two* sphalerite. Morphology of growth faults is distinctive and differs from the deformation fabrics of section 8.6. Field of view ~ 6 microns.

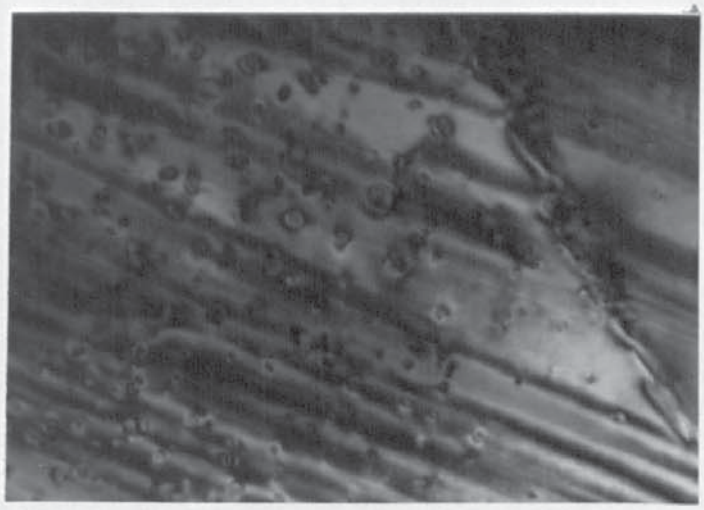

PLATE 6.27

Transmission electron micrograph of a region of *type-one* banded sphalerite with both localised defects and planar or rod-like defects developed. Planar defects strike perpendicular to crystal growth direction i.e. {111}. Localised defects have paired strain fields. Field of view ~ 2.5 microns.

6.9 XRD Studies of the Zinc Mineralisation.

Goniometric and Debye-Scherrer studies of powdered ZnS show the presence of only the 3C-sphalerite ZnS polytype. Reflections consistent with a wurtzitic component for the mineralisation are not recorded. For wurtzite the following principal reflections were searched for:

(100)	d_{th} = 3.309	(101)	d_{th} = 2.927
(110)	d_{th} = 1.911	(103)	d_{th} = 1.762
(002)	d_{th} = 3.128		

The (002) reflection for wurtzite is masked by the (111) reflection for sphalerite. Principal reflections indicating sphalerite were:

(111)	d_{th} = 3.123	(200)	d_{th} = 2.705
(220)	d_{th} = 1.912	(311)	d_{th} = 1.633
(400)	d_{th} = 1.351	(331)	d_{th} = 1.240
(422)	d_{th} = 1.034	(511)	d_{th} = 1.0403

Where d_{th} corresponds to the interplanar spacing for pure ZnS containing no impurities (see Vaughan and Craig, 1978). Measurement of the angles for the (331) and (422) reflections enables the cell edge for the sphalerite to be calculated from the Bragg equation given in equation (6.1).

$$\sin^2 \emptyset = \lambda^2 N (4a^2)^{-1} \qquad (6.1)$$

where λ = wavelength of the radiation Cu $k\alpha_1$ (5.40405×10^{-10} m).

$N = h^2 + k^2 + l^2$ for the reflecting plane.

a = the cell edge of the diffracting crystal.

$\emptyset$ = the angle corresponding to the Cu $k\alpha_1$ reflection.

For the reflection angles measured, variation was small. Cell edge values vary from a = 5.4094 Å to a = 5.4125 Å. Substitution of the cell edge values into equation (6.2) give the theoretical possible range of mole percentages for FeS and CdS substitution.

$$a = 5.4093 + 0.000456FeS + 0.00424CdS. \qquad (6.2)$$

FeS ranges 0 ~7 mole % CdS ranges 0 ~ 0.75 mole %

Observed FeS and CdS levels in the sphalerite do not differ significantly from the predicted ranges and generally lie within the ranges (see section 7.1).

CHAPTER 7: Analytical Studies and Copper Related Alteration.

7.1 Electron Microprobe Studies.

Type-one and *type-two* sphalerite were both analysed for the following elements; Zn, Cu, Fe, Sb, As, Cd, Ni, Co, Ag and S. Analytical conditions are as detailed in section 3.3.

7.1.1 *Type-One* Sphalerite.

For the *type-one* sphalerites analysed, nickel, cobalt, and silver were not detected. Arsenic is present, but at levels too low for the results to be reliable. Trace levels of copper and antimony are detected in much of the sphalerite. Also recorded are low levels of iron and cadmium.

Both the banded and unbanded regions were analysed. Differences in elemental concentrations are apparent between the bands and unbanded material. Figures 7.1a and 7.1b show iron and cadmium profiles respectively. A sharp rise in iron and cadmium levels is observed for the banded regions. Iron levels, generally around 2 wt. percent, rise in excess of 3 wt. percent. Cadmium levels, generally around 0.2 wt. percent, rise to greater than 0.6 wt. percent. Figure 7.4a shows the correlation between iron and cadmium.

Copper levels, generally between 0.1 and 0.3 wt. percent, show no consistent correlation with banded regions. Banded areas may host

higher or lower copper concentrations than the unbanded material.

Likewise antimony levels, generally around 0.1 to 0.15 wt. percent, may be enriched or depleted across the banded areas (figures 7.1c and 7.1d). For the banded sphalerite analysed (figures 7.3c and 7.3d) antimony and copper levels are lower in the banded regions. Whilst no consistent correlation may be deduced between banded regions and either antimony or copper levels, a correlation between antimony and copper levels is apparent in *type-one* sphalerite overall (figure 7.4b).

Typical analyses for *type-one* material are given in appendix 2. Unbanded regions show fairly constant levels of iron (approximately 1.5 wt. percent), and cadmium (around 0.25 wt. percent). Copper and antimony levels fluctuate; 0.1 to greater than 0.4 wt. percent for copper, and 0.1 to 0.25 wt. percent for antimony. A correlation between copper-rich areas and patchy areas of sphalerite alteration may be deduced (see section 7.3).

For the *type-one* sphalerite, no apparent relationship between the iron-cadmium trend and the copper-antimony trend may be deduced. The scatter in a plot of copper against iron (figure 7.4c) implies that the following two processes are unrelated:

1. Enrichment of iron and cadmium across the banded regions.
2. The sporadic enrichment of, or depletion of, copper and antimony levels across the banded regions.

7.1.2 *Type-Two* Sphalerite.

Silver, nickel, and cobalt are not detected in the *type-two* sphalerite. Arsenic and antimony are detected, but in levels too low to be considered reliable. Copper is detected in trace amounts, and iron and cadmium in minor amounts.

Banded areas were systematically probed for elemental variations, particularly of cadmium, copper and iron. All three elements show some relation to band development.

Levels of iron increase with the intensity of band colour. Low levels of iron (1 to 2 wt. percent) correlate with the paler coloured varieties (e.g. pale yellow bands), whilst higher levels of iron (5+ wt. percent) correspond to the darker orange and red-brown sphalerite varieties (figure 7.2a). Figure 7.2b shows that cadmium behaves likewise. A plot of cadmium against iron shows a positive correlation (figure 7.5b).

Copper values show some correlation with band colour. The darkest bands host little, if any, copper, whilst the paler bands may host up to 0.35 wt. percent (figure 7.2c). A plot of copper against iron confirms this trend (figure 7.5a).

Typical probe analyses of *type-two* sphalerite are given in appendix 2.

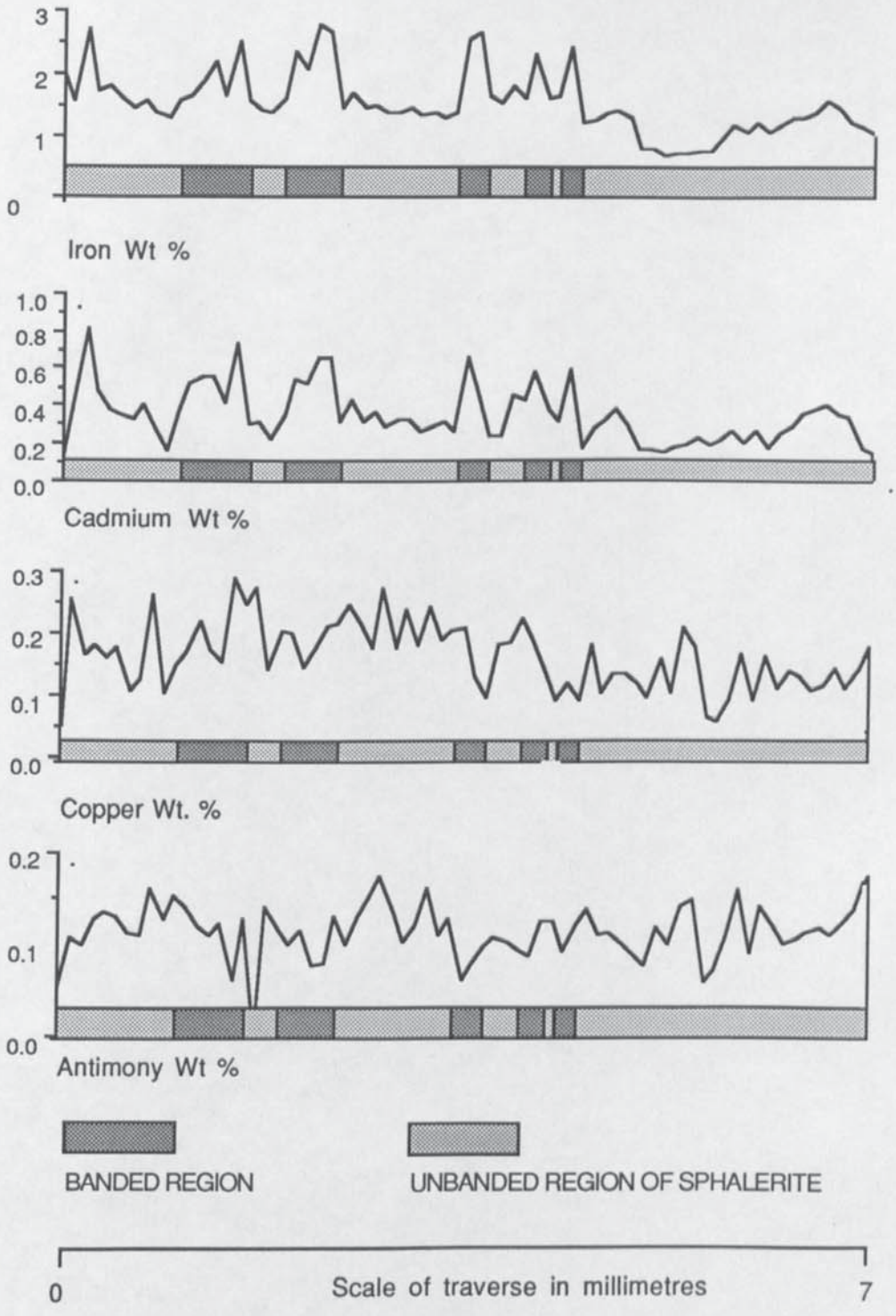

FIGURE 7.1

Element profiles across *type-one* banded sphalerite. Data of appendix 2 (NH06 B1).

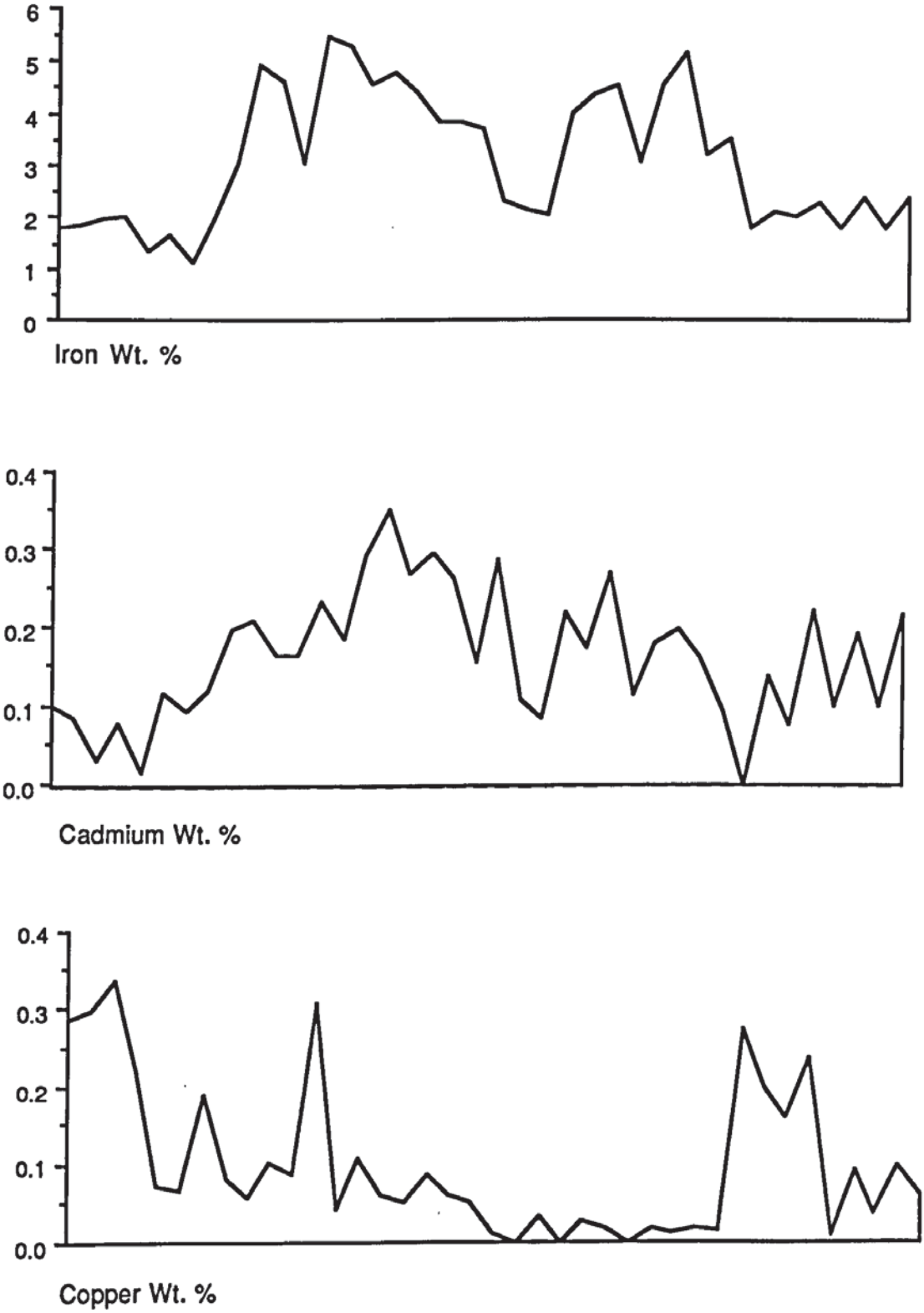

FIGURE 7.2

Element profiles across *type-two* banded sphalerite. Traverse is approx 4 millimetres across. Data of appendix 2 (NH06 B2 Set 2).
a. Iron variation. b. Cadmium variation. c. Copper variation.

7.1.3 *Type-one* and *Type-two* Sphalerite: A Comparison.

Concentration profiles for the trace metals were obtained from a region of banded *type-one* sphalerite developed adjacent to a banded region of *type-two* sphalerite. From the data collected (appendix 2) a number of observations can be drawn:

1. Iron and cadmium concentrations differ between the two sphalerite types (figure 7.3a and b). *Type-two* sphalerite is relatively enriched in iron. However, as illustrated in figure 7.3b, the reverse trend is true for cadmium; *type-one* is relatively enriched. Both generations show the same positive correlation between iron and cadmium for any one generation.

2. Both antimony and copper levels are relatively enriched in *type-one* sphalerite. *Type-two* sphalerite is devoid of antimony altogether (figures 7.3c and d)

3. Both antimony and copper levels are greatly enriched in the region where a prominent dissolution surface separates the two generations of sphalerite.

4. Two different processes act to govern copper distribution: in *type-one* sphalerite copper values show an occasional correspondence to band development, and a positive correlation with antimony but in *type-two* material copper is inversely related to and does not correlate with antimony.

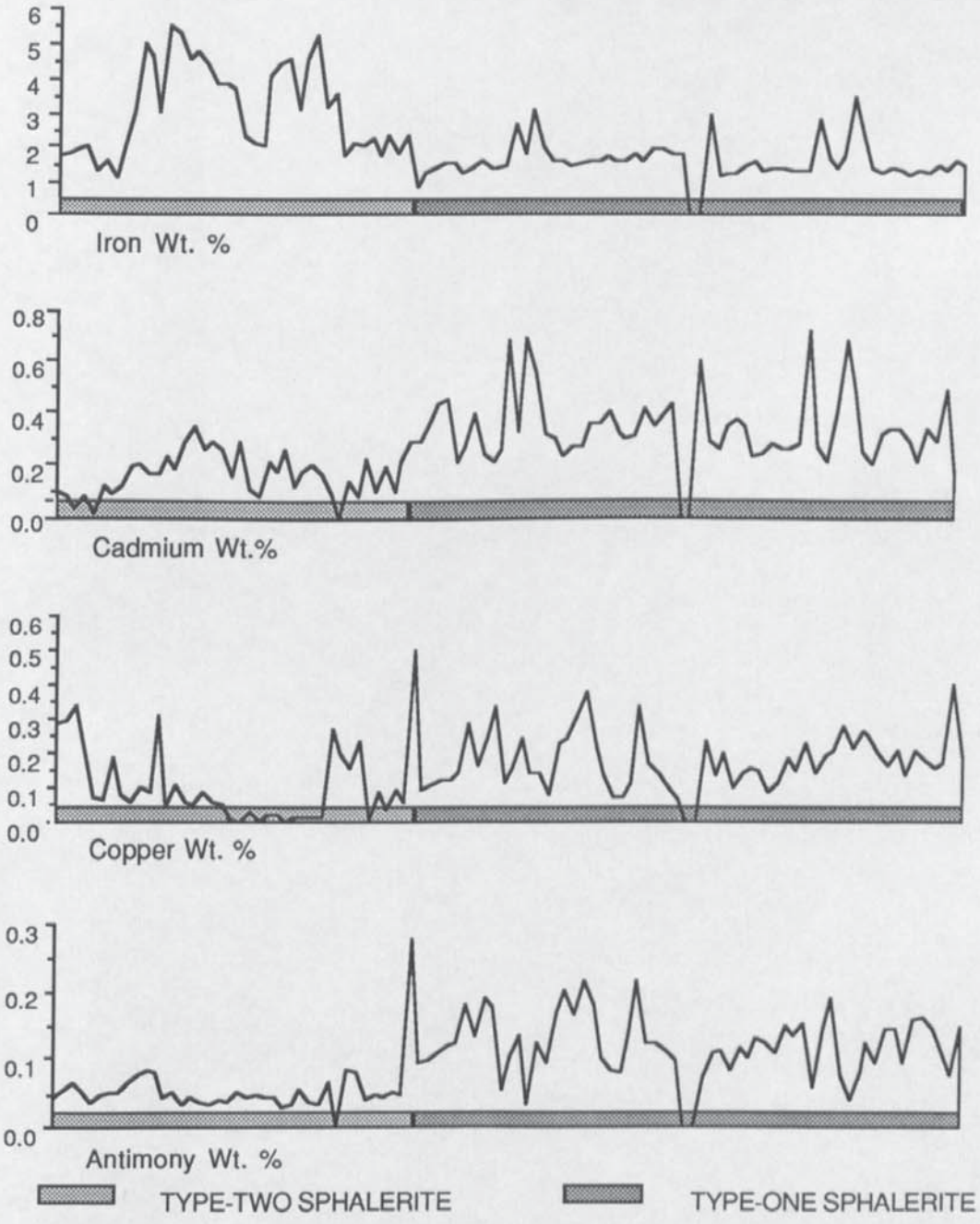

FIGURE 7.3

Comparative elemental profiles across a region of type-one banded and type-two banded sphalerite. Data of appendix 2 (NH06 B2, Sets1 and 2).

a. Iron variation. b. Cadmium variation.
c. Copper variation. d. Antimony variation.

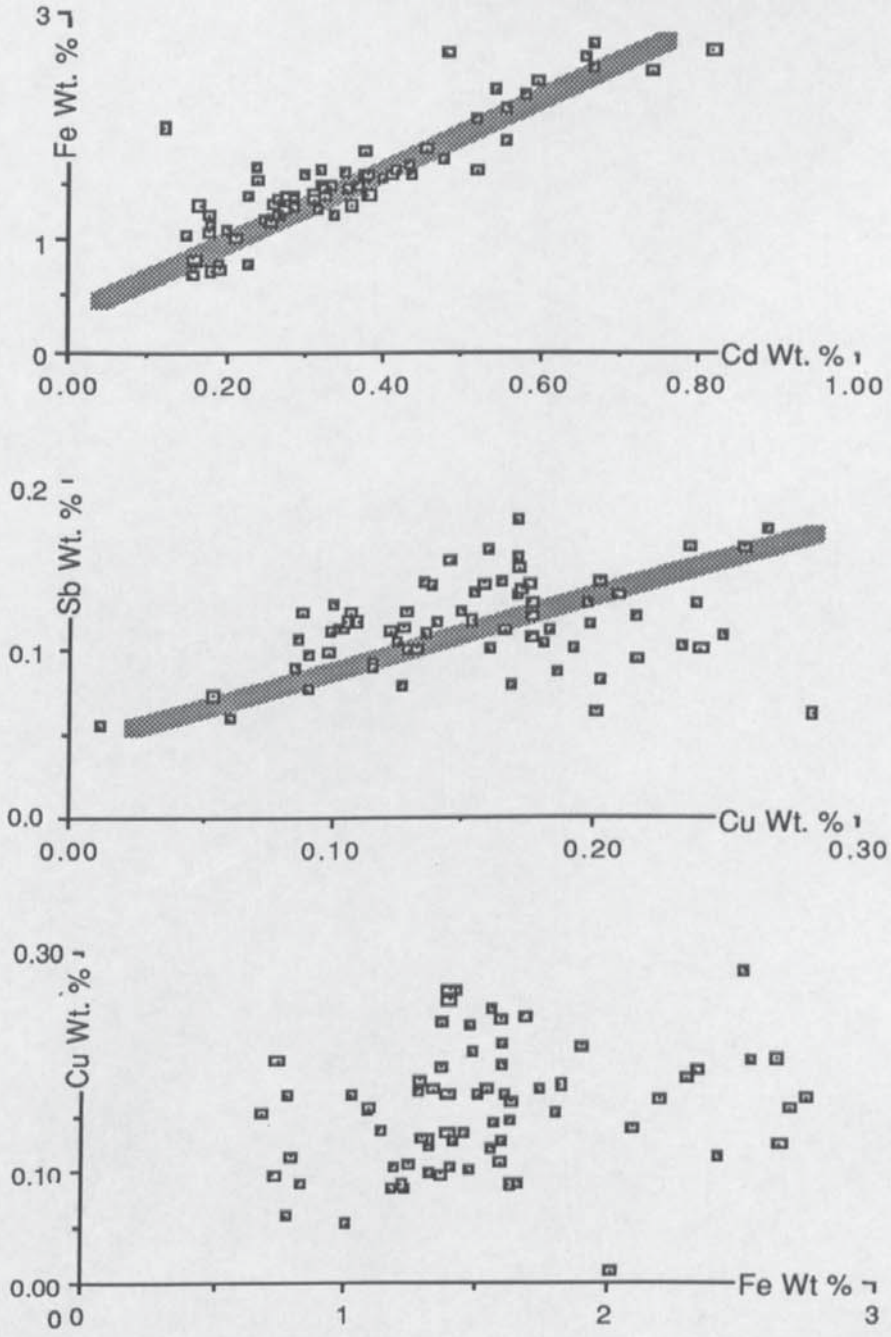

FIGURE 7.4

Variation diagrams for a) *Type-one* sphalerite: Iron verses cadmium.
b) *Type-one* sphalerite: Antimony verses copper.
c) *Type-one* sphalerite: Copper verses iron.

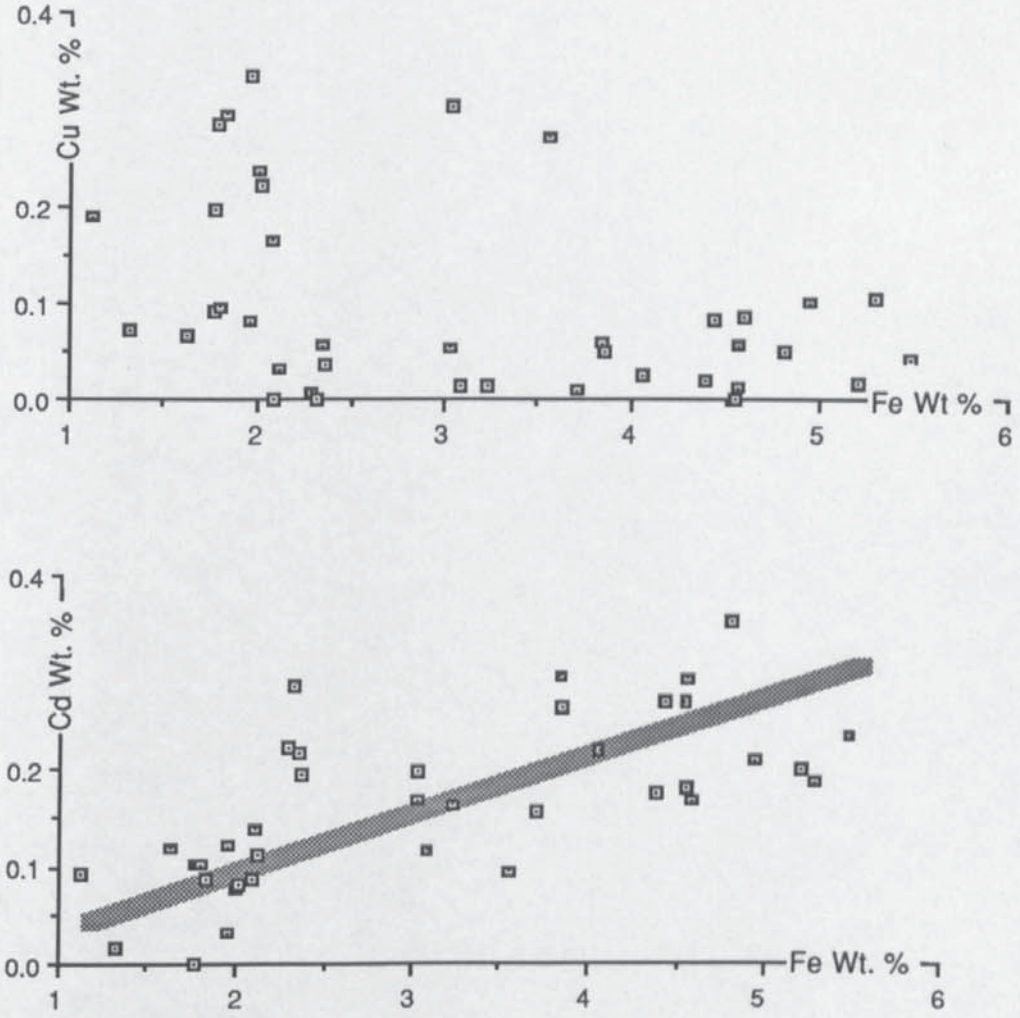

FIGURE 7.5

Variation diagrams for a) *Type-two* sphalerite: Copper verses Iron.
b) *Type-two* sphalerite: Cadmium verses Iron.

7.2 Organic Studies.

Petrographic and analytical work was undertaken to test for the presence of organic matter within the Pennine sphalerite. In particular, banded regions of *type-one* sphalerite were examined. Also examined were some of the larger semi-opaque inclusions. Following the procedures outlined in section 3.4.1, the samples were viewed using an ultraviolet petrographic microscope to detect any luminescent phases present (hydrocarbon and other organic phases). For regions of banded *type-one* material, additional analytical work was undertaken using F.T.I.R. spectroscopic techniques (see section 3.4.2).

Neither the banded material nor the semi-opaque inclusions luminesced under the ultra-violet beam. It would appear that neither the bands nor the inclusions contain any detectable organic content (the inclusions are further discussed in section 7.4).

Due to the inverse relation shown between the intensity of phase luminescence and the maximum temperature attained by the hydrocarbon phases, the banded material was examined spectroscopically (F.T.I.R) in the hope of detecting any hydrocarbons that had suffered heating. Electron microprobe studies of the banded material (section 7.1) show the bands to host a range of trace metals, particularly cadmium. A correlation between cadmium and organic-banded material has been reported for many M.V.T. ores (e.g. Craig, Solberg and Vaughan, 1983).

F.T.I.R. spectroscopic analysis of *type-one* samples was undertaken by Dr. A. Gize at the Geophysical Laboratory, Carnegie

Institution, Washington D. C., for both banded and unbanded material. The spectral profiles are given in figure 7.6, and 'ratioed' in figure 7.7. 'Ratioing' of the two profiles reveals little difference between the banded and unbanded material. Also absent is any spectroscopic indication of a carbon or hydrocarbon component (i.e. the absence of strong bands in the region 3000-2700 cm^{-1} for methyl and ethyl groups, the absence of strong bands in the region 2700 cm^{-1} for aromatic groups, and the absence of bands in the region 1750-1700 cm^{-1} for C=O groups).

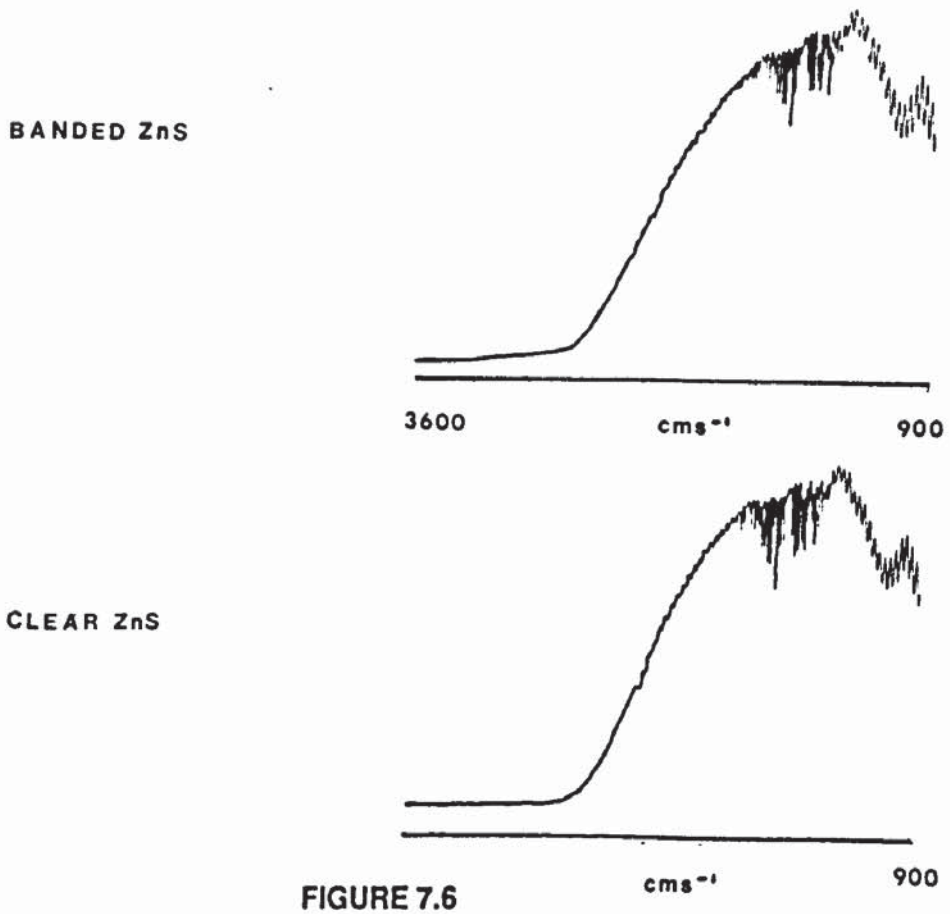

FIGURE 7.6

F. T. I. R. Spectroscopic (transmittance) profiles of banded and unbanded regions of *type-one* sphalerite from the Nenthead Area (sample NP 06).

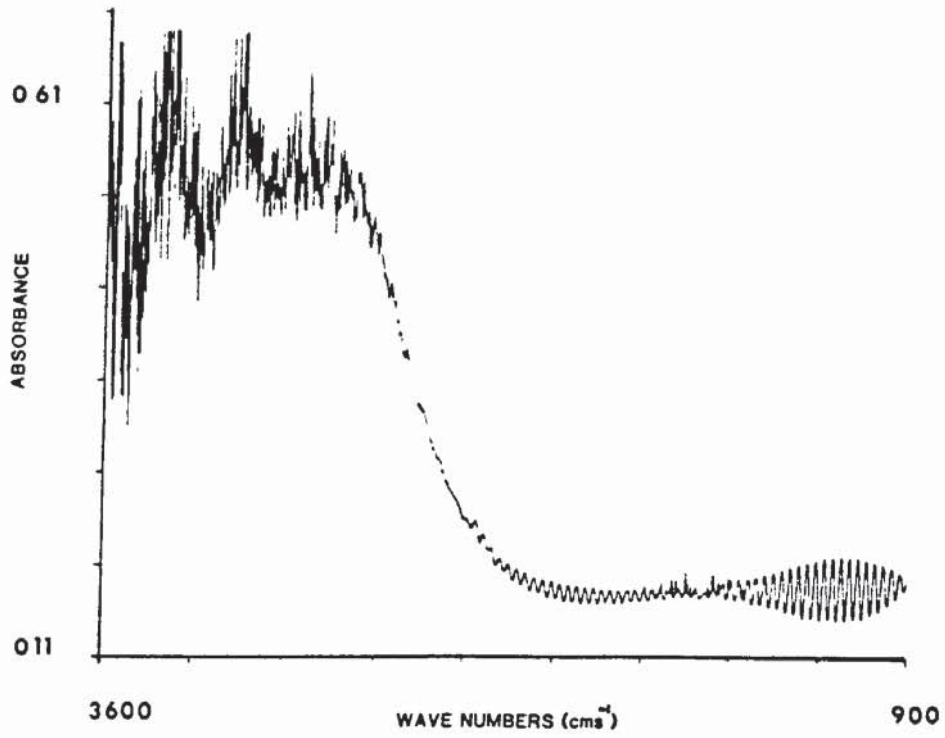

FIGURE 7.7

Ratioed absorption spectral profile from the banded and unbanded *type-one* sphalerite. Little difference is observed in the spectra obtained from the banded and unbanded material, and no banding due to organic groups.

It is concluded that banded *type-one* material is devoid of any hydrocarbon content. Also apparent from the spectroscopic profiles is a low concentration of additional phases present (if any) in the banded material, relative to the unbanded material.

7.3 Fluid Inclusion Thermometric Analysis.

Heating and freezing data obtained during thermometric analysis of quartz-hosted fluid inclusions (two-phase) along with heating data from sphalerite hosted two-phase inclusions are presented. The extensively altered sphalerite proved unsuitable for freezing studies due to the small size of the primary inclusions. Freezing data from the quartz-hosted inclusions is indicative of a highly saline mineralising fluid that contains other salts in addition to NaCl.

Heating results obtained from Quartz-hosted inclusions

Homogenisation temperatures for sphalerite -containing quartz grains are presented in figure 7.8. A narrow temperature range is apparent with a bimodal inclusion population recognised. Optically no difference is discernible between the inclusions that comprise the two populations. Homogenisation temperatures range from 101.4 °C. to 130.7 °C. (mean = 110.8 °C., Sd = 6.8, n = 54) with the majority between 101.4 °C. and 120.1 °C., and a small cluster centred around 130.7 °C. Typical errors of measurement are less than ±1.75 °C.

For the two populations recognised:

mean T_{h1} =104.1 °C. Sd_1 = 1.49 n_1 = 18

mean T_{h2} =114.2 °C. Sd_2 = 5.80 n_2 = 36

Temperatures of homogenisation are considered as representative of a minimum temperature for gangue quartz deposition. Corrections for overburden pressure-related effects are considered below.

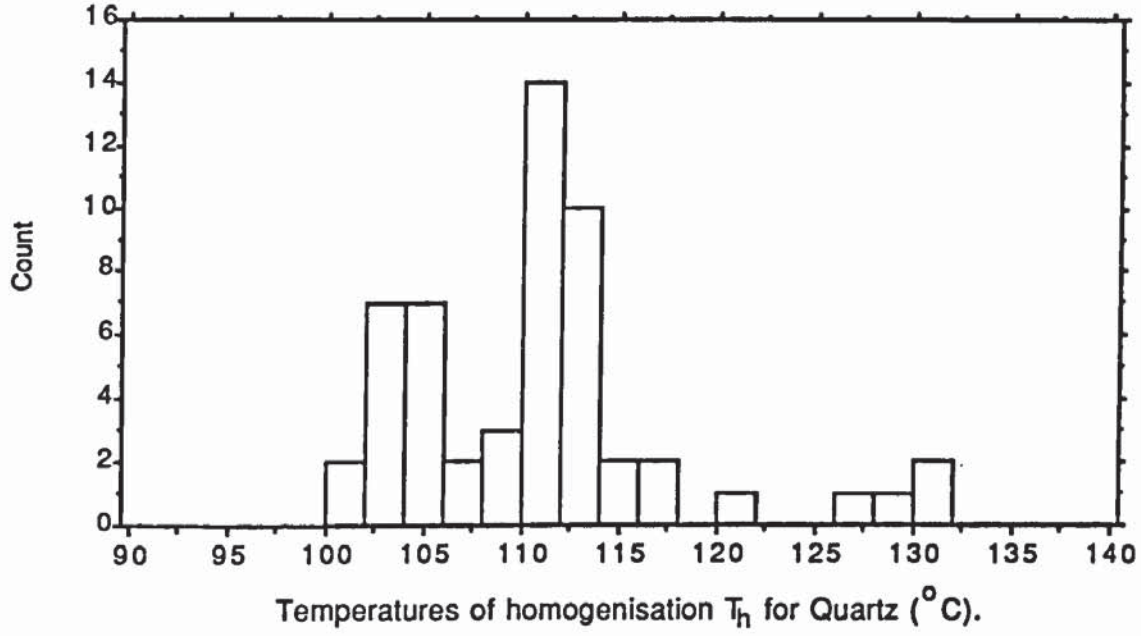

FIGURE 7.8

Histogram showing range of homogenisation temperatures for two-phase fluid inclusions from sphalerite bearing gangue quartz.

Heating results obtained from sphalerite-hosted inclusions.

Homogenisation temperatures for sphalerite-hosted two-phase inclusions are presented in figure 7.9. A narrow temperature range is recorded, from 93.4 °C. to 101.7 °C. (mean = 102.4 °C. Sd = 4.31 n = 24), with apparently two populations (as in quartz). One population is centred around 97 °C. (n = 7), the second around 105 °C. (n = 16). The recognition of a bimodal distribution must be tentative in view of the small data set.

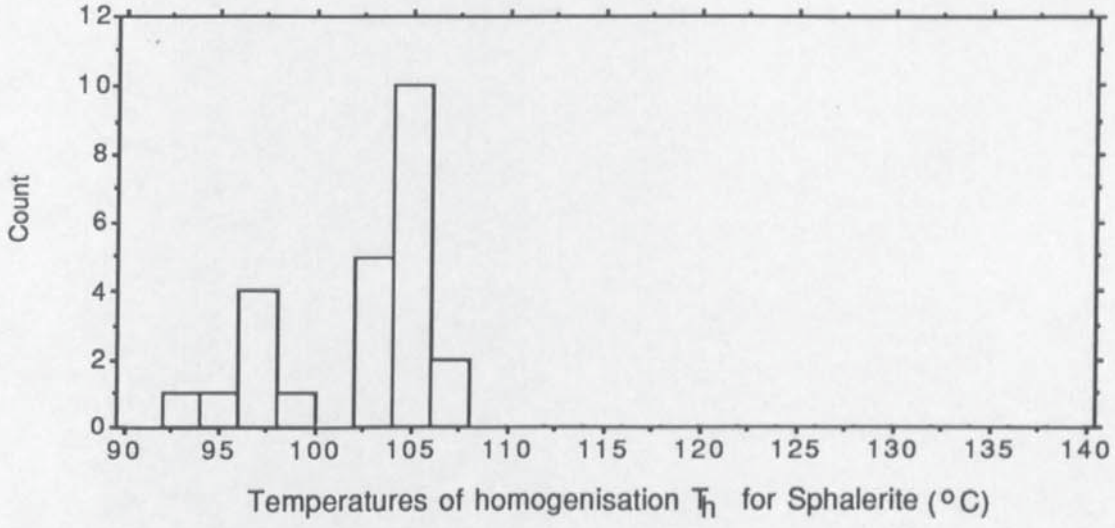

FIGURE 7.9

Histogram showing range of homogenisation temperatures for two-phase fluid inclusions from sphalerite mineralisation.

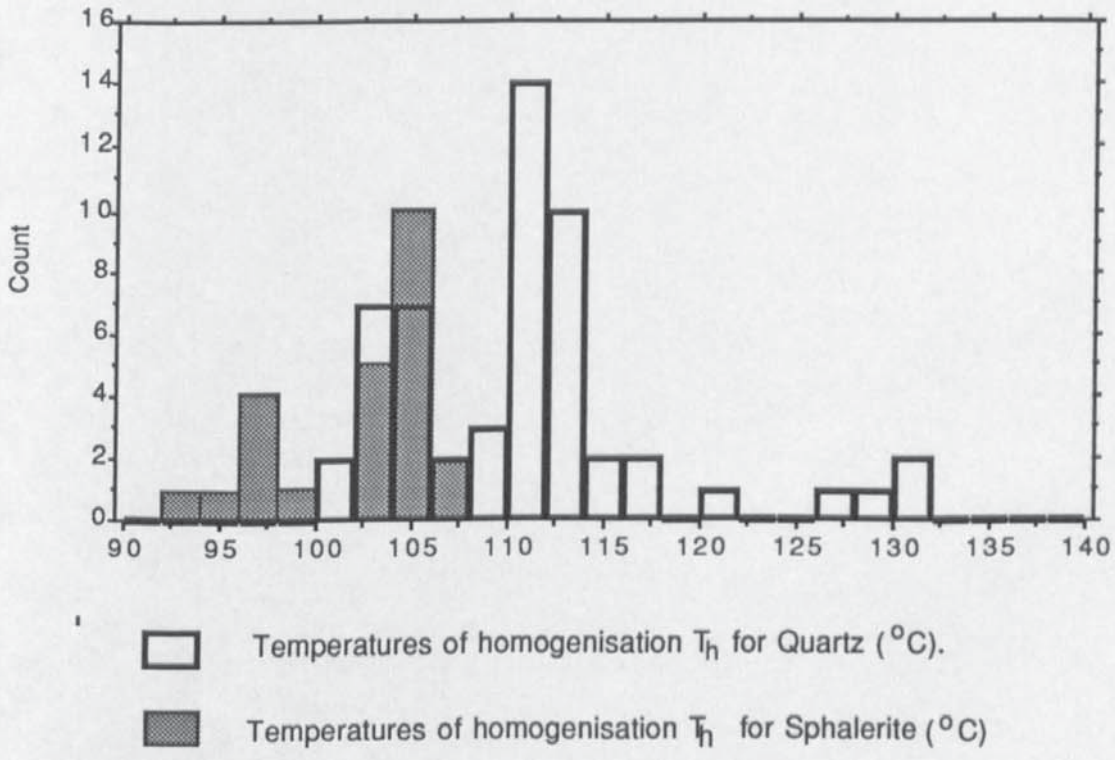

FIGURE 7.10

Histogram showing the degree of overlap in homogenisation temperatures from two-phase inclusions in the sphalerite and accompanying gangue quartz mineralisation.

Homgenisation temperatures for the quartz-hosted and sphalerite-hosted inclusions overlap (figure 7.10). Mineralization temperatures for sphalerite and accompanying gangue quartz are considered as approximately the same for the purposes of discussion (in a 'regional' or geological context- i.e. ch. 9).

Freezing results obtained from quartz-hosted inclusions.

Temperatures for the final melting of ice (depression of freezing point DFP) for quartz-hosted two-phase inclusions are presented in figure 7.11. DFP temperatures range from -22.3 °C. to -17.1 °C. with no apparent distribution peak (mean = -19.9 °C., Sd = 1.92, n = 14). Errors of measurement are typically less than ± 0.5 °C.

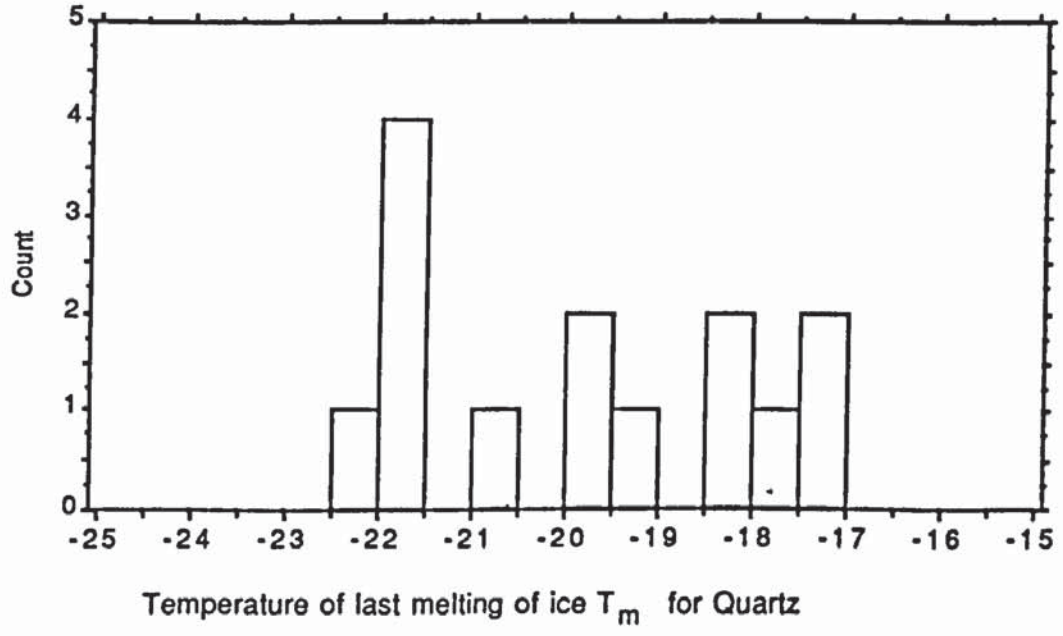

FIGURE 7.11

Histogram showing the range of temperatures (°C) for last melting of Ice for two-phase inclusions in sphalerite-bearing gangue quartz.

The range in DFP temperatures encompasses the eutectic temperature (-20.8 °C.) for the NaCl-Water system (see figure 7.12) implying the presence of other salts in solution in addition to NaCl. The presence of small amounts of other salts is reported as having little effect upon the DFP temperatures. The fluid salinity is estimated by treating the solution as a simple NaCl solution (Roedder, 1984). Potter and Brown (1977) relate the freezing point depression to the fluid salinity for a simple NaCl solution as below:

$$W_s = 1.76958Ø - 4.2384x10^{-2} Ø^2 + 5.2778x10^{-4} Ø^3 \ (\pm 0.028) \qquad (7.1)$$

where Ø is the depression of freezing point in °C.

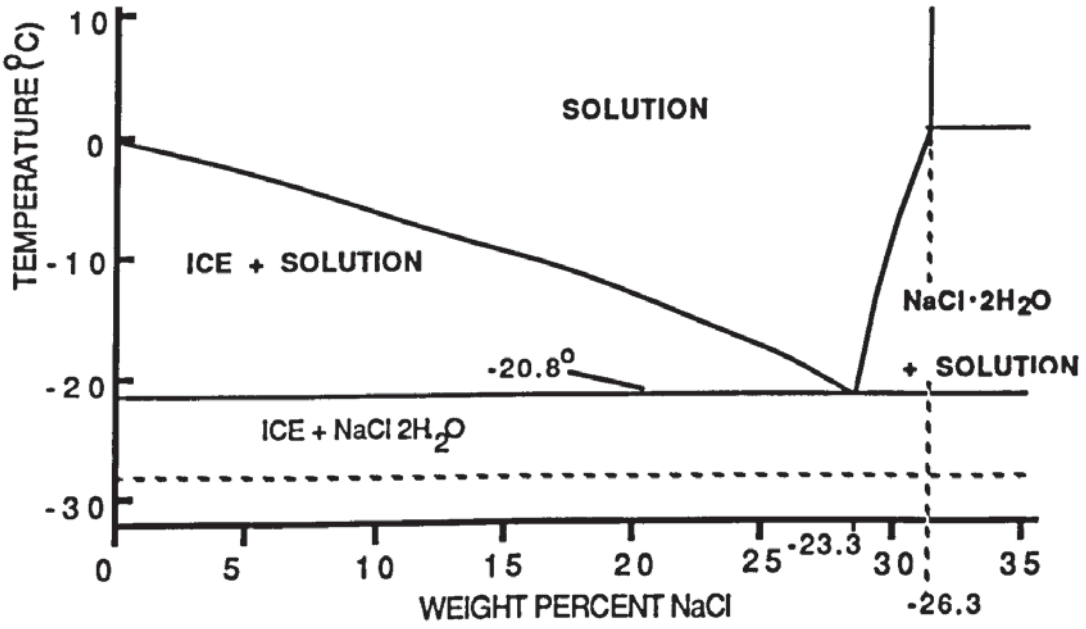

FIGURE 7.12

Temperature composition diagram for part of the NaCl-H_2O System showing the main phases developed at low temperatures.

A temperature of -17.1 °C. corresponds to a salinity of approximately 20.5 wt. % equivalent NaCl, and the mean temperature (-19.9 °C) implies a salinity of approximately 22.6 wt. % equivalent NaCl. The absence of daughter minerals at room temperature, namely NaCl, suggests the salinity to be less than 26.48 wt. % equivalent NaCl (Roedder, 1984).

Pressure-related corrections for temperatures of homogenisation.

Temperatures of homogenisation represent possible minimum temperatures for inclusion trapping (i.e. for primary inclusions the temperature of mineralisation). Such temperatures need to be corrected for overburden pressures present at the time of entrapment if they are to be used to model possible mineralisation temperatures.

If the maximum overburden of 1100 metres of Sawkins (1966) is assumed to be correct then possible pressures at the time of inclusion trapping are estimated from equation 7.2:

$$\text{The overburden pressure} \quad P = Hpg \qquad (7.2)$$

Where H = thickness of overburden

g = acceleration due to gravity

p = density of overlying material (1.00 g cm^{-3} for hydrostatic load; 2.70 g cm^{-3} for lithostatic load).

If a 100 % lithostatic overburden component is assumed P ~ 290 bars.
If a 100 % hydrostatic overburden component is asssumed P ~ 110 bars.

The true value for the overburden will lie between the two extremes above. Previous studies (i.e. Sawkins, 1966) use an intermediate value of 200 bars. However maximum and minimum values of 290 bars and 110 bars are also considered here. Using the data of Haas (1976) and Potter and Brown (1977) liquid-vapour curves with the relevant isochores are constructed for 20 wt. % and 25 wt. % equivalent NaCl (figures 7.13 and 7.14). Pressure-temperature corrections taken from figures 7.13 and 7.14 are given in table 7.1.

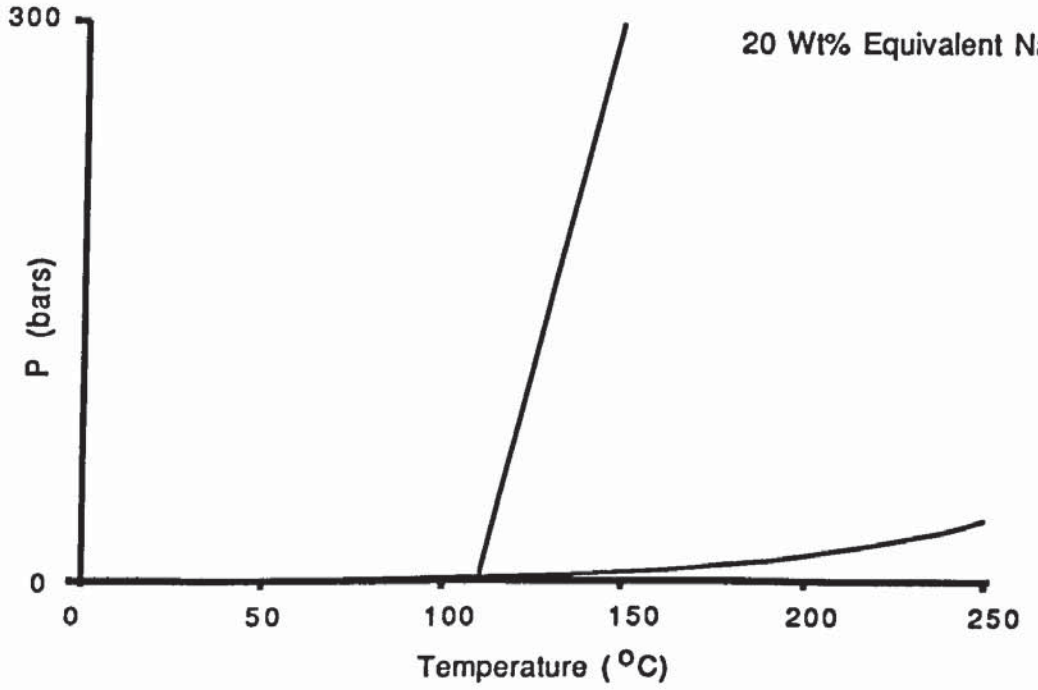

FIGURE 7.13

Pressure-temperature correction curve for 20 wt. % equivalent NaCl

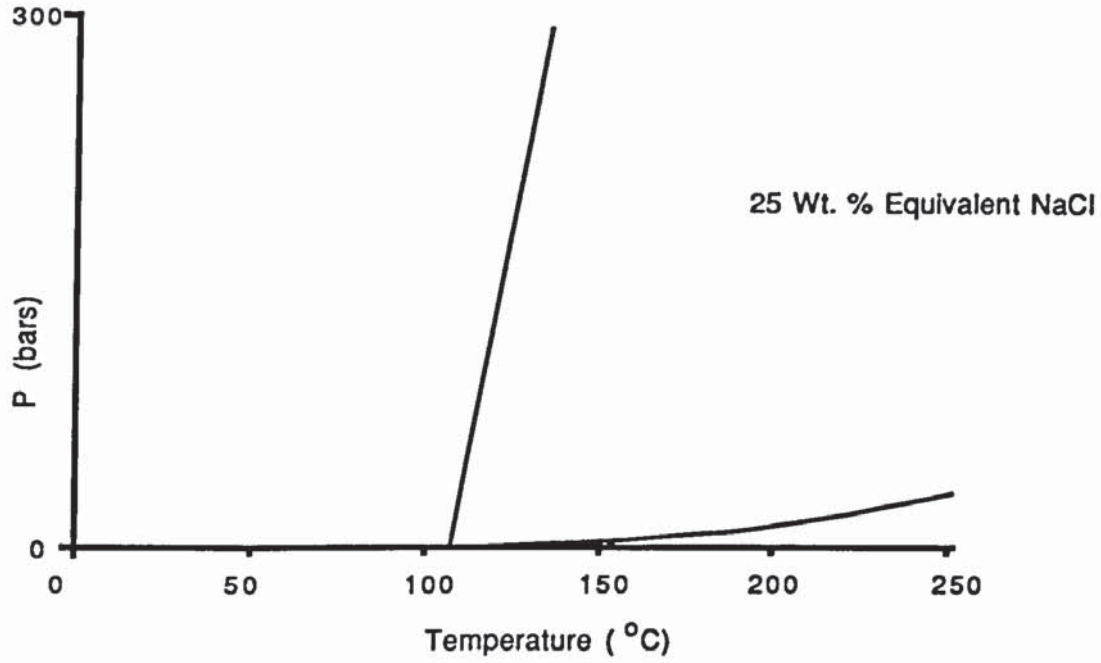

FIGURE 7.14

Pressure-temperature correction curve for 25 wt. % equivalent NaCl

Pressure	P (bars)	Salinity of fluid	Temperature correction
100 % Lithostatic	290	20 wt .% NaCl	37 °C
		25 wt .% NaCl	28 °C
100 % Hydrostatic	110	20 wt .% NaCl	13 °C
		25 wt .% NaCl	12 °C
Sawkins (1966)	200	20 wt .% NaCl	24 °C
		25 wt .% NaCl	24 °C

Table 7.1

Range of fluid inclusion homogenisation temperature corrections.

In summary, thermometric studies of the two-phase fluid inclusions indicate a low temperature, highly saline (20 to 25 wt. % equiv. NaCl) mineralising fluid. The minimum average temperature of homogenisation is approximately 100 °C. for sphalerite and a slightly higher 110 °C. for gangue quartz. The true temperature of mineralisation is higher, with the actual value dependent on the nature and degree of overburden-related temperature correction employed. A maximum possible correction of up to 40 °C. may be added to the homogenisation temperatures if a lithostatic load of 1100 metres is assumed.

Errors of temperature measurement (less than ± 2 °C.) are insignificant when contrasted with the uncertainty in mineralisation temperatures due to overburden-related pressure (between 12 and 40 °C.). In considering the effect of depositional environment on mineral textures and microstructures, temperatures between 100 and 150 °C will be considered. If the pressure correction of previous studies (i.e. P = 200 bars) is used then mean temperature for mineralisation is 122 ± 12 °C. (for discussion of temperature uncertainty see Sawkins, 1966).

7.4 Copper Related Alteration of Sphalerite.

Alteration of sphalerite, resulting in a cuprian variety, is recognised optically by the development of a distinctive texture, apparent only in transmitted light. Altered regions are characterised by small opaque triangular patches within the sphalerite. These occasionally occur singly, but typically in clusters. Patch size ranges from less than 5 microns to greater than 100 microns across. Altered areas often take on a planar form that comprises numerous co-planar patches. A stack-like form composed of numerous triangular patches stacked on each other is also observed. Both alteration textures are sporadically seen in both *type-one* and *type-two* sphalerite.

Individual triangular patches tend to be diffuse, with at best only one sharp edge. Plate 7.1 illustrates a typical co-planar triangle assemblage. Elongation of some patches occurs at the expense of the common triangular morphology.

Many of the stack-like textures are associated with healed micro-cracks. The axis of the "stalk" created bears no apparent crystallographic relation to the host sphalerite. Plate 7.2 shows such a "stalk" composed of well-developed triangular patches. Not all the "stalks", however, comprise such well developed triangular patches (plate 7.3).

The smaller patchy areas of alteration may coalesce giving rise to opaque regions several hundreds of microns across (plate 7.4). These extensive areas of alteration are more suited to electron probe and electron optical examination than the individual triangular patches. Chalcopyrite is rarely seen in these regions except where the

sphalerite is cross-cut by major fractures, which may host occasional small chalcopyrite grains.

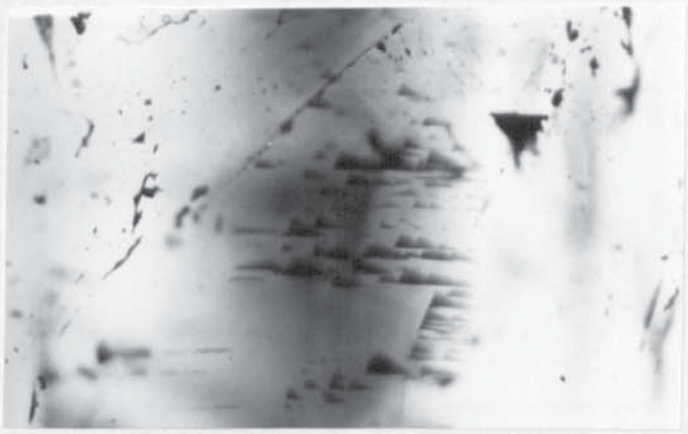

PLATE 7.1

Coplanar development of small triangular patches due to Cu-related alteration of sphalerite. PPL transmitted light. Field of view 1125 microns.

PLATE 7.2

"Stalk" composed of stacked triangular patches due to Cu-related alteration of sphalerite. PPL transmitted light. Field of view 560 microns.

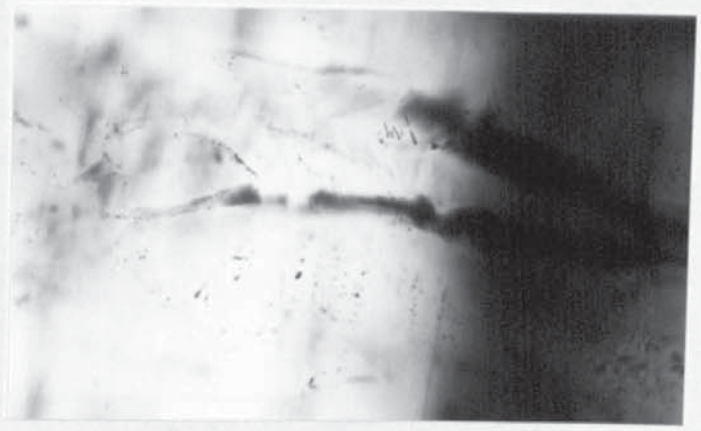

PLATE 7.3

"Stalk" composed of stacked patches due to Cu-related alteration of sphalerite. Characteristic triangular patch morphology is absent. PPL transmitted light. Field of view 560 microns.

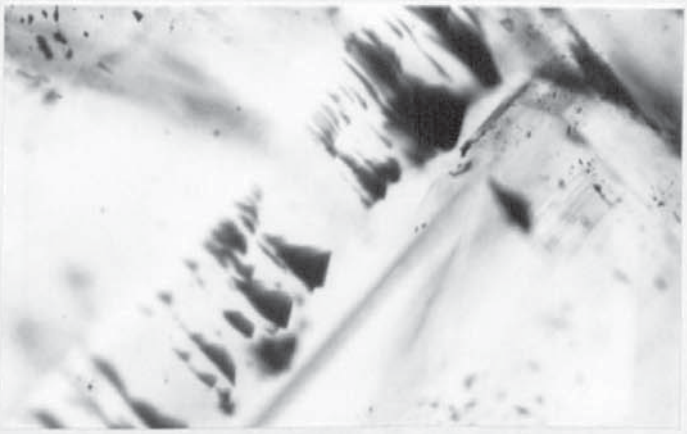

PLATE 7.4

Narrow band subject to development of Cu-related alteration patches. Some of the smaller triangular patches coalesce to create more extensive regions of alteration. PPL transmitted light. Field of view 1125 microns.

Electron microprobe analysis of the larger opaque patches indicates some copper enrichment and a slight antimony enrichment. No cadmium or iron enrichment, however, is recorded for these cuprian regions, unlike the growth-banded regions (section 7.1). Typical analyses for the cuprian regions are given in table 7.2.

Many of the heavily altered areas are associated with either some form of dissolution surface, micro-crack, or prominent glide or twin-plane. Rarely is the alteration associated with chalcopyrite euhedra in the sphalerite, or with chalcopyrite anhedra in gangue filled cracks. Some of the smaller chalcopyrite grains within the sphalerite are in areas of patchy alteration.

Transmission electron microscopy of the opaque patches confirms an alteration origin. Electron microscopy also reveals an apparent relation between the alteration texture and deformationally induced textures. Electron microscopy documents the presence of sub-micron euhedral patches within the sphalerite, developed along with regions subject to more extensive alteration. The more extensive altered regions were semi-quantitatively analysed using an analytical electron microscope. Antimony, not indicated on spectral profiles, was not analysed for.

Plate 7.5 details a region of sphalerite that hosts both small euhedral alteration patches, and a more extensive alteration. Much of the alteration is observed to develop along the planar microstructure, here comprising {111} twin planes, produced by crystal deformation (see section 9.6 for possible textural origins). Texturally, the alteration appears to have exploited the deformation microstructure, by using the planes as channelways either for the diffusion of copper,

or for the passage of copper-bearing fluids.

Semi-quantitative analytical electron microscopy of the altered regions confirms the cuprian nature suggested by the data of table 7.2. Analysis takes the form of a traverse from an unaltered region to the core of the altered region. The background effect due to the sphalerite host may then be corrected for, assuming no zinc component is present in the alteration mineralogy. The data in figure 7.15 imply a copper-rich, sulfur-deficient, alteration assemblage. For zero percent zinc, i.e. zero percent matrix, the alteration mineralogy is inferred to contain greater than 70 percent copper along with no sulfur. The assemblage probably comprises copper carbonates, copper hydroxides or a mixture of both.

The presence of non-sulfide bearing alteration assemblages suggests a supergene environment of alteration, rather than alteration by a late-stage Cu-bearing ore-fluid.

PLATE 7.5

T.E.M. micrograph of Cu-altered region of sphalerite. Alteration is seen developed along twin and slip-planar fabric. A.T.E.M. analysis details a Cu-rich S-deficient alteration mineralogy. Field of view ~ 5.4 microns.

Zn	65.40	64.59	64.01	63.62	63.61	63.65	64.44
Cu	0.51	0.23	0.25	0.31	0.38	0.34	0.41
Fe	0.81	1.59	1.48	1.53	1.57	1.65	1.62
As	0.12	0.06	0.05	0.13	0.04	0.05	0.06
Sb	0.30	0.30	0.24	0.27	0.27	0.31	0.49
Cd	0.28	0.17	0.20	0.17	0.22	0.22	0.08
S	32.24	32.93	33.07	32.91	32.97	32.93	32.54
TOTAL	99.66	99.89	99.30	98.94	99.06	99.15	99.64

Table 7.2

Typical electron microprobe analyses for copper-related alteration patches developed within the Nenthead sphalerite. Analyses are taken from *type-one* altered material and are given in wt. percent.

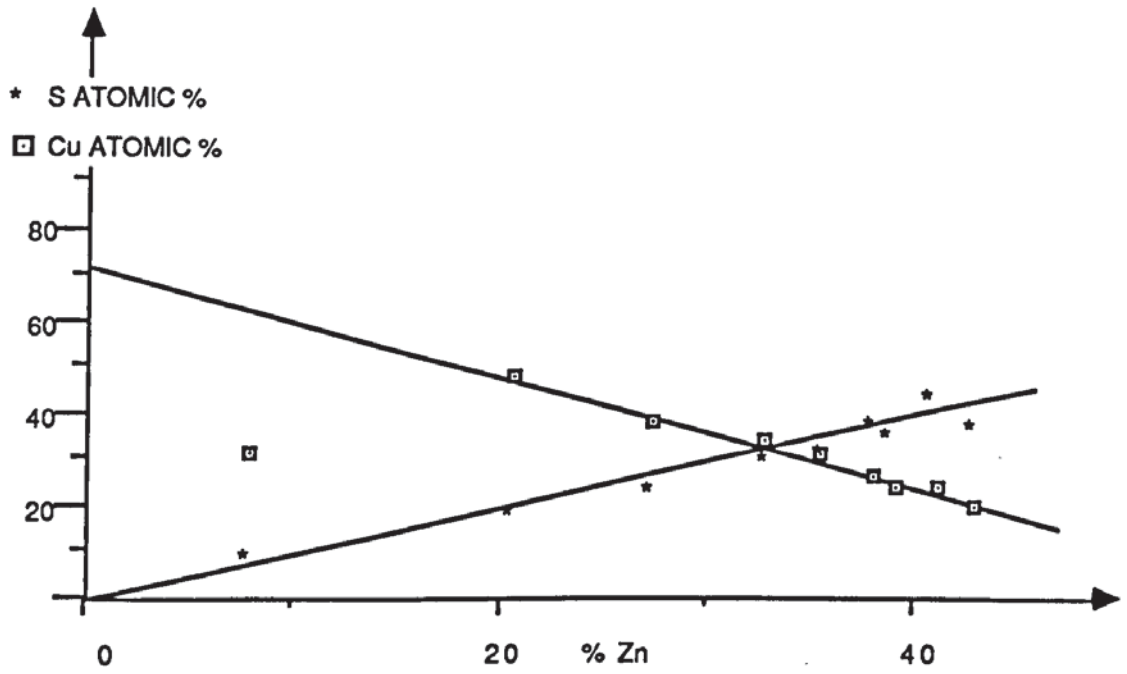

FIGURE 7.15

A.T.E.M. data for cuprian region of type-one sphalerite. Regression of the data to 0 % matrix (i.e. 0 % zinc) indicates a copper-rich, sulfur-deficient, alteration mineralogy.

CHAPTER 8: General Petrography Part Two: Deformation Microstructure, Twinning and Anisotropy.

Both brittle and ductile deformational processes are observed to have acted upon the sphalerite ores. Brittle deformation, chiefly manifest as brecciation and fracturing of the sphalerite ore, occurs both on a large scale and within individual grains. Ductile deformation, principally intracrystalline, is apparent when the ores are examined with a combined reflected and transmitted light petrographic microscope. Deformationally-induced strain is indicated by the development of twin- and slip-plane related fabrics. Also apparent locally is some minor recrystallisation of the sphalerite ore. A pronounced optical anisotropy is observed throughout the sphalerite.

8.1 Brittle Deformation.

Examination of doubly-polished thin sections of the ore reveals fracturing to be widespread, with brecciation of both the host rock and the mineralisation.

8.1.1 Intercrystalline Fracture and Brecciation.

Examination of the veined-ore samples reveals fracturing and brecciation of the silicified wall rock. The rock was originally a crinoidal micritic carbonate but has undergone silicification, fracturing, and brecciation, which is assumed to have occurred prior

to the main mineralising events. A variety of sharp, angular fragments, ranging in size from less than one millimetre to greater than twenty millimetres, are observed, set in a gangue and ore-mineral matrix (figure 8.1). Repeated fracturing with subsequent ore and gangue deposition has locally created an ore-breccia similiar in character to many reported for carbonate hosted lead-zinc deposits (e.g. Ohle, 1985).

Large fractures running throughout the vein ores may be traced for tens of centimetres. Examination shows fracture development to both coincide with, and post-date, some of the mineralising episodes. Those fractures which coincide with mineralisation host both a gangue assemblage and an ore-mineral assemblage, often interlayered in the crustiform style described by Craig and Vaughan (1981, page 113). Syn- and post-mineralisation fractures transect the various episodes of sphalerite deposition and often host a carbonate-quartz assembage. Additionally fluorite or dolomite may be present in small amounts. Fractures commonly bifurcate or wedge-out along their length.

Many of the smaller fractures developed in banded gangue-ore assemblages show an apparent reverse component of 10 to 15 millimetres with some variation in character along the 'fault' length. As the fracture cuts up through the banded ore, the visible slip component becomes progressively smaller until no offset is seen. The fracture then thins and wedges out. The observed variation in slip component and wedging out of the fracture is similiar to that described for many 'growth faults' . Reading (1978) describes such faults as having developed during sedimentation. Some syn-

depositional (i.e. syn-mineralisation) faulting of the Nenthead ores is assumed.

Reflected light petrography shows many of the fractures to be irregular and jagged, with grain shattering and cataclasis common. A mechanical rather than chemical origin is invoked for fracture development.

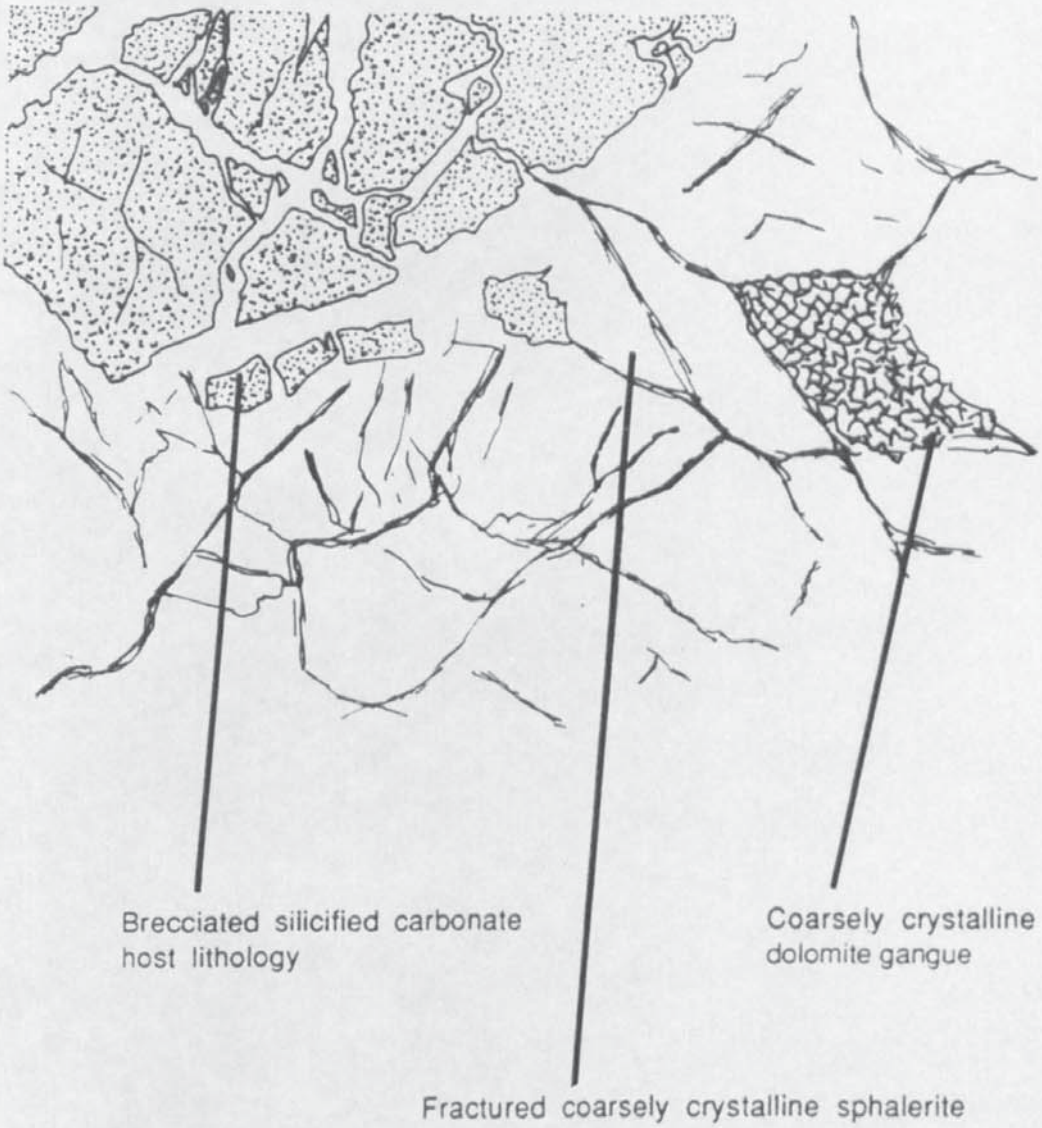

FIGURE 8.1

Diagram to illustrate typical brecciated and fractured nature of the ore and host carbonate.

8.1.2 Intracrystalline fracture development.

Individual sphalerite grains, especially those greater than 1000 microns in diameter, have often undergone multiple fracture development, with fractures ranging in scale from centimetre wide gangue-filled fissures to healed microcracks. The gangue-filled cracks commonly carry other sulfides, especially when the gangue assemblage comprises a quartz-carbonate component.

Throughout the mineralisation numerous microcracks are seen. These thin anastomosing cracks often terminate at cleavage planes, or in a chain of elongate fluid-filled inclusions. The latter texture indicates some post-fracture healing by later stage, sphalerite-bearing, fluids. Also present are planes of secondary, fluid-filled inclusions developed when healing along cleavage planes or fractures is only partially complete.

8.2 Ductile Deformation.

In addition to microstructures that may be ascribed to brittle deformation-related processes, ductile related microstructures are recognised. Glide-plane and twin-plane development, along with some recrystallisation-related textures (sub-grain development) are observed in the deformed sphalerite ores.

8.2.1 Glide Plane and Twin Plane Development.

Throughout the sphalerite a planar fabric comprising numerous

closely-spaced sub-parallel twin and slip planes is observed. This fabric, not apparent using conventional reflected light microscopy, is best observed using either chemically-etched polished sections or doubly-polished wafers. Most easily observed in the more delicately banded sphalerite grains, a variety of textures are developed where the fabric cross-cuts the banding.

Although the fabric is seen throughout much of the sphalerite, the accompanying gangue phases and other sulfides do not appear to have deformed in a similar manner. Careful examination of smaller, millimetre-sized lenses of gangue enclosed within areas of deformed sphalerite fail to show any comparable fabrics.

Extending over several hundeds or thousands of microns, this planar fabric may be developed in continuity across adjacent grains. For the *type-two* sphalerite, the fabric is observed developed throughout the various generations. Some of the larger grains host more than one fabric-dominated region, each region differing in the direction of the fabric. Textural evidence suggests much of the deformation-twinning and glide-planes to be associated spatially with the simple growth twinning observed cross-cutting the sphalerite generations.

8.2.2 *Type-One* Sphalerite: Fabric Related Textures.

A variety of textures related to the planar fabric are recognised. The majority relate to the action of the fabric on growth banding. Three common textural effects are recognised where the banding is cut by one or more of the twin and slip-planes. These may

be developed either singly or in combination. They are:

1. A change in growth-band width across the slip or twin plane.
2. Changes in growth-band colour. A sharp colour change occurs across the plane. Changes from dark grey or black to light grey or intermediate shades of grey are all seen. Occasionally, the slip plane may act so as to remove all traces of the band from the plane of section.
3. Changes in band intensity or texture. A thick opaque band may be transposed against a thin, poorly-developed translucent growth band by the action of the plane. If a plane has a large component of slip out of the plane of section, then it may act to isolate a segment of band (plate 8.1).

Pairs of planes may act together to produce a distinctive texture that implies twin-plane development. Twinning is recognised on the basis of the textural effects observed across the twin-plane (plate 8.20). The twin composition plane acts as a mirror with growth banding and 'rod-like' textures apparently reflected across it. Examination of chemically etched sections indicates the development of deformation twinning to be widespread (see section 8.5).

Two other textures are commonly observed and are thought to represent a combination of twin and slip plane development:

1. Development of transparent lamellae running throughout the growth-banded material. Lamellae range in thickness from a few microns to one or two hundred microns.

2. Development of black lamellae in non-banded material. These lamellae are similar in size and morphology to the transparent ones.

Plate 8.2 illustrates a region of *type-one* sphalerite with a well-developed planar fabric cross-cutting the growth bands. Both twin-plane and slip-plane related fabrics are developed along with their associated textures. Some kinking of the lamellae is apparent across one of the growth bands, as is seen in plate 8.1. Plates 8.1 and 8.3 illustrate twin and slip-related textures.

8.2.3 *Type-Two* Sphalerite: Fabric Related Textures.

The most commonly observed textures due to slip- and twin-plane development are sphalerite colour change across the twin or slip planes. Variations of colour from orange-brown, red-bown to yellow are observed principally due to the action of twinning (see section 8.4). Where the planar fabric cross-cuts a polysynthetically twinned region, the range of textures similar to those described for type-one sphalerite is not always seen. Polysynthetic twinning may post-date much of the fabric development.

Plate 8.4 illustrates a section of banded *type-two* sphalerite cut by a 'sheaf' of slip and twin-planes. The colour banding may be seen offset by amounts that range from a few microns to greater than 70 microns. Plate 8.5 illustrates fabric related textures in a polysynthetically twinned region. Small slip components on the twin lamellae are seen, with an apparent slip component ranging from one

to five microns in the plane of section. Some thin transparent lamellae are also developed.

8.2.4 Recrystallisation and Subgrain Development.

Many of the larger sphalerite grains, especially those isolated and set in a gangue matrix, show textural evidence of sub-grain development and some (minor) recrystallisation. Areas of mineralisation which have been heavily fractured and brecciated best exhibit these textures.

Subgrain development and recrystallisation textures are best observed using doubly-polished, chemically-etched thin sections. Equant polygonal grain development, characterised by 120 degree grain boundary junctions, is seen. In many grains, the deformational twinning appears to be superceded by the development of broad simple annealing or recrystallisation twins (see etch studies. Section 8.4.2). Sphalerite grains that have recrystallised often have a blotchy and irregular internal colouration rather than well-defined growth banding. Such grains also tend to host fewer fluid inclusions.

Subgrain development is texturally indicated in etched samples. The etchant preferentially attacks grain surfaces of a specific orientation, hence many of the subgrains are only poorly picked out by the etching process. However, these subgrains are better observed by their development of a distinctive anisotropy texture, as may be seen in plate 8.6. Localised regions of undulose anisotropy are observed, with the regions having different extinction positions. These regions, sub-spherical in shape, outline the subgrains (section 8.3.5).

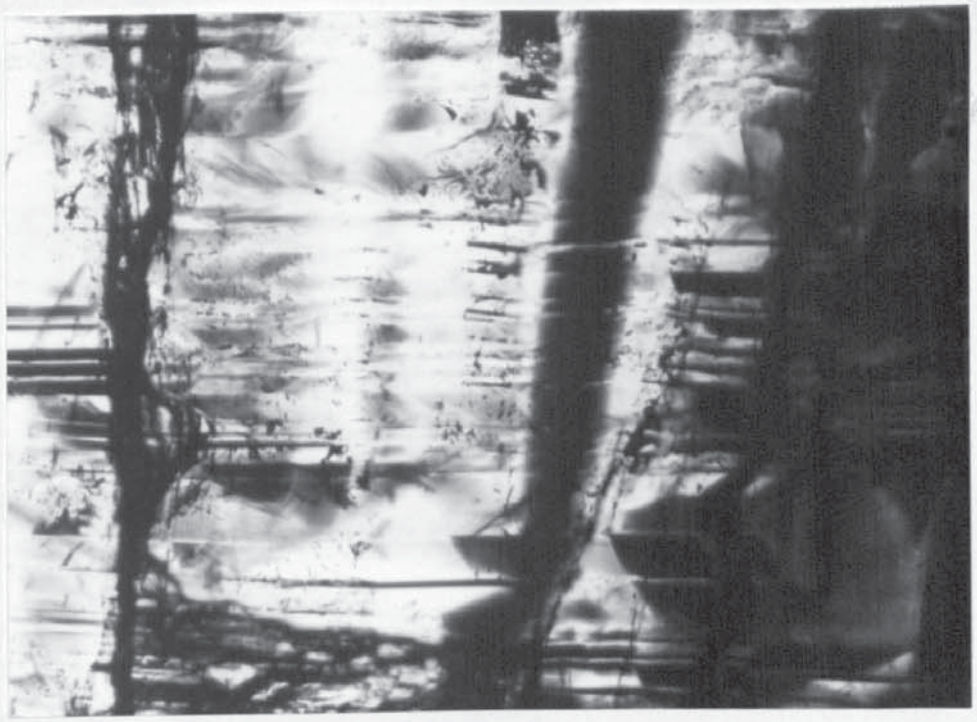

PLATE 8.1

{111} Twin and slip-plane fabric cross-cutting *type-one* banded sphalerite. Growth twins in the fabric are recognised on the basis of reflection effects across the composition plane (twin A). PPL Transmitted light. Field of view 890 microns.

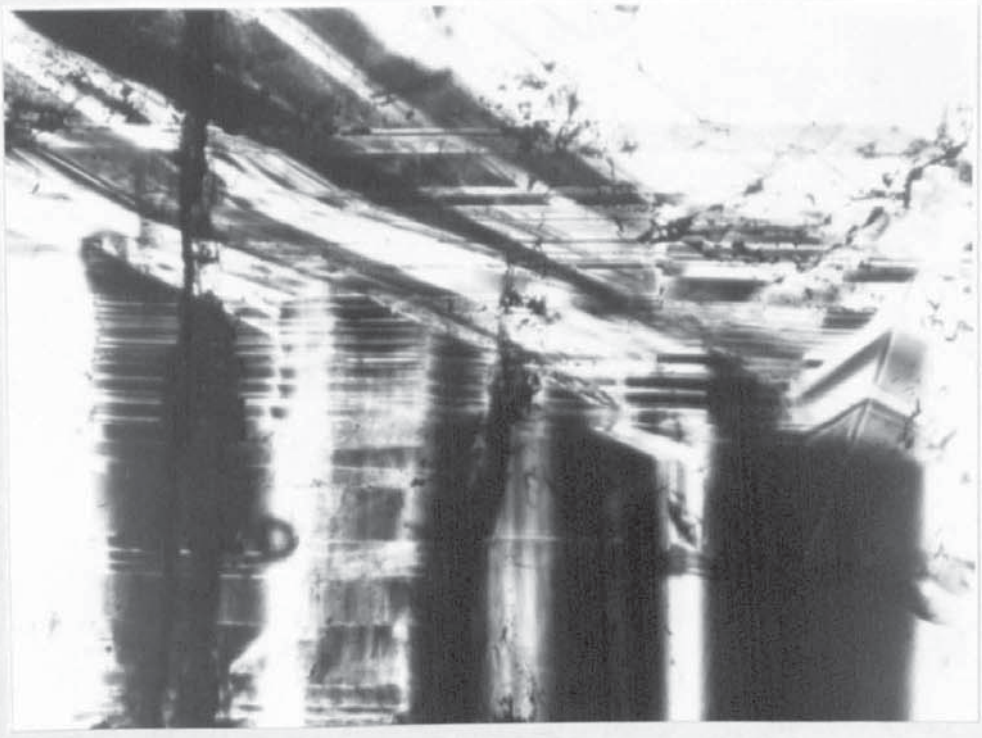

PLATE 8.2

{111} Twin and slip-plane fabric cross-cutting *type-one* banded sphalerite. Planes typically appear to have a slip-component of less than 15 microns in the plane of section. PPL Transmitted light. Field of view 890 microns.

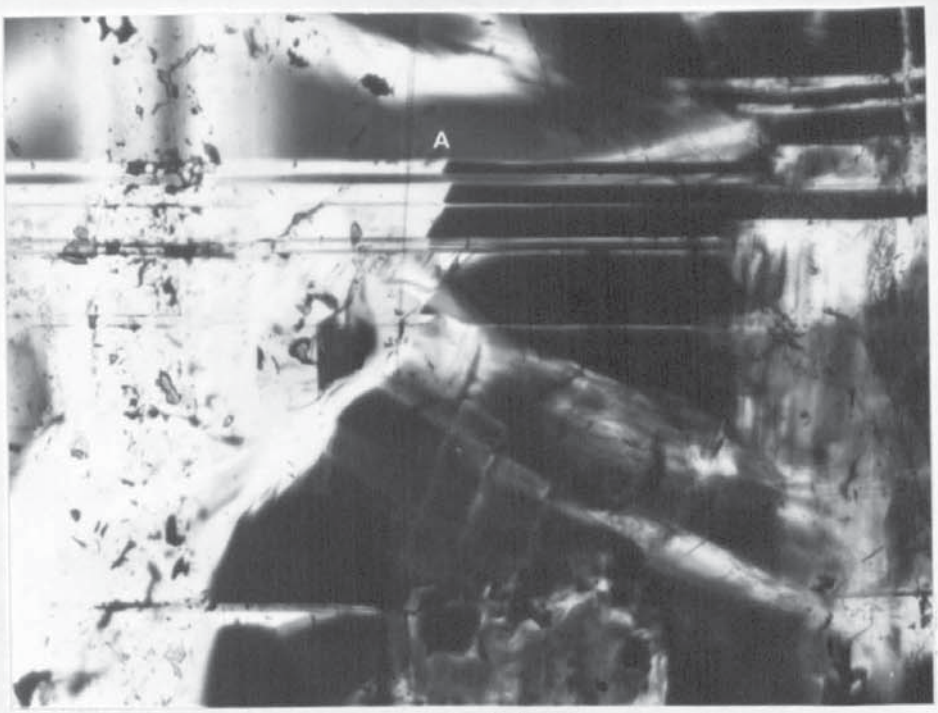

PLATE 8.3

{111} Twin and slip-plane fabric cross-cutting more than one generation of sphalerite deposition. Growth twinning is marked by pronounced change in sphalerite colour (twin A). PPL Transmitted light. Field of view 890 microns.

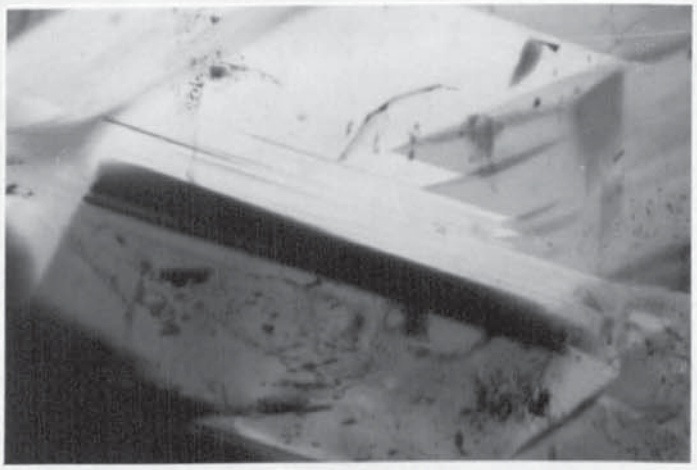

PLATE 8.4

Planar fabric cross-cutting *type-two* sphalerite. PPL Transmitted light. Field of view 350 microns.

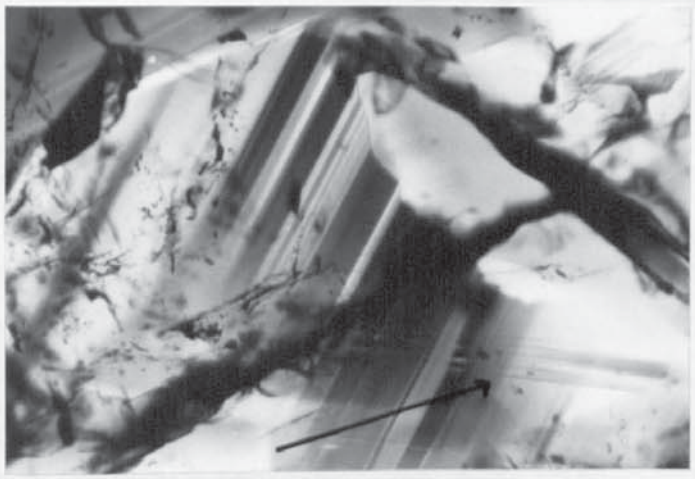

PLATE 8.5

Planar fabric cross-cutting region of polysynthetically twinned sphalerite. Fabric is observed to have little effect upon the twinned region (arrowed), and probably pre-dates twin development. PPL Transmitted light. Field of view 350 microns.

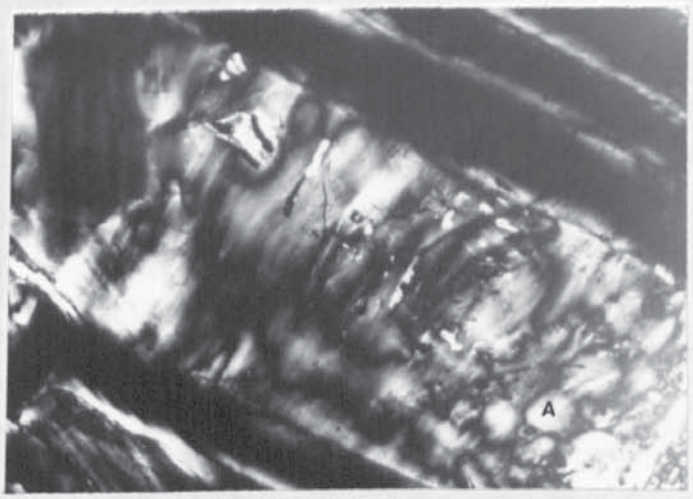

PLATE 8.6

Region of banded *type-one* sphalerite with patchy and undulose anisotropy developed. Subgrains apparent in region A. XPL Transmitted light. Field of view 3220 microns.

8.3 Optical Anisotropy.

Petrographic studies using cross-polarised light reveal a well-developed optical anisotropy. Best observed in slightly thick sections (150 microns thick), the anisotropy exhibits a low retardation of less than 270 nanometrres (1st order white). A retardation of less than 270 nanometres indicates a birefringence of 0.0018 or less. The studies of Nelkowski and Pfutzenreuter (1971) state that a 7.5 % hexagonal component is consistent with a sphalerite birefringence of 0.0018. Examination of the same material in reflected light reveals only a uniform grey, apparently isotropic sphalerite showing numerous red-brown internal reflections. A close correlation between the type of anisotropy developed and growth-related or deformation-related textures may be deduced over much of the ore. Two principal textural forms of anisotropy are commonly recognised; grid-iron (as described by Seal et al., 1985) and lamelliform. A third form is termed undulose.

8.3.1 Grid Iron Anisotropy.

This textural form is best observed in the *type-one* sphalerite. It is, however, developed throughout the sphalerite ores. Similar to microcline twinning in appearance, the anisotropy takes the form of numerous small laths of a diffuse nature, set in two principal directions mutually at right angles. This texture is not uncommon in both deformed and undeformed regions of sphalerite and is documented in the literature (e.g. Seal, Cooper, and Craig, 1985).

Plate 8.7 illustrates such a grid-iron anisotropy developed in *type-one* sphalerite. The dark line running from N.W. to S.E. (growth band) corresponds to one of the two principal lath directions. The second lath direction is set perpendicular to the first. The laths, whilst sharply bounded at the margins, internally exhibit an undulose or diffuse anisotropy.

8.3.2 Undulose Anisotropy.

This textural form is widely developed in *type-two* sphalerite and occasionally in *type-one* sphalerite. The undulose fabric comprises a region tens or hundreds of microns across which exhibits a patchy and undulose anisotropy of low birefringence. Optically this texture closely resembles the sweeping undulose extinction developed in strained quartz.

Plate 8.6 illustrates such an anisotropic area developed between two growth bands in *type-one* sphalerite. A large central region characterised by undulose extinction is recognised along with a series of smaller 60 to 100 micron wide areas. The small areas are interpreted as representing subgrain development. No grid-iron texture is recognised as in plate 8.8.

8.3.3 Lamellar Anisotropy.

Lamelliform, or twin-like anisotropy is not as widely developed as the undulose and grid-iron forms. Occurring typically within a region dominated by grid-iron anisotropy, this textural

variety is best observed where the glide and twin plane fabrics are present (see section 8.2). Bounded by a pair of sharp parallel boundaries the anisotropy is twin-like in appearance with a sharp, rather than undulose, extinction.

Plate 8.8 illustrates a region of *type-one* sphalerite dominated by a grid-iron anisotropy. Within this region, however, there are small domains where a lamellar, twin-like, fabric is developed.

8.3.4 Anisotropy Development in Relation to Crystal Growth.

With many of the growth banded ores, especially the delicately banded *type-one* ores, it is possible to correlate crystal growth direction with grid-iron anisotropy development. Crystal growth direction, perpendicular to banding, is observed to coincide with one of the two principal lath directions developed in the grid-iron texture.

Plate 8.9 illustrates a region of finely growth-banded *type-one* sphalerite. The grid-iron texture is observed to vary its principal lath direction in response to changes in growth band direction. In plate 8.9, superimposed on the growth directed grid-iron anisotropy is a deformation microstructure comprising twin planes and glide planes. In regions where the deformation and growth fabrics coincide, grid-iron anisotropy is somewhat overprinted and obscured.

The observed relationships between grid-iron anisotropy and crystal growth direction suggests two possible causes, the second of which is favoured.

1. Anisotropy development is deformational in origin with the deformational processes acting upon certain crystallographic planes, namely the {111} planes for sphalerite.
2. Grid-iron development is a growth-induced microstructure predating the deformational overprint. The report of similar microstructures in undeformed vug-infilling sphalerites (Seal et al., 1985) suggests growth-related controls to fabric development (stacking faults and twin planes) rather than a deformationally-induced origin.

8.3.5 Anisotropy Development in Relation to Deformation.

Superimposed on the growth-related anisotropy are deformationally-induced varieties. Best observed in the delicately banded *type-one* sphalerite, the intersection of the twin- and glide-plane deformation fabric with the growth-related fabric produces a variety of textural effects:

1. The development of the lamellar or twin-like anisotropy. This is best developed where the twin and glide planes occur in large numbers and intersect the growth banding.
2. The development of areas of diffuse anisotropy between some of the more prominent glide and twin planes. Where subgrain development is apparent the development of diffuse or undulose anisotropy occurs at the expense of the grid-iron anisotropy.
3. Variations in the birefringence and grid-iron fabric across

the more prominent twin and glide planes.

Plate 8.9 illustrates some of the textural varieties outlined above. Regions of growth-related grid-iron anisotropy are observed overprinted by a distinct deformation-related anisotropy. Where the deformational overprint is strongest, both lamellar and undulose anisotropic fabrics are seen. Many of the growth bands illustrate band deformation due to both twin-related and slip-related processes.

From the above observations two conclusions may be drawn:

1. Lamelliform, or twin-like anisotropy reflects a deformationally-induced microstructure.
2. The development of undulose extinction in areas dominated by a deformational microfabric is attributed to deformational and not growth-related processes, in particular subgrain development (plate 8.6). For areas subject to apparently low levels of deformation, it is not possible to assign a deformational origin for the undulose anisotropy. Growth related proceses cannot be ruled out (see Seal, Cooper and Craig, 1985).

PLATE 8.7

Grid-iron anisotropy developed in *type-one* sphalerite. Two mutually perpendicular lath directions are recognised (arrowed). Subgrains are also apparent (region A). XPL Transmitted light. Field of View 890 microns.

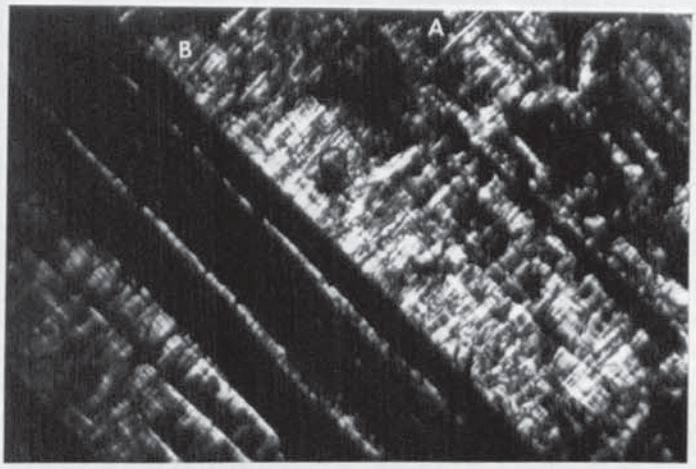

PLATE 8.8

Region of *type-one* sphalerite with both grid-iron and lamelliform anisotropy developed. Areas of lamelliform anisotropy correlate with planar fabric (A and B). XPL Transmitted light. Field of View 2220 microns.

PLATE 8.9

Type-one banded sphalerite with undulose (A and B), grid-iron (C and D), and lamelliform (E and F) anisotropy developed. Principal lath direction for grid-iron and lamelliform anisotropy varies in response to crystal growth directions (arrowed). XPL Transmitted light. Field of view 2220 microns.

8.4 Etch Studies and Observations on Twinning.

Twin development, whether pre-deformational, deformational, or post-deformational, is best observed by reflected light microscopy of chemically-etched polished sections. Examination of etched samples reveals widespread twin development. Growth twins, deformation twins, or a combination of both types may be developed in any one sample.

8.4.1 Growth Twinning.

Growth twinning is characterised by a simple twin morphology. The twins are typically simple lamelliform twins and widely spaced. Texturally, they are similiar to those documented by Richards (1966) in a study of the mechanically-deformed Broken Hill sphalerite ores. Any one twinned grain will usually only host one or two such twin lamellae. This contrasts sharply with deformation twinning, where multiple lamellae are common. The term growth twin is used in the sense of Frater (1985); i.e. growth twins are taken as representing all simple lamelliform twins which are either pre-deformational or due to recrystallisation, where there is no other textural evidence to suggest a deformational origin (i.e. primary twinning of Spry, 1969).

Growth twinning is best developed in the large individual mineral grains that constitute much of the *type-two* (iron banded) sphalerite. These grains are usually developed as isolated lenses of sphalerite set in a gangue matrix. Plates 8.10 and 8.11 illustrate such sections of sphalerite which host numerous growth twins. Minor

fracturing and cataclasis of the grains is apparent, along with some grain recrystallisation; the recrystallisation being characterised by triple grain boundary development. Some of the triple points additionally host other (gangue quartz) phases (plate 8.10).

Growth twinning is also seen in the banded *type-one* sphalerite, where it is overprinted by a later deformational twin and glide-plane fabric. Growth twinning is often associated with the deformation twinning and glide-planes. The growth twinning would appear to have promoted the deformation twinning and glide-plane development.

Many of the larger sphalerite grains in plate 8.10 host large simple lamelliform twins. No preferred twin plane orientation is apparent. These large simple twins are interpreted as being primary growth twins. The possibility that some of the twins could be secondary annealing twins due to grain recrystallisation cannot be discounted (see section 8.2.4), and for the more patchily coloured sphalerite grains is probable.

Not all of the twins developed in the sphalerite which are interpreted as of growth or recrystallisation origin have a simple growth morphology. Variations may be occasionally observed. Multiple twinning may be developed, each twin being simple in form, in addition to multiple, narrow, parallel twins that cut across more than one episode of sphalerite deposition (especially those which form the basis for the *type-one* fabric of 8.2.2).

Plate 8.12 illustrates an etched section of *type-one* sphalerite cut by gangue filled fractures (the gangue comprises a quartz-carbonate matrix carrying small zoned gerdsorffite grains).

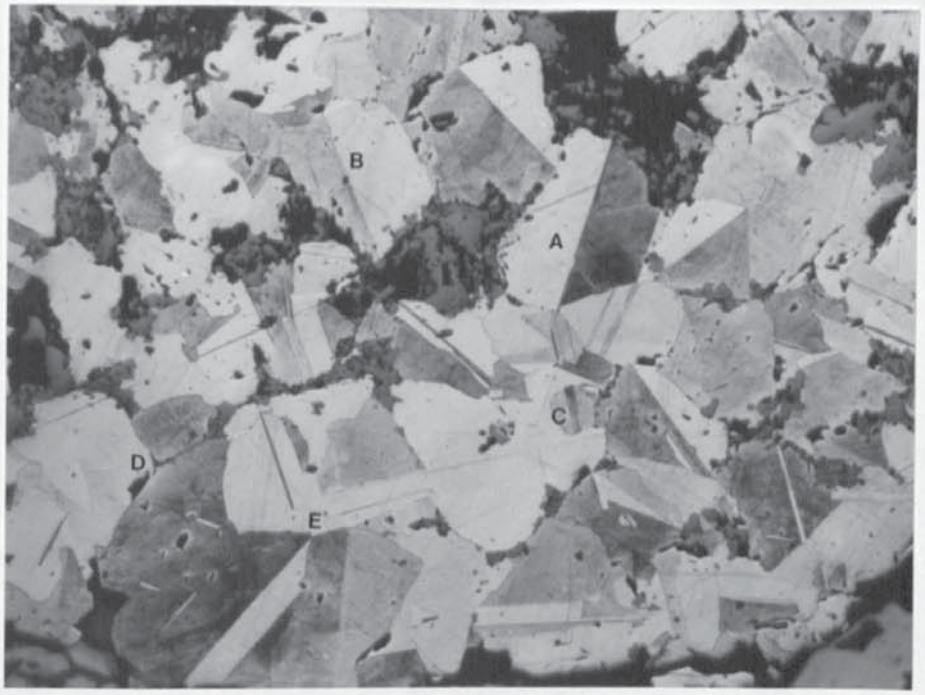

PLATE 8.10

HI etched *type-two* sphalerite. Simple lamelliform growth (? annealing) twins developed (twins A and B). Some thin deformation twinning locally developed (Twins C). Possible recrystallisation of some grains indicated by triple grain boundary development (pts D and E). PPL Reflected light. Field of view 2220 microns.

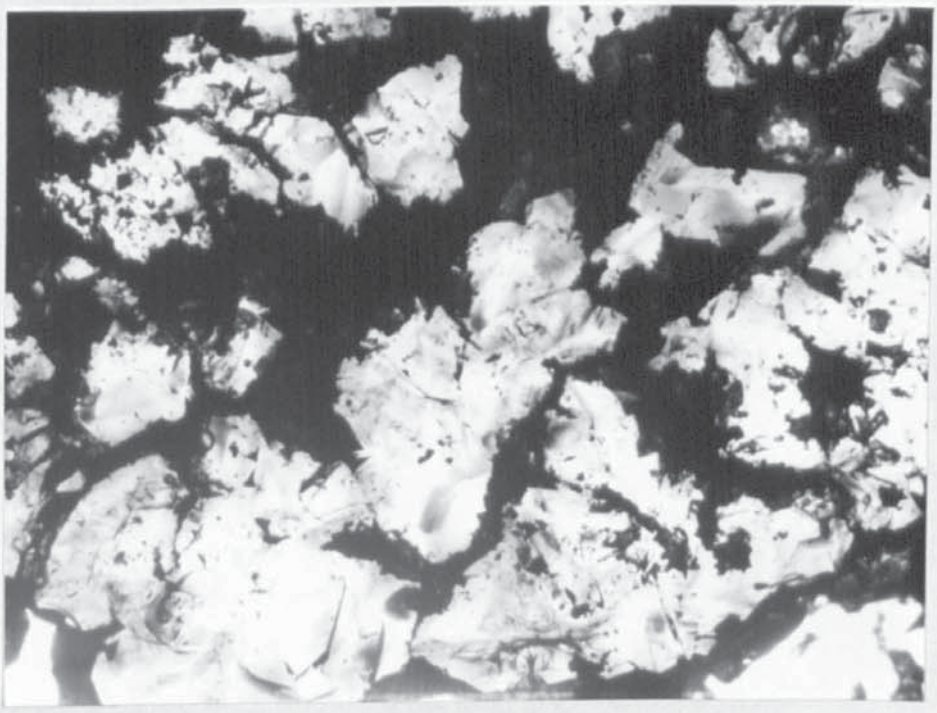

PLATE 8.11

Sphalerite and siliceous gangue of plate 8.10. Much of the patchy colouration is probably due to grain recrystallisation. PPL Transmitted light. Field of View 2220 microns.

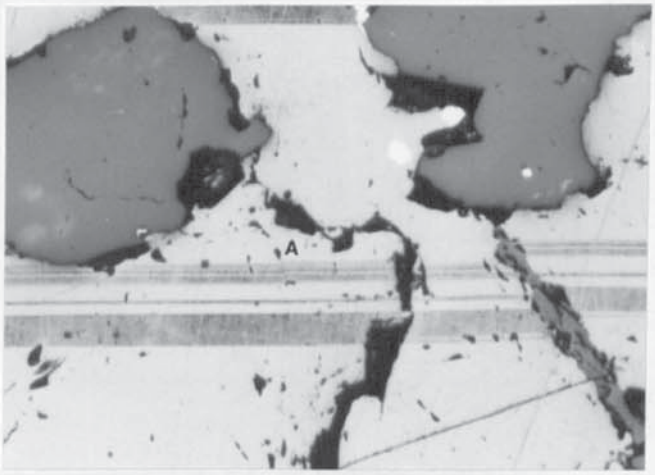

PLATE 8.12

HI etched sphalerite with fracture offset of lamelliform growth twinning. Twin lamellae are also offset by a small fault (A). PPL Reflected light. Field of view 1100 microns.

PLATE 8.13

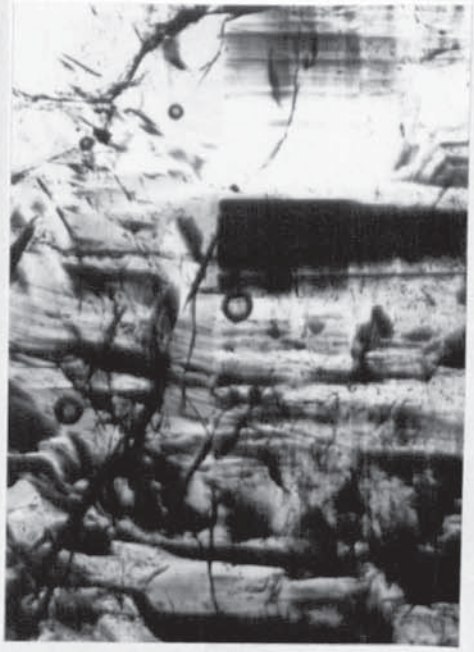

PLATE 8.14

8.13 HI etched sphalerite with large simple growth twin developed. Twin cuts more than one sphalerite generation. PPL Reflected light. Field of view 2200 microns.

8.14 Sphalerite generations cut by the growth twin of 8.13. PPL Transmitted light. Field of view 2200 microns.

8.4.2 Deformation Twinning.

Unlike growth twins, deformation twins are characterised by a complex and varied mophology. Best developed and observed in the larger grains, they are seen to vary greatly both in shape and size. Locally such twins may be present in large numbers.

Plates 8.15 and 8.16 illustrate typical deformation twinning and the highly variable twin morphology. Present in abundance, the twins vary greatly in width but are typically less than 30 microns. Some deformation twins may thin to less than one micron in width. Another feature common of deformational twinning is the splitting and merging of the twin lamellae.

The deformation twinning may be seen to wedge and 'kink' in a manner similar to that described by Richards (1966) and Spry (1969). Such a fabric development has been attributed to two possible causes (Spry, 1969).

1. The intersection of deformation twins with a cross-cutting twin or slip plane.
2. Post-twin deformation of the ore causing multiple slip of the twins, with the slip direction perpendicular to the twin axis.

'Kink' development in sphalerite is illustrated in plate 8.15 Where the deformation twins are observed cross-cutting sub-grain boundaries an angular deflection of the twin lamellae is seen (twin B, plate 8.15). Twin lamellae are often continuous across other twin

planes or a subgrain boundary. Wedging of the twin lamellae, i.e. a gradual narrowing of the lamellae prior to termination, is commonly seen (twins A, plate 8.16). This texture is best developed in twins less than 15 microns wide.

Etching of polished ore sections locally reveals a patchy subgrain development, with the subgrain boundaries often acting as a locus for twin nucleation. Twins projecting from such subgrain boundaries are often spindle-shaped and wedge out. Subgrain development may also give rise to annealing twins; large simple twins developed due to grain recrystallisation.

Plates 8.10 and 8.15 illustrate regions of sphalerite subject to subgrain development. Plate 8.15 displays thin, five micron wide, needle twins which can be seen to nucleate from the subgrain wall. Also apparent are thin deformation twins nucleating from subgrain boundaries (plate 8.10). Some of the twins are discontinuous and wedge out, whereas others may be traced across gangue phases present.

8.4.3 Deformation Fabric-Related Twin Development.

Deformational twinning may act on planes also subject to glide-plane development and primary (growth) twinning. Where both twinning and gliding occur in the same crystal, slip plane development is often enhanced by twin development (Bell and Cahn, 1957). For sphalerite crystals, both twin planes and slip planes may develop on the {111} crystallographic planes. A close correlation between the deformation twinning and the planar fabric is observed in

transmitted light studies of much of the ore.

Micrographs 8.17 with 8.18, and 8.19 with 8.20, illustrate typical deformation twinning developed along with simple narrow sub-parallel growth-twins in *type-one* sphalerite and its correlation to the observed planar fabric. The majority of twin planes correlate directly with planes constituting the fabric. The fabric contains additional planes not revealed by the etchant, which may represent slip planes devoid of any twinned component. The planar fabric would appear to comprise twin planes (growth and deformational), glide or slip planes, and planes with both a twin-component and slip-component.

Some regions of sphalerite, principally *type-two*, also have developed a second planar fabric. This fabric is visible as numerous closely-spaced parallel planes inclined at an acute angle to the main fabric. Selectively picked out by the etchant, the fabric is only developed in certain twinned lamellae. The trend of this fabric appears to correspond to that of polysynthetic twin development.

Plate 8.20 illustrates an etched region of *type-two* sphalerite where the fabric is developed. Seen to be present in selected lamellae only, the fabric is inclined at approximately 70 degrees to the principal fabric. It may be seen that the direction of the second fabric is coincident with that of the polysynthetic twinning developed. Also apparent is the absence of the second fabric where the polysynthetic twinning is developed. The development of polysynthetic twinning may be related to localised recrystallisation of the sphalerite, removing all trace of this second micro-fabric. The strong control exerted by the principal planar fabric upon polysynthetic twin

development suggests this form of twinning postdates the main phase of twin and glide plane development. The patchy texture seen in some areas of the fabric corresponds to a patchy colouration and may be related to subgrain development (section 8.2.4).

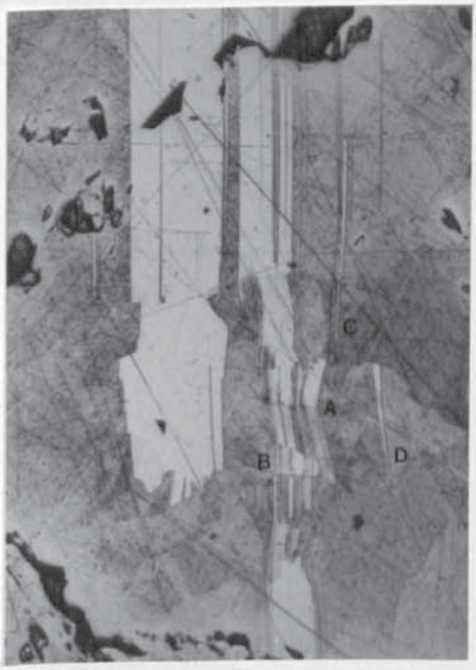

PLATE 8.15

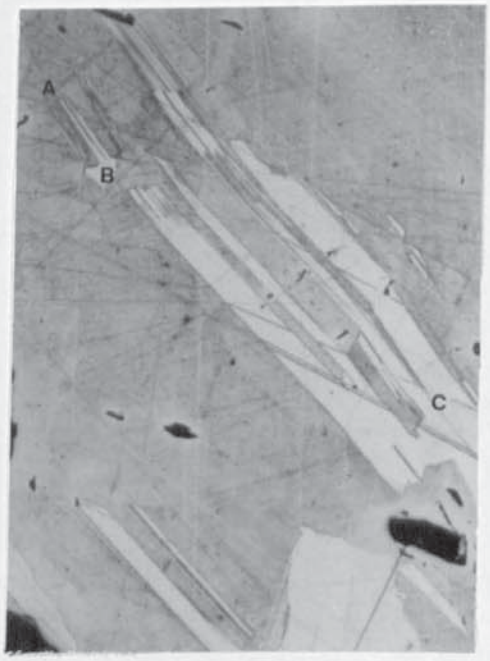

PLATE 8.16

8.15 HI etched sphalerite with well-developed deformation twinning. Multiple thin lamellae apparent with wedging out of lamellae developed (C and D). Change of lamellae direction (A) possibly due to retwinning of the sphalerite. Subgrain developed at B also affects twin morphology. PPL Reflected light. Field of view 1125 microns.

8.16 HI etched sphalerite with well developed deformation twinning. Bifurcating (B) and merging (C) of individual lamellae seen in addition to wedging out (A). PPL Reflected light. Field of view 2220 microns.

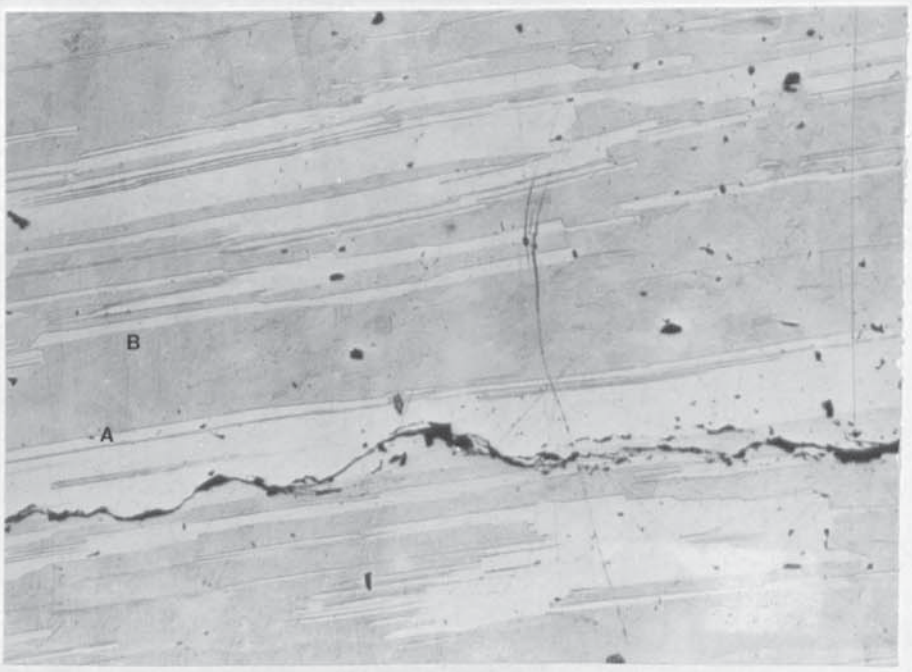

PLATE 8.17

HI etched *type-one* sphalerite with planar fabric developed. Some of the more laterally extensive lamellae are primary growth twins (twins A and B); recognised on the basis of reflection textures (plate 8.18). PPL Reflected light. Field of view 2200 microns.

PLATE 8.18

Transmitted light micrograph of plate 8.17. Primary growth twins A and B recognised from reflection textures. Such twins promote deformation textures, esp. slip-plane development. PPL Transmitted light. Field of view 2200 microns.

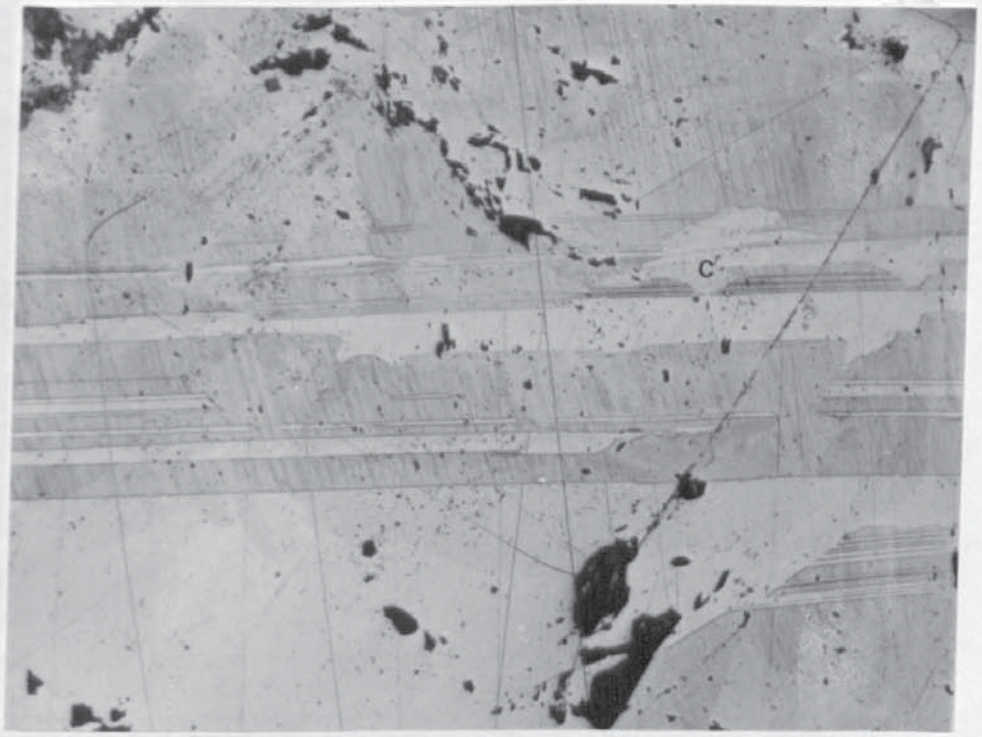

PLATE 8.19

HI etched *type-two* sphalerite. {111} slip and twin-planes cutting more than one sphalerite generation (A and B in 8.20). A second, less well developed, fabric is observed, with fabric direction parallel to that of polysynthetic twin development (plate 8.20). Irregularities in the planar fabric correspond to areas of polysynthetic twin development (C) and possible recrystallisation.PPL Reflected light. Field of view 2220 microns.

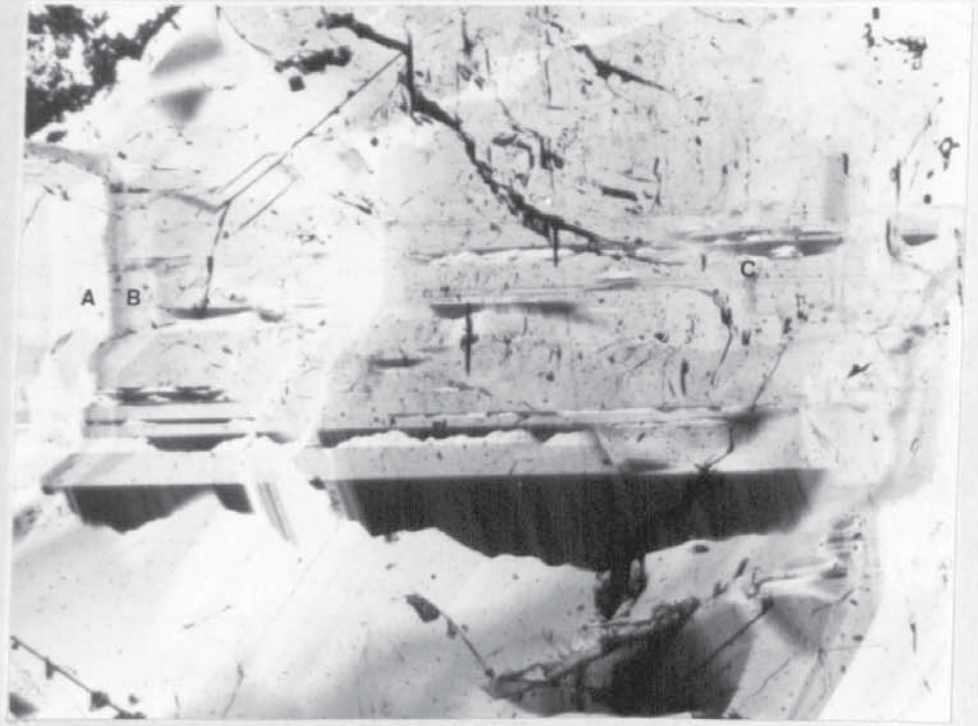

PLATE 8.20

Transmitted light micrograph of plate 8.19 detailing planar fabric and polysynthetic twinning. Legend as for plate 8.19. PPL Transmitted light. Field of view 2220 microns.

8.5 Electron Optical Observations of Deformation-Related Textures.

Regions with a well-developed (optically) planar fabric were examined under the electron beam. A similar planar fabric is seen when examined using the TEM, with diffraction analysis implying both a twin component and a stacking fault component to the fabric. Fabric direction seen electron optically corresponds to that seen optically.

TEM examination of ion-thinned foils details a closely spaced fabric of parallel to sub-parallel planes. Where planes intersect the foil margin, wedging of the planes is apparent due to thickness variations in the foil (e.g. plate 8.23). Planes are not observed to bifurcate or coalesce. They occasionally, however, wedge out laterally.

Separation between the planes, i.e. lamella width, varies, typically between 0.05 and 1 microns. Maximum plane density may is estimated to be in the order of 15,000 planes per millimetre. Plate 8.21 illustrates a region of sphalerite foil with a well developed planar fabric.

Diffraction pattern studies of the fabric indicate the presence of twin planes and stacking faults with a {111} composition plane. Glide planes may be regarded as a variety of stacking fault. Twinning is primarily recognised from the pairing of diffraction spots. Plates 8.22 and 8.23 illustrate a region of twinned sphalerite and the corresponding diffraction pattern. The diffraction pattern implies a $\{1\bar{1}1\}$ composition plane or equivalent (see figures 8.2 and 8.5).

The presence of stacking faults will typically cause streaking of diffraction pattern spots, with the trace of the streak direction

perpendicular to the planes or faults responsible. Diffraction patterns 8.24 and 8.25 illustrate such streaking in a $\{1\bar{1}1\}$ trace and {421} trace respectively (figures 8.4 and 8.5). Stereographic analysis of the {421} trace is consistent with {111} stacking-faults (figure 8.6).

Streaking of diffraction spots may also be expected for a series of closely spaced twin planes or if there exists strain in the region of the twin interface (Hirsch et al., 1965. p 131). Many areas of sphalerite imaged show the development of both paired spots and streaked spots simultaneously, with a {111}, or equivalent, composition plane always implied (e.g. plate 8.22). Caution must be applied before assuming that any region imaged with {111} streaked diffraction spots is dominated by stacking faults only.

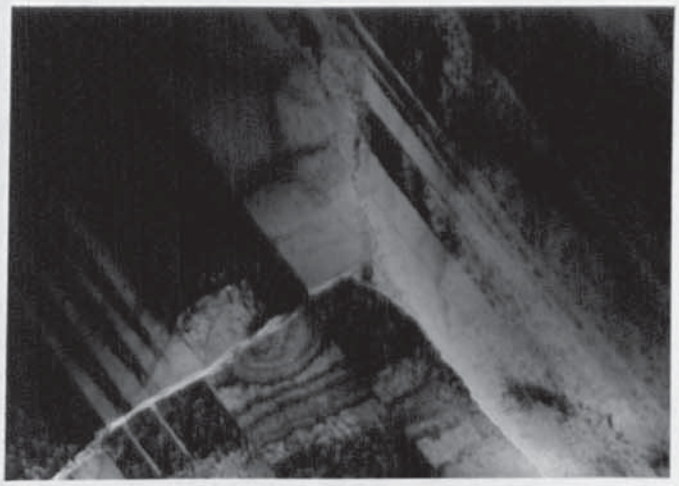

PLATE 8.21

TEM image of sphalerite with well developed planar fabric composed of sub-parallel twin planes and stacking faults. Fracturing of the foil is additionally seen. Field of view ~ 4 microns.

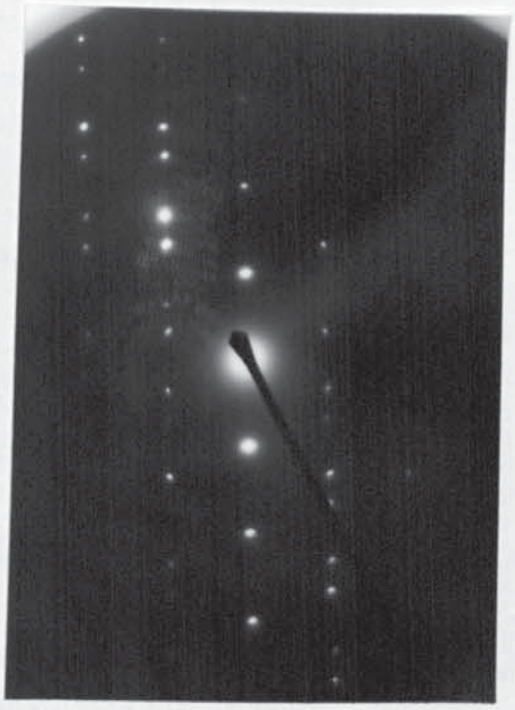

PLATE 8.22

PLATE 8.23

8.22 Electron diffraction pattern of lamellae in plate 8.23. Pairing of the diffraction spots due to $\{1\bar{1}1\}$ twinning is apparent for a beam direction [011]. See figure 8.2 for interpretation.

8.23 Lamelliform sphalerite of diffraction micrograph 8.22. Differential ion-thinning is apparent. Planar fabric (faint) is additionally developed within the lamellae. Beam direction is [011] or equivalent.

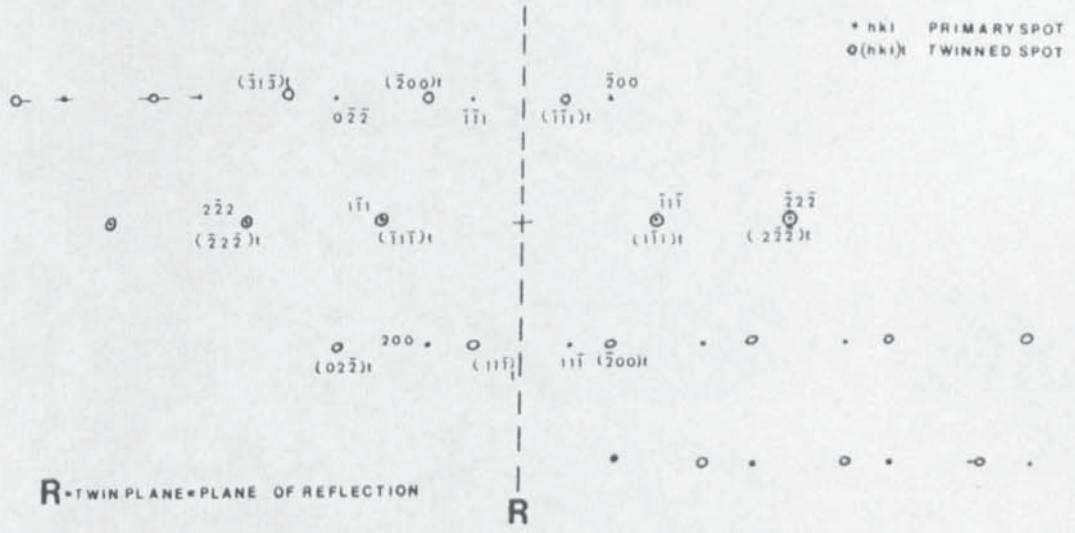

FIGURE 8.2

Interpretation of diffraction pattern of plate 8.22. Twinning on a {211} trace plane of reflection for a [011] beam direction. Some spot streaking with a $\{1\bar{1}1\}$ trace developed.

PLATE 8.24

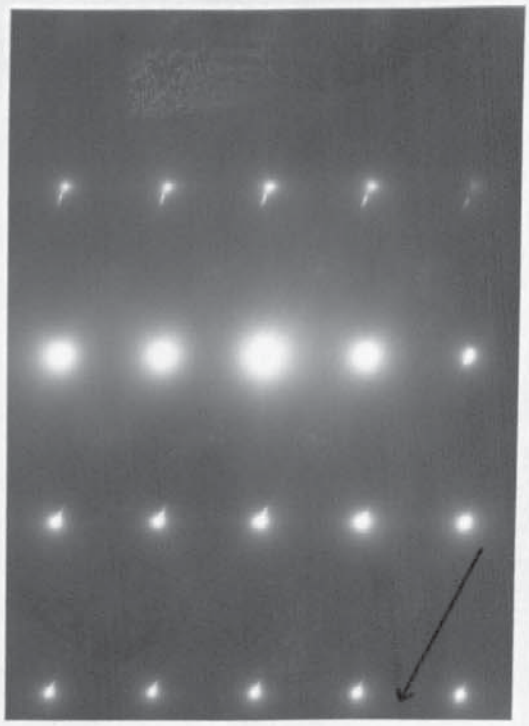

PLATE 8.25

8.24 Diffraction pattern with streaked spots due to stacking faults in sphalerite. Trace of streak direction is $\{1\bar{1}1\}$; for a beam direction [011].

8.25 Diffraction pattern for same region as plate 8.24 different orientation. Trace of streak direction is approx. {311}, actually {421}; for a beam direction $[\bar{1}12]$.

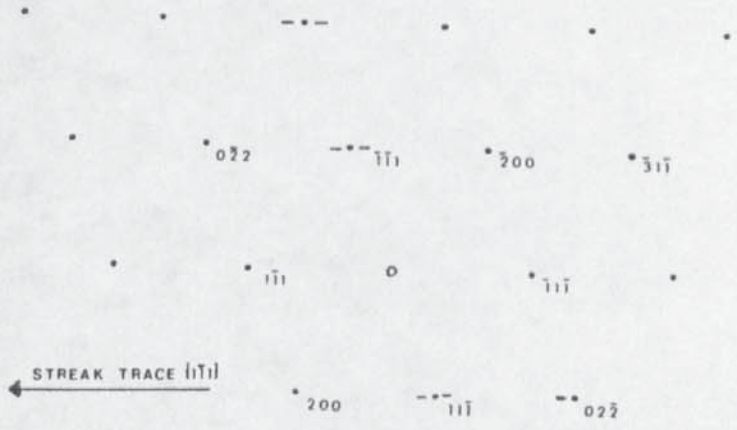

FIGURE 8.3

Interpretation of diffraction pattern of plate 8.24. Streak direction of $\{1\bar{1}1\}$ for a beam direction of [011].

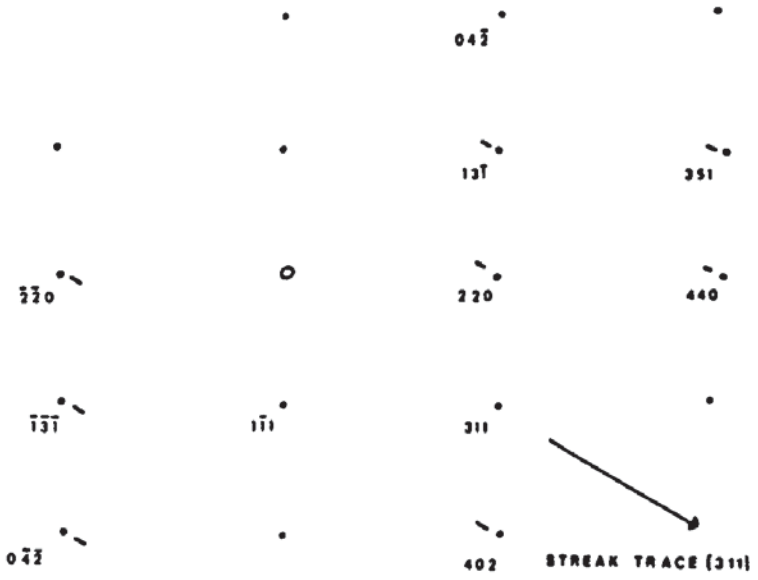

FIGURE 8.4

Interpretation of diffraction pattern of plate 8.25. Streak direction of approx. {311} for a beam direction of $[\bar{1}12]$. The true trace direction is {421}.

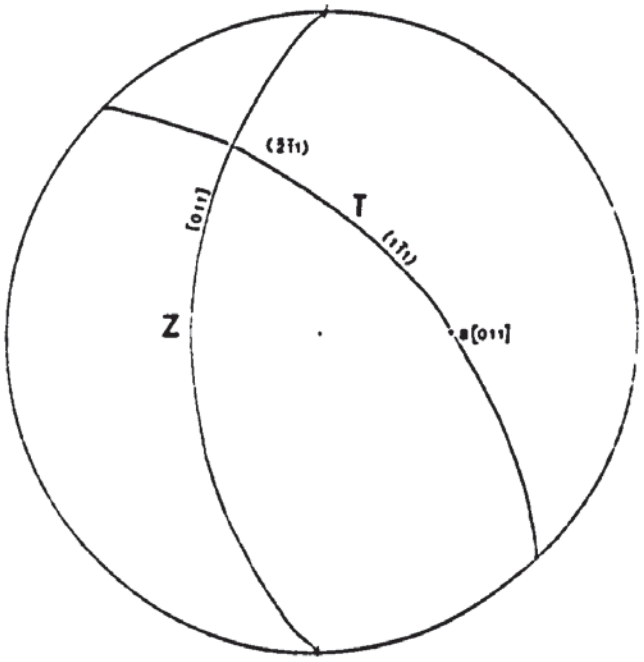

FIGURE 8.5

Stereographic trace analysis of streak directions from plate 8.22. Trace analysis indicates that the trace direction of $\{\bar{2}\bar{1}1\}$ for a [011] projection is consistent with a $\{1\bar{1}1\}$ twin-plane. Z represents the zonal plane [011], T the twin plane $(1\bar{1}1)$, and B the diffraction vector [011].

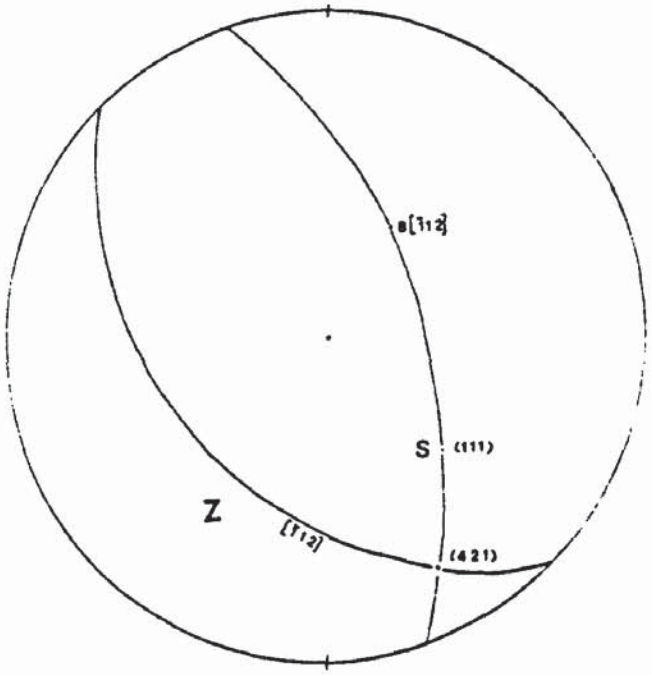

FIGURE 8.6

Stereographic trace analysis of streak directions from plate 8.25. The stereogram indicates that a streak trace direction of {421} for a [$\bar{1}$12] projection is consistent with a {111} plane (stacking fault) responsible for streaking. Z represents the zonal plane [$\bar{1}$12], S the stacking fault or glide plane (111), and B the diffraction vector [$\bar{1}$12].

pole of the

CHAPTER 9: Textural Discussion of the Nenthead Sphalerite.

9.1 Growth-Related Microstructures and Possible Textural Origins.

Of the two principal textural varieties of sphalerite described from the Nenthead mineralisation, *type-two* sphalerite represents a variety typical of sphalerite developed in lead-zinc deposits world-wide. The growth-banded *type-two* sphalerites host a range of textures that are described for many growth-banded M.V.T. sphalerites. *Type-two* sphalerite, with its low trace-metal content, reflects a fluctuating iron component in the ore-fluid. The iron content, whilst generally low, is sufficient to cause variations in sphalerite body colour. Of particular note is the relation seen between iron and the other metals present within *type-two* sphalerite. Early *type-two* varieties are iron-enriched, cadmium-enriched and antimony-poor, unlike late *type-two* sphalerites which tend to be iron-poor, cadmium-poor and antimony-enriched.

Banded *type-one* sphalerite texturally is non-typical of M.V.T. sphalerites. The range of microstructures and textures developed within this variety are unusual. *Type-one* banded sphalerite is developed as a paragenetically early phase of zinc mineralisation, with remnants and patches of *type-one* material seen both as separate early phases and as isolated patches enclosed within later

type-two mineralisation. Type-one sphalerite (banded) is enriched in a range of metals not typically reported for M.V.T. sphalerites (Hagni, 1983). In addition to iron and cadmium the more 'unusual' metals copper, antimony and occasionally arsenic are detected. The banding characterising *type-one* sphalerite differs both optically and chemically from that defining *type-two* sphalerite.

For *type-one* sphalerite, a chemical origin for the banding, i.e. the direct substitution of metals for zinc, may be discounted. No apparent change in sphalerite body-colour across the banded region is observed, as would be expected for the substitution of zinc by antimony or iron. The principal variations in *type-one* banding apparent are the shades of 'colour'. 'Colour' varies from pale-grey through shades of intermediate grey to black for the well developed 'marker' bands. The majority of the 'colour' variations are due to variations in band intensity. Some variation, however, is related to the orientation of the banded regions to the plane of thin section. Near-vertical banded regions will be 'darker' than near-horizontal banded regions. The observed changes in iron concentration across well-developed banded regions, i.e. approximately 1 to 2 mole percent, are insufficient to cause the opaque bands. Iron concentrations in excess of 10 mole percent would be necessary to give rise to the observed variations in transparency. The concentration variations in the other metals present (copper, antimony and arsenic) do not correlate with the banding and, therefore, are unlikely to be the origin of the banding. Cadmium, the only other metal present in significant quantities in the banded regions, has little effect upon sphalerite body-colour (Boldish,

1973).

A hydrocarbon origin for *type-one* banding can be discounted (see section 7.2) although organic-related banding would not be unexpected for cadmium-bearing sphalerite and a link between M.V.T. lead-zinc mineralisation and hydrocarbon-bearing fluids has been suggested (Barton, 1967; Barnes, 1983). F.T.I.R. spectroscopic analysis of the banded and unbanded *type-one* sphalerite regions indicated a hydrocarbon-free sphalerite. Also apparent from the spectroscopic studies is the compositional similarity between banded and unbanded material. Hence, any possible phases that may be concentrated within the banded regions occur only at very low concentrations.

Optical examination of less developed banded regions shows a number of similarities between the banded texture of the Nenthead sphalerite and the 'bead chain' textures of Barton and Bethke (1987), Barton (pers. comm.). Barton and Bethke (1987) describe the presence of numerous rods or 'bead chains' within sphalerite from Creede, Colorado which are considered representative of primary growth features. There are several differences, texturally, between the rods developed in the *type-one* banded regions and those of Barton and Bethke (1987). Rod morphology in the Pennine examples is generally simple, with rods that are poorly-developed compared to the 'bead chains' of Barton and Bethke (1987). They report 'bead chains' developed throughout much of the sphalerite sampled. They do not, however, describe the presence of opaque regions in the sphalerite due to locally high concentrations of such 'bead chains'. Rods developed in the North Pennine sphalerite do not trace out

geometrically complex patterns. One possible origin for the thin rod-like texture would be the development of growth-defects (chain-like dislocations) generated during crystal growth. The defect, carried by the growing crystal face, would be drawn out in the direction of growth i.e. perpendicular to growth banding. Defect climb (e.g. in a 'cross-slip' manner) may generate rod-like defects inclined at an angle to growth banding. 'Blotching' of the rods, attributed to defect decoration by Barton and Bethke (1987), possibly by Cu-Fe sulfides, is absent for all but a few of the rods developed. Blotched rods tend to be developed in the more iron-rich (dark red-brown) patches. Cu-Fe sulfides are not seen associated with the regions hosting blotched rods in the Nenthead samples.

The decoration of crystal defects by other mineral phases (Fe or Cu-Fe sulfides in the case of sphalerite) is not unexpected. Crystal defects may act as a site for the nucleation of submicroscopic phases. The activation energy required for the nucleation of a second phase will be reduced by an amount equivalent to the energy associated with the crystal defect. Partial or complete obliteration of the defect by the nucleating second phase releases the energy associated with the defect site (disorded energy or entropy), thus reducing the activation energy required for the nucleation of a second phase. The slight increase in metal concentrations observed for the banded regions may represent the localised decoration of point and chain-like defects. The blotching seen developed for the thicker rods associated with iron-rich patches of sphalerite may represent the decoration of the rod by other minerals. Post-ore copper-bearing fluids are observed to have

locally altered the sphalerite (section 7.4). The precipitation of secondary Cu-minerals at the defect site, in a manner analogous to the twin and slip-plane alteration (section 7.4), could account for the 'blotched' rod texture. A similar origin (i.e. defect decoration) has been suggested for the 'blotched' rods developed in the Creede sphalerite (Barton and Bethke, 1987).

Electron optical studies of the banded *type-one* material shows areas containing numerous localised or 'point' defects along with rod-like and planar defects. In addition to a range of defect types, numerous micron and sub-micron inclusions are observed. Many of these inclusions probably host a liquid phase (section 6.7). A high concentration of sub-micron defects and inclusions will render the host sphalerite translucent or opaque.

The banded regions developed in *type-one* sphalerite are attributed to a combination of defect-related causes. A high concentration of defects (point, rod-like and planar) some of which are decorated by other minerals are locally complemented by numerous micron to sub-micron fluid inclusions. The defect and inclusion concentration is sufficient to locally render the sphalerite opaque with only minor changes in sphalerite composition and body colour. The fine sub-micron 'dust-like' texture is attributed to sphalerite regions that locally host high concentrations of 'point' defects and sub-micron inclusions.

9.2 Mineral Deposition and the Ore Fluid.

The range of growth banded and dissolution textures developed

in *type-one* and *type-two* sphalerites reflects a fluctuating environment of mineral deposition. Within any one episode of mineralisation, fluctuations in the fluid chemistry are indicated texturally by the development of fine scale growth banding within any one mineral grain. Also apparent is a chemically changing ore fluid, texturally manifest by a change from finely banded *type-one* sphalerite to an iron-poor late-stage *type-two* sphalerite.

The ore fluid, carrying a low concentration of metals (Cu, Sb, Fe, Cd ± As, Co and Ni), deposited a defect-rich, impure sphalerite (banded *type-one*) with a cobalt-nickel bearing gangue (quartz, iron carbonate and gersdorffite). A phase of sporadic *type-one* mineralisation followed, punctuated by phases of sphalerite dissolution and the deposition of iron and cadmium poor *type-two* sphalerite. The *type-one* and early *type-two* mineralisation represent phases of iron-rich mineralisation relative to the later *type-two* mineralisation.

The small grains of *type-two* sphalerite occuring as isolated grains in the quartz-carbonate gangue texturally record the changing nature of the ore-fluid. The majority of these isolated grains display an iron-rich (8 to 10 mole percent) red-brown core which is surrounded by a pale orange-yellow iron-poor (1 to 2 mole percent) rim. Mineral deposition is punctuated by episodes of mineral dissolution. Fluid inclusion data imply a steady temperature during the drop in sphalerite iron content. The decreasing iron content of the sphalerite may reflect a fall in the activity of sulfur or iron for the mineralising fluid.

In addition to a changing iron concentration in the ore fluid a

changing antimony concentration is apparent. For the *type-two* sphalerite an increase in antimony content is seen accompanying the drop in iron content. The rise in antimony content during *type-two* mineralisation is paralleled by other evidence of an increase in the availability of antimony. Paragenetic studies of the Alston block assemblages (Ixer, 1986; Ixer and Stanley, 1987) detail a change from a quartz-fluorite gangue with sphalerite and early Co-Ni sulfarsenides (zone 2a of Ixer, 1986) to a barite gangue with sphalerite and late Ni-As sulfides and sulfantimonides (zone 2b of Ixer, 1986); i.e. the appearance of antimony mineralisation late in the ore paragenesis

Mineralisation by the ore fluid is observed to have fluctuated between periods when the fluid was supersaturated with respect to sphalerite (sphalerite deposition) and when the ore fluid was undersaturated with respect to sphalerite (sphalerite dissolution). For much of the mineralisation, levels of dissolved ZnS fluctuated around saturation level (see figure 9.1). Much of the sphalerite is delicately growth-zoned with occasional areas that appear to be sector zoned (especially for the isolated *type-two* grains set in the quartz-carbonate gangue). Running through much of the banded material are numerous dissolution disconformities. Occasionally, more pronounced solution unconformities are seen. Textural evidence of extreme levels of fluid supersaturation or undersaturation are absent (see figure 9.1). Similar textures for M.V.T. sphalerite from the Creede orefield are reported by Barton et al. (1963). They suggest that the sphalerite was deposited under 'quasi-equilibrium' conditions, with the concentration of sphalerite

in solution varying just above and below sphalerite saturation level.

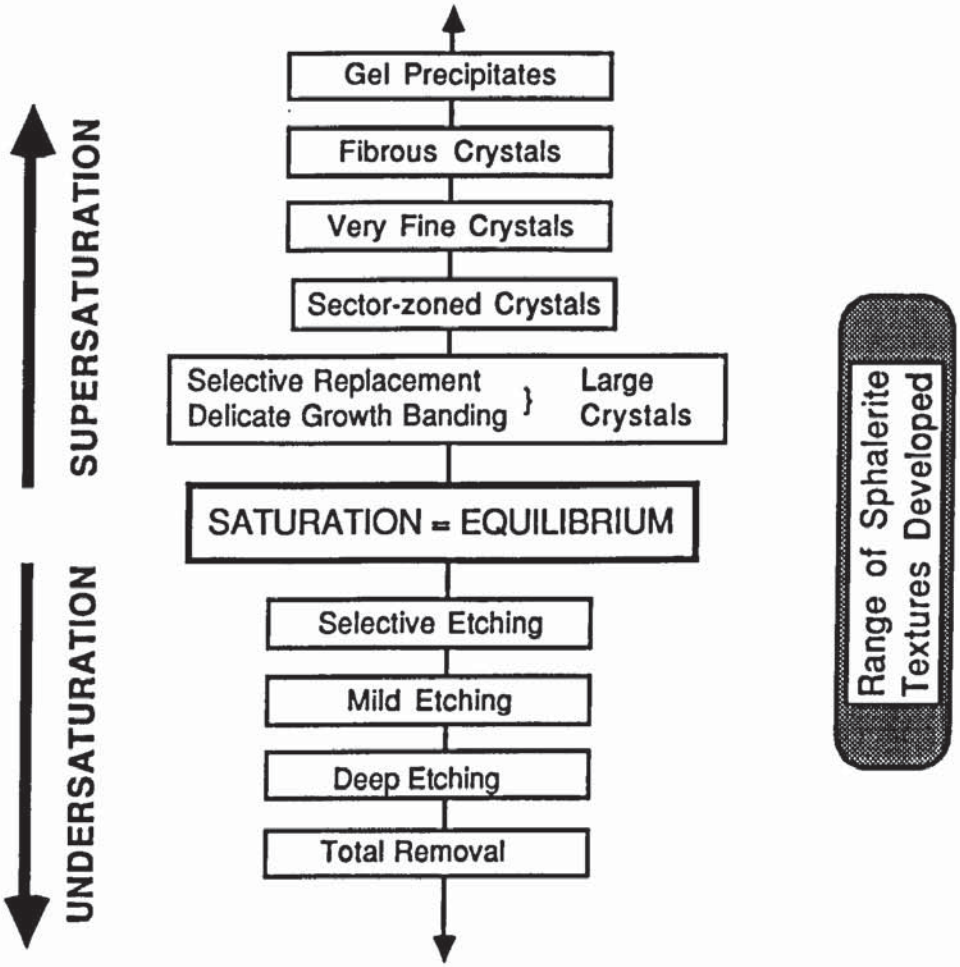

FIGURE 9.1

Relationship between crystal texture and saturation level of mineralising fluid (after Barton et al., 1963).

Sphalerite saturation levels do not have to be very high to promote crystal growth. For a saturation level just above equilibrium, i.e. a slight degree of supersaturation, the kinetic energy barrier for sphalerite growth will be greatly reduced if a nucleus or seed is present. Crystal growth may then proceed by a

spiral dislocation mechanism, a mechanism that requires a low activation energy (Frank, 1949). For the Pennine sphalerite such a 'seed' is provided by the previous generation of ZnS.

The iron-banded sphalerites texturally reflect the relationship between crystal composition and the chemistry of the mineralising fluid. There exists a state of 'near equilibrium' between the growth surface of the crystal and the mineralising fluid. Crystal surfaces often grew at different rates and adsorbed different concentrations of metals present in solution, thus accounting for some of the lateral variations in band colour seen in the sphalerites. For the development of the fine scale banding seen throughout the Pennine sphalerites, a rapid response by the growing crystal to the fluid chemistry is necessary.

Fluid inclusion data obtained from both the sphalerite and coexisting quartz indicate a low temperature, highly saline brine as the mineralising fluid. Salinities of greater than 20 equiv. weight percent NaCl are indicated along with a possible Ca or Mg component to the fluid (not unexpected considering the widespread presence of fluorite and carbonate mineralisation in the ore field). Assuming the temperature-pressure corrections of section 7.3 to be a reasonable estimate of the possible mineralisation conditions range a mean temperature of 124 ° ± 12 °C is suggested. This temperature is much lower than that which has been suggested for the cupola-related mineralisation (250° C., Vaughan and Ixer, 1980), and is reflected by the simpler mineralogy of the Nenthead ores. Pyrrhotine is absent and only small amounts of chalcopyrite are seen (cf. The Great Sulphur Vein: Vaughan and Ixer, 1980).

9.3 Polytypism in relation to the Environment of Deposition.

X-ray diffraction, transmission electron microscopy and petrographic studies all indicate a disordered 3C-polytypic form for the Nenthead zinc sulfide, rather than sphalerite generated by the inversion of a wurtzitic precursor. For sphalerite derived by the inversion of wurtzite, equal proportions of twins in all <111> directions would be expected throughout the resultant 3C-sphalerite. No morphological or textural evidence for a hexagonal precursor to the sphalerite is seen. In particular, the bladed-hexagonal grain morphology often seen characterising wurtzite (Hollenbaugh and Carlson, 1983; Oudin, 1983; Koski et al., 1984) is absent.

Sphalerite was originally considered to represent the low temperature ZnS polymorph, with wurtzite as the high temperature form, assumed to be metastable at geologically reasonable ore-forming temperatures. A variety of other factors, apart from temperature, are now known to influence polytype precipitation, one factor possibly being sulfur fugacity.

The free energy of formation (ΔG_f at a temperature of approx. 130 °C) of sphalerite and wurtzite differ by only approx.12 kJ mol^{-1}, a very small number when compared to the actual energies of formation as given below (after from Robie et al., 1978):

Sphalerite	ΔG_f at 400 K	-200.655 kJ mol^{-1}.
Wurtzite	ΔG_f at 400 K	-188.401 kJ mol^{-1}.

The precipitation of wurtzite as a metastable phase within the

M.V.T. hydrothermal regime cannot be discounted, especially from a ZnS saturated fluid (and hence a rapid rate of ZnS deposition). Barton (Vaughan. pers comm. 1986) advocates a possible, but as yet unspecified, kinetic control that favours the precipitation of sphalerite rather than wurtzite for most ore-depositing environments.

Scott (1968) and Scott and Barnes (1972), however, do not advocate a kinetic control for sphalerite-wurtzite deposition. They cite sulfur fugacity as a possible control for polytype development. Wurtzite may be considered as being sulfur-deficient relative to sphalerite. Wurtzite should, therefore, be favoured by a low sulfur fugacity or reducing environment; a concept born out in many natural low temperature occurrences of wurtzite (e.g. low fS_2 sideritic black shales: Hollenbaugh and Carlson, 1983). Scott and Barnes (1972) define a stability field for wurtzite that lies outside the range of sulfidation states encountered in most ore-depositing environments. However, low sulfur fugacities are not unusual within M.V.T. depositional environments. Barton and Skinner (1967) report sulfur fugacities as low as 10^{-24} atm. for a low iron (1 mole %) sphalerite and low temperature (100° C) ore depositing fluid. Wurtzite is a mineral component reported from many M.V.T. lead-zinc ores (e.g. McKnight and Fischer, 1970).

The presence of impurities within a sphalerite may stabilise non-cubic regions (Kullerud, 1953; Scott and Barnes, 1972; Geilikman, 1982). Seal et al. (1985) noted a correlation between cadmium-rich areas and high birefringence patches for the

anisotropic sphalerite of the Elmwood-Gordonsville deposit, Tennessee. North Pennine sphalerite, enriched in both cadmium and iron, however, shows no such apparent correlation between birefringence and impurities present.

Assuming a maximum possible temperature of 150° C for the Nenthead mineralisation, and a range in FeS concentration from 1 mole % to 10 mole %, the fugacity ranges from approximately 10^{-17} atm. to 10^{-19} atm. (table 9.1). The sulfur fugacity is much lower for temperatures less than 150° C, and if the minimum possible temperature of 100° C is assumed, the estimated sulfur fugacity ranges from $10^{-20.2}$ atm. to $10^{-22.2}$ atm. (table 9.1).

For 100° C.	a_{FeS} = 0.025.	log fS_2 ~ -20.3
	a_{FeS} = 0.25.	log fS_2 ~ -22.3
For 130° C.	a_{FeS} = 0.025.	log fS_2 ~ -18.9
	a_{FeS} = 0.25.	log fS_2 ~ -20.9
For 150° C.	a_{FeS} = 0.025.	log fS_2 ~ -17.0
	a_{FeS} = 0.25.	log fS_2 ~ -19.0

Table 9.1

Approximate sulfur activities for an ore-fluid depositing sphalerite containing 1 to 10 mole % FeS (a_{FeS} = 0.025 to 0.25), at 100, 130 and 150° C. Data derived from Vaughan and Craig (1978).

Figure 9.2 shows a temperature-sulfur fugacity plot for sphalerite in equilibrium with pyrite, along with the sulfur fugacities of table 9.1.

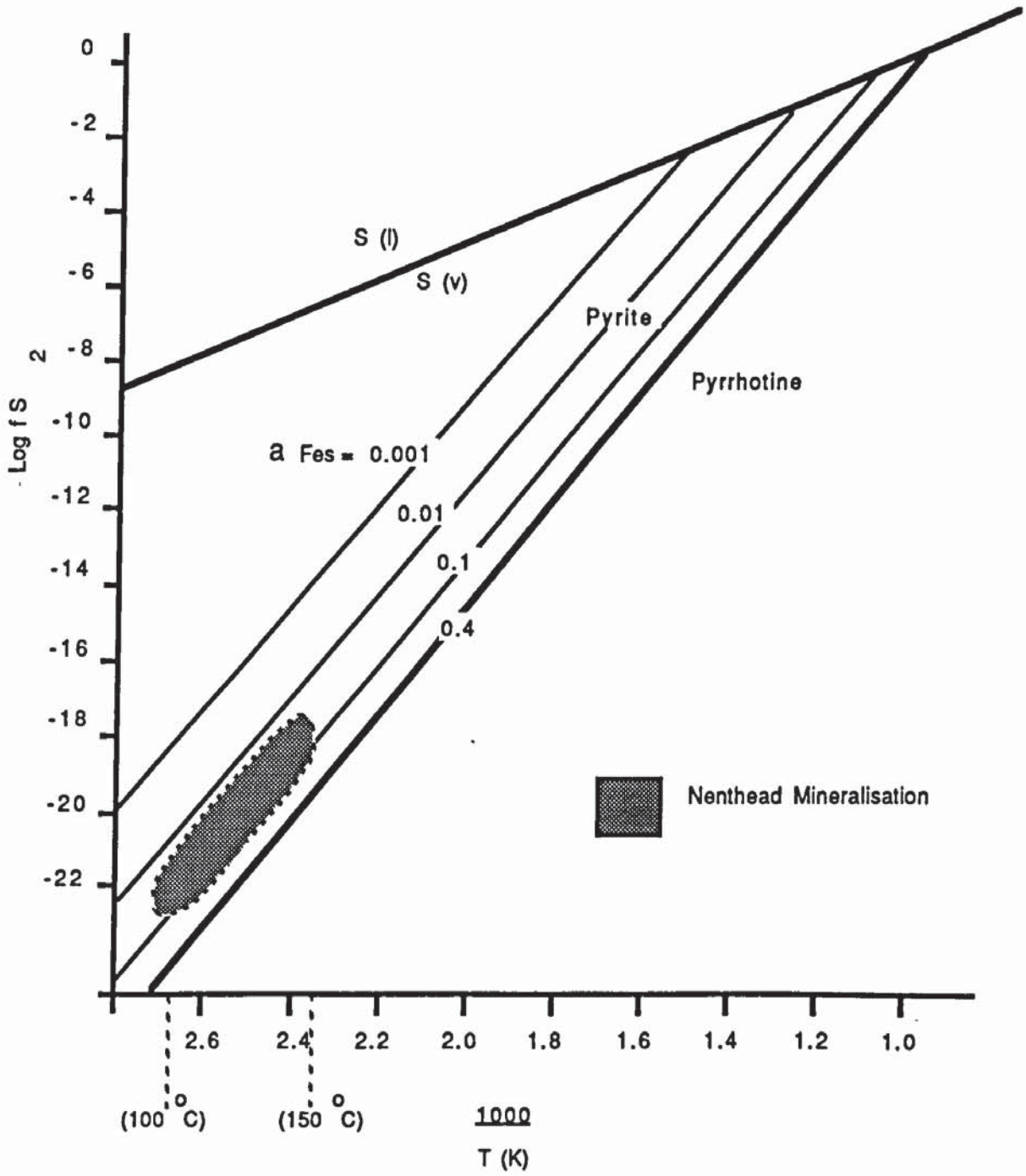

Figure 9.2

Temperature- fS_2 plot of sphalerite in equilibrium with pyrite. Iso-compositional curves of FeS in sphalerite are also plotted. Adapted from diagram in Vaughan and Craig (1978). The stippled area represents Nenthead mineralisation conditions as plotted from data of table 9.1

Estimated sulfur fugacity values for the environment of deposition of the Nenthead sphalerite may be plotted on the sphalerite-wurtzite stability field of Scott (1968). Figure 9.3 shows the Pennine range of sulfur fugacities plotted on this diagram. The fugacity values plot close to the sphalerite-wurtzite boundary, within the sphalerite stability field.

For the Nenthead ores, the textures indicate the deposition of a disordered 3C-sphalerite. The development of a disordered sphalerite may reflect the close proximity of depositional conditions (temperature and fS_2) to the stability field for the deposition of hexagonal ZnS, i.e. wurtzite. The precipitation of non-cubic ZnS layers during crystal growth would be favoured by the low temperature and sulfur fugacity of the depositing fluid. Also favouring the deposition of non-cubic ZnS layers would be the presence of trace amounts of Cd and Fe in the precipitated phase (Geilikman, 1982). For Fe-bearing ZnS some displacement of the sphalerite-wurtzite boundary to slightly higher sulfur fugacities may be expected (Scott and Barnes, 1972). The introduction of iron into ZnS increases the temperature range of the wurtzite stability field.

However, for the low temperatures of Nenthead sphalerite deposition (100-150 deg. C.) there is unlikely to be any significant shift of the wurtzite-sphalerite stability field due to the low levels of iron substitution for zinc permitted in the sphalerite structure. Below 240 °C. a maximum of 11.5 mole % FeS is permitted for sphalerite in equilibrium with pyrite (pyrrhotine absent).

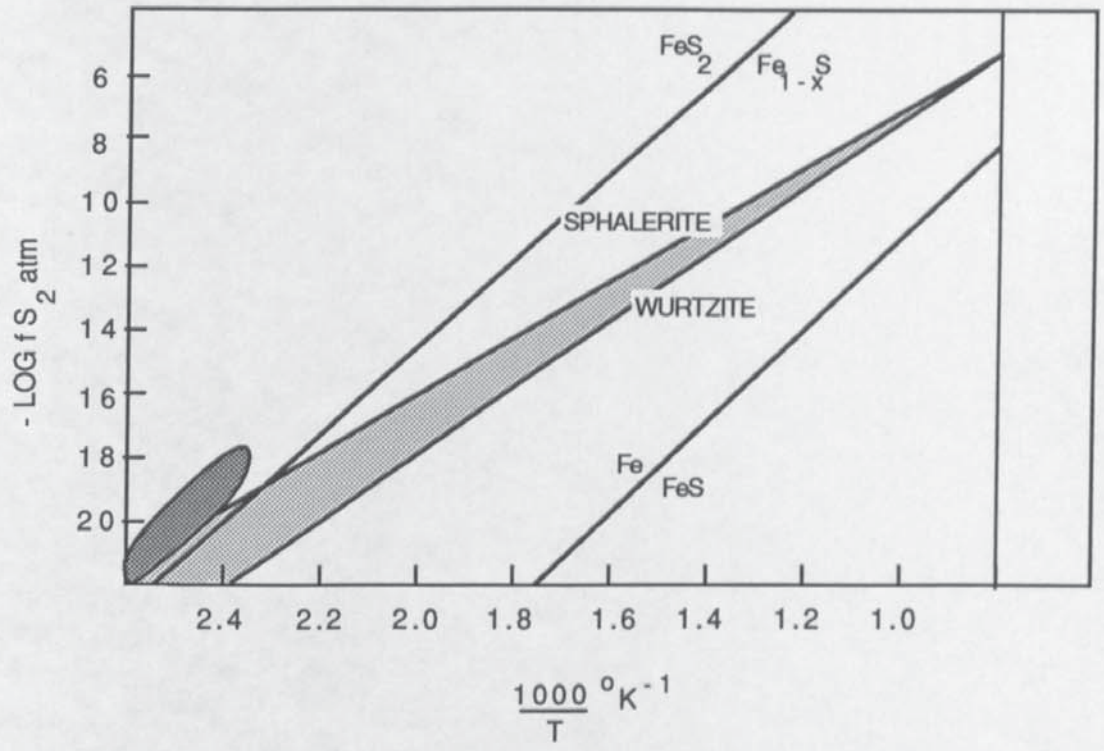

Figure 9.3

The sphalerite-wurtzite equilibrium boundary as a function of log sulfur fugacity and temperature. The stippled area represents uncertainty in the boundary extrapolation. Modified from Scott (1968).

Figure 9.4 shows the estimated range of sphalerite iron contents possible for the low temperature portion of the Fe-Zn-S system, along with the recorded iron contents.

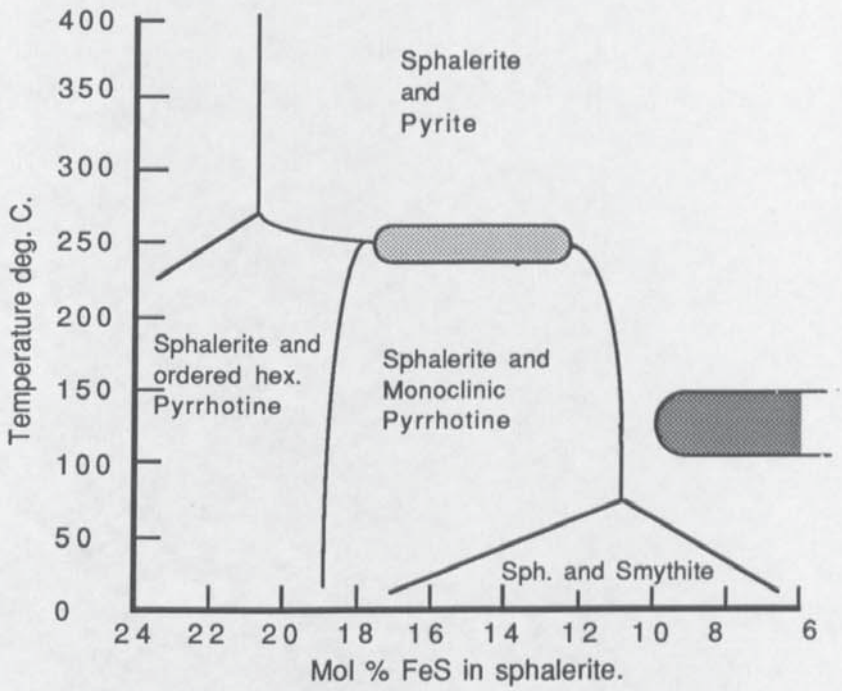

Nenthead Mineralisation of Thesis.

Qz - Po - Sphalerite assemblages of
Vaughan and Ixer 1980.

FIGURE 9.4

T-X projection of part of the FeS-ZnS-S system. Modified from Scott and Kissin (1973).

In conclusion; the deposition of a defect-rich, impure and structurally disordered, 3C-ZnS from a low temperature and low fS_2 fluid, is not inconsistent with either previous experimental studies or the other data from M.V.T. deposits.

9.4 Post-Ore Deformational Processes.

For the different generations of sphalerite little difference is apparent in their response to deformation from the microstructures developed. The only differences noted are optical, with deformation textures most obvious optically when developed in finely-banded *type-one* material. The same mechanisms are inferred to be operative in all varieties of sphalerite examined. Deformation is probably both syn and post-depositional.

Brittle and ductile processes are observed to operate within the grains; the former shown by fracture development and the latter by glide and twin-plane development. Some evidence for recovery is seen through localised subgrain development.

Sphalerites sampled from Nenthead may be called 'wet' (using the terminology of Clark and Kelly, 1973), because this sphalerite, deposited from a fluid medium, hosts numerous fluid inclusions and crystal defects. These may significantly modify the mechanical properties of the mineral.

Figure 9.5 shows the pressure vs. temperature fields for brittle (with minor ductile) and ductile-only deformation in a dry (relatively pure gem-like crystal) and a 'wet' (impure, inclusion and defect-rich) sphalerite, as experimentally determined by Clark and Kelly (1973). The majority of natural sphalerite samples will plot in a zone between the wet and dry transition boundaries. Between 100° and 150° C, a dry sphalerite will deform in a ductile manner only for a confining pressure of greater than 400 bars. Wet sphalerite will continue to deform in a brittle manner up to a confining pressure of

700 bars. The brittle field of deformation for wet sphalerite is increased due to fluid inclusions rupturing and inducing mineral fracture. Brittle deformation in sphalerite may be accompanied by up to 5% straining of the mineral before fracture (Clark and Kelly, 1973). Twin-planes, slip-planes, and polygonisation may result due to straining of the mineral (Spry, 1969).

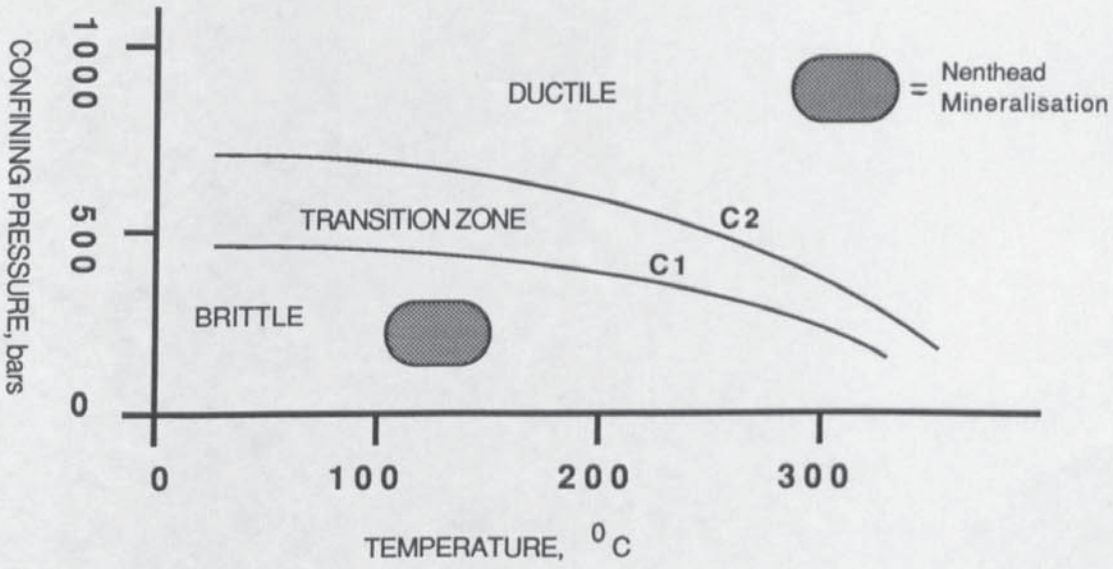

FIGURE 9.5

Temperature-Pressure diagram for the brittle to ductile transition for natural sphalerites. Curve C1 is for relatively 'dry' sphalerite, curve C2 for 'wet' sphalerite. The extent of the brittle field should be regarded as a maximum possible (adapted from Clark and Kelly, 1973).

The confining pressure for the transition from brittle with minor ductile to ductile-only deformation may be significantly lower for natural strain rates (strain rate value of 0.072 per sec. used by Clark and Kelly, 1973) and for straining in the presence of a fluid medium (ore-fluids or circulating ground waters). The field for ductile rather than brittle deformation, however, is not sufficiently reduced to induce ductile-only deformation for the Nenthead environment of deformation (see figure 9.5).

The confining pressure for the Nenthead mineralisation lies between a maximum of 275 bars (assuming a 100 % lithostatic component) and 110 bars (assuming a 100% hydrostatic component) if an overburden of 1100 metres is assumed (Sawkins, 1966 assumed an overburden of 1100 metres and an intermediate value of 200 bars for the confining pressure). A minimum of approximately 2800 metres (100 % lithostatic component) of overlying strata would be neccessary to induce ductile-only deformation for the temperatures of Nenthead mineralisation.

At higher temperatures of mineralisation (greater than 350° C) or at higher pressures (greater than 0.75 kbars) ductile deformational processes may be expected to take over, with recrystallisation textures in particular expected. The sphalerites studied by Henry et al., 1979, (5.5 kbar) and Hutchison and Scott, 1981, (6.0 k.bar) illustrate such behaviour.

Throughout the Nenthead sphalerites, a pervasive deformation microstructure is seen to overprint growth-related textures. Microstructures due to deformation (slip-planes, twin-planes, and some recovery textures) may be correlated with optical anisotropy .

Two 'end-member' anisotropic textures are distinguished: a growth-induced or 'grid-iron' anisotropy, and a widely seen deformation-induced overprinted anisotropy (lamelliform anisotropy). Relict grid-iron anisotropy is best observed in isolated, relatively undeformed grains of sphalerite set in the quartz-carbonate gangue. The large, growth-banded crystalline sphalerite masses host a well-developed lamelliform anisotropy.

The origin of the third or undulose form of anisotropy is problematical. Both growth-related and deformation-related origins are possible. Studies of undeformed Appalachian ores (chapter 4) and those of Seal, Cooper, and Craig (1985) show undulose anisotropy of a growth origin, related to the development of primary stacking disorder and growth defects within the sphalerite. Defect-rich sphalerite (e.g. banded regions of *type-one* sphalerite) could be expected to show an undulose anisotropy. Such anisotropy reflects lattice strain developed due to a high defect concentration. Deformational straining of the lattice, however, may also induce undulose anisotropy (cf. strained quartz). Regions of undulose anisotropy are seen associated with areas of sphalerite that have undergone some recovery by sub-grain development. For areas of sphalerite with a well-developed deformational microstructure, it is not always possible to distinguish growth-related undulose anisotropy from deformation-induced undulose anisotropy. For regions that display an undulose anisotropy, the associated textures and microstructures have to be considered before assigning a textural origin. For much of the Pennine sphalerite showing undulose anisotropy, the associated textures imply a deformation origin.

Despite widespread deformational overprinting of the Nenthead sphalerite, growth-related textures and microstructures can be recognised. Deformation is not sufficiently advanced to obliterate growth-related features (e.g. banding, inclusions), either by cataclasis or by recrystallisation. Such growth-related textures and microstructures are important in evaluating conditions of ore-deposition.

9.5 Copper-Related Alteration Processes.

Cuprian sphalerite is observed in much of the ore sampled from Nenthead. Copper enrichment is due to an alteration process, post-dates ore-deposition and probably post-dates chalcopyrite development. Alteration is independent of both episodes of chalcopyrite mineralisation (which form part of the primary mineral assemblage). Alteration of chalcopyrite locally may take the form of a 1 to 10 micron wide covelline rim. While much of the cuprian sphalerite shows no textural evidence for an alteration origin under the optical microscope, transmission electron microscopy of the triangular patches developed provides evidence of such an origin. The observation of sulfur-deficient copper compounds along twin- and slip-planes suggest a post-ore paragenesis. Pennine sphalerite is iron-poor relative to many 'diseased' sphalerites (e.g. Kuroko-type zinc ores). The low levels of iron may account for the development of a copper rather than a copper-iron alteration mineralogy. Copper-iron sulfides are documented from a variety of sphalerite ores which have undergone Cu-related alteration (Dickinson, 1984 and pers. comm.,

1986).

The development of sub-microscopic copper minerals in sphalerite may account for many of the anomalously high Cu levels reported for sphalerite. Phase equilibrium studies (see section 2.5) necessitate Cu-levels below those reported from 'diseased' and cuprian sphalerites (e.g. Sugaki et al., 1987). Cuprian sphalerites hosting up to 15 wt percent copper have been reported from a supergene environment (Clark and Sillitoe, 1970). The development of sub-microscopic copper-bearing phases is also reported from 'diseased' sphalerite (Dickinson, 1984; Dickinson and Pattrick, 1986). Numerous copper and copper-iron sulfides appear to develop as precursors to 'chalcopyrite disease'. Nenthead material sampled has developed only copper-bearing, sulfur-deficient, phases rather than Cu and Cu-Fe sulfides. This is attributed to the passage of post-ore supergene fluids. Such fluids differ in both chemistry and temperature from those thought to be responsible for 'chalcopyrite disease', which in Kuroko style ores, have a reported temperature of greater than 250° C (see Ohmoto et al., 1983, for a full discussion of the nature of the fluids responsible for post-sphalerite chalcopyrite development in the 'Black' and 'Yellow' Kuroko ores of Japan).

The studies of Eldridge et al. (1983), Barton and Bethke (1987) and DeWaal and Johnson (1981) suggest the replacive mechanisms involved in 'chalcopyrite disease' development utilise the iron-component of the host sphalerite. The replacement of sphalerite by chalcopyrite along certain horizons is attributed to the preferential replacement of iron-rich growth bands and patches. Pennine sphalerite, relatively iron-poor, shows only a low degree of

copper enrichment (up to 1 wt. %). These factors may promote the development of Cu-carbonates and hydroxides rather than sulfides.

Conditions outlined in Eldridge et al. (1983), and Ohmoto et al. (1983), for the the Cu-alteration models of the Kuroko style ores, sharply contrasts with those possible for the alteration of the Nenthead samples. For the Kuroko ores replacement of an iron-bearing sphalerite is ascribed to hot (up to 350° C.) copper-rich fluids. For the Nenthead alteration a maximum fluid temperature for the iron-bearing sphalerite is 150 °C., assuming a syn-mineralisation alteration. However, if the alteration is assumed to be late-stage and post-dating ore deposition, an alteration temperature of 25 °C. is more probable. Such differences in temperature between the Kuroko and Nenthead fluids may give rise to very different resultant alteration mineralogies and textures. The role of antimony, detected in many copper-rich areas, is unknown for the Pennine ores sampled.

The Nenthead copper-related alteration textures are seen as a possible first stage in the Cu-alteration of sphalerite. The use of deformation-related and growth-related pathways (twin-planes, glide-planes, and grain boundaries) overcomes the 'impervious' and refractory nature of the host phase.

9.6 Summary.

Textural and microstructural observations for the Nenthead samples are briefly summarised below:

1. Growth-related textures and microstructures differ from later deformation-related ones. Although modified, the growth-related textures and microstructures are distinguishable despite deformational overprinting.

2. Fluid inclusion and analytical studies indicate a low temperature (100° to 150°C.), highly saline (20 to 25 wt. % equivalent NaCl) fluid with a fluctuating sulfur fugacity (approx. 10^{-17} to 10^{-22} atm.). Levels of ZnS in solution fluctuated from supersaturation to undersaturation.

3. The fluctuating fluid chemistry is texturally recorded by delicately growth-zoned crystals, many of which are cross-cut by dissolution surfaces. Two varieties of growth-banded sphalerite are recognised; a widespread iron-banded variety, and a paragenetically early variety, banded due to the presence of horizons rich in submicroscopic inclusions and localised crystal defects.

4. The zinc sulfide studied takes the form of a disordered 3C-sphalerite polytype. Disorder is both growth-related (localised defects and stacking faults) and deformation-related (glide- and twin-planes). Areas of sphalerite principally hosting deformational

defects typically develop a lamelliform anisotropy. Areas of sphalerite dominated by a growth-related microstructure exhibit an undulose or grid-iron anisotropy. Undulose anisotropy is also developed locally where deformed sphalerite has undergone some recovery, sub-grain development or recrystallisation.

5. The deformationally-induced slip- and twin-plane fabric permitted the passage of later copper-bearing fluids; these appear to have been both associated with late-stage ore formation processes and post ore formation. Twin- and slip-planes are seen decorated by copper-rich, sulfur-deficient, minerals. Altered areas of sphalerite are 'Cu-rich' when analysed with the electron microprobe.

CHAPTER 10: Conclusions and Suggestions for Future Research.

10.1 Conclusions.

The thesis sucessfully demonstrates the wealth of information regarding mineralisation conditions that can be gleaned from a textural and mcrostructural study of one particular ore mineral. The range of optical, electron-optical, analytical and inclusion techniques that were applied in the study enabled the temperature, salinity, and sulfur fugacity of the mineralising fluid to be estimated.

The use of doubly-polished thin sections, as opposed to polished blocks, is essential for the examination of many of the textures developed. Many previous 'definitive' studies of zinc-bearing ores employed only polished blocks and, as the studies of Barton (1978) show, much relevant information regarding the mineralisation processes and conditions must have been missed in such studies.

The transparency of sphalerite enabled the observation and study of the delicate growth-related textures developed in the Pennine material. Despite a later deformation textural overprint, the refractory nature of the phase ensured textural preservation. For both the Pennine and the Appalachian material studied, the techniques employed successfully allowed growth-related textures to be distinguished from deformation-related textures and micro-structures. Similiar textural studies of other zinc-bearing ores should also yield much information regarding conditions and

processes of mineralisation.

10.2 Suggestions for Future Research.

Possible future areas of interest are suggested from the petrographic, analytical, and electron optical studies of the Appalachian and Pennine material. Such areas are given below:

1. An Analytical T.E.M. investigation of 'cuprian' sphalerite from the Nenthead region and elsewhere, to identify copper-related alteration minerals. The possibliity of a relationship between alteration mineralogy (i.e. sulfide or non-sulfide) and degree of copper enrichment of the host sphalerite should be investigated.

2. A T.E.M. study of defect-rich or disordered sphalerite similar to that described by Barton and Bethke (1987) could be undertaken to determine the nature of the defects. Analytical T.E.M techniques could be employed to identify the nature of the 'blotching' seen decorating many of the defects.

3. Petrographic and T.E.M. studies of deformed sphalerite (natural and synthetic) to confirm the observed relationship between the density of {111} slip- and twin-planes and the degree of crystal deformation.

Specifically for the Pennine material, further studies could also involve:

4. A T.E.M. study of deformed sphalerite from the 'copper-rich' higher temperature assemblages of the Alston Block (e.g. the cpy-po assembages of Tynebottom Mine and The Great Sulphur Vein, as described in Vaughan and Ixer, 1980).

2. A high resolution T.E.M. examination of the defect-rich banded regions of *type-one* sphalerite to determine the nature of the submicroscopic defects and inclusions.

3. Petrographic and analytical studies to determine the extent of *type-one* sphalerite development in the Alston Block.

APPENDIX 1

Data Correction Procedures for Thermometric Analysis of Fluid Inclusions.

A computer based method for correcting thermometric data was employed. The correction procedure is based on the program 'FLINCOR' of Robinson (1985). The program was modified by J. Naden of the Department of Geological Sciences, University of Aston in Birmingham.

The program uses 'calibration' data derived from a variety of standard compounds (see table 3.1) for various heights above the sapphire window (see section 3.5.1). Standards are chosen so as to span the temperature range of interest (-30° C. to 200° C.). Data processing is in three parts:

1. The measurement of vertical thermal gradients for the stage and the correction of measurements to a reference datum height above the stage (0.1 millimetres).

2. A calibration correction to correct the observed temperatures (now corrected to the reference datum height) for the deviation of the temperature sensor's response from linearity. This correction utilises the differences recorded between the observed melting temperature and the true melting temperature of the standards.

3. The calculation of the error due to the spread of measurements obtained for any single inclusion.

A series of calibration curves were constructed for each standard compound of temperature deviation due to vertical thermal gradients. From the calibration curves the gradient and intercept for each curve is calculated and input into the program along with the true melting temperature of the standard. The observed melting temperatures are input into the program and the corrected temperature computed along with possible measurement error at the 95% confidence level. Program structure is given in figure A2.1.

The error value computed $S_F = \sqrt{[S_{VTGC}^2 + S_{CC}^2 + S_M^2]}$ (A2.1)

Where;

S_{VTGC} is the standard error of the vertical temperature gradient correction calculated at T_m (obs) °C. for a distance t mm above the sapphire window.

S_{CC} is the standard error of the calibration correction at T_m (obs) °C.

S_M is the standard error of the mean measured T_m (obs) °C.

The 95% confidence interval for the final inferred temperature is $T_{corrected} \pm 4S_F$ (Robinson, 1985).

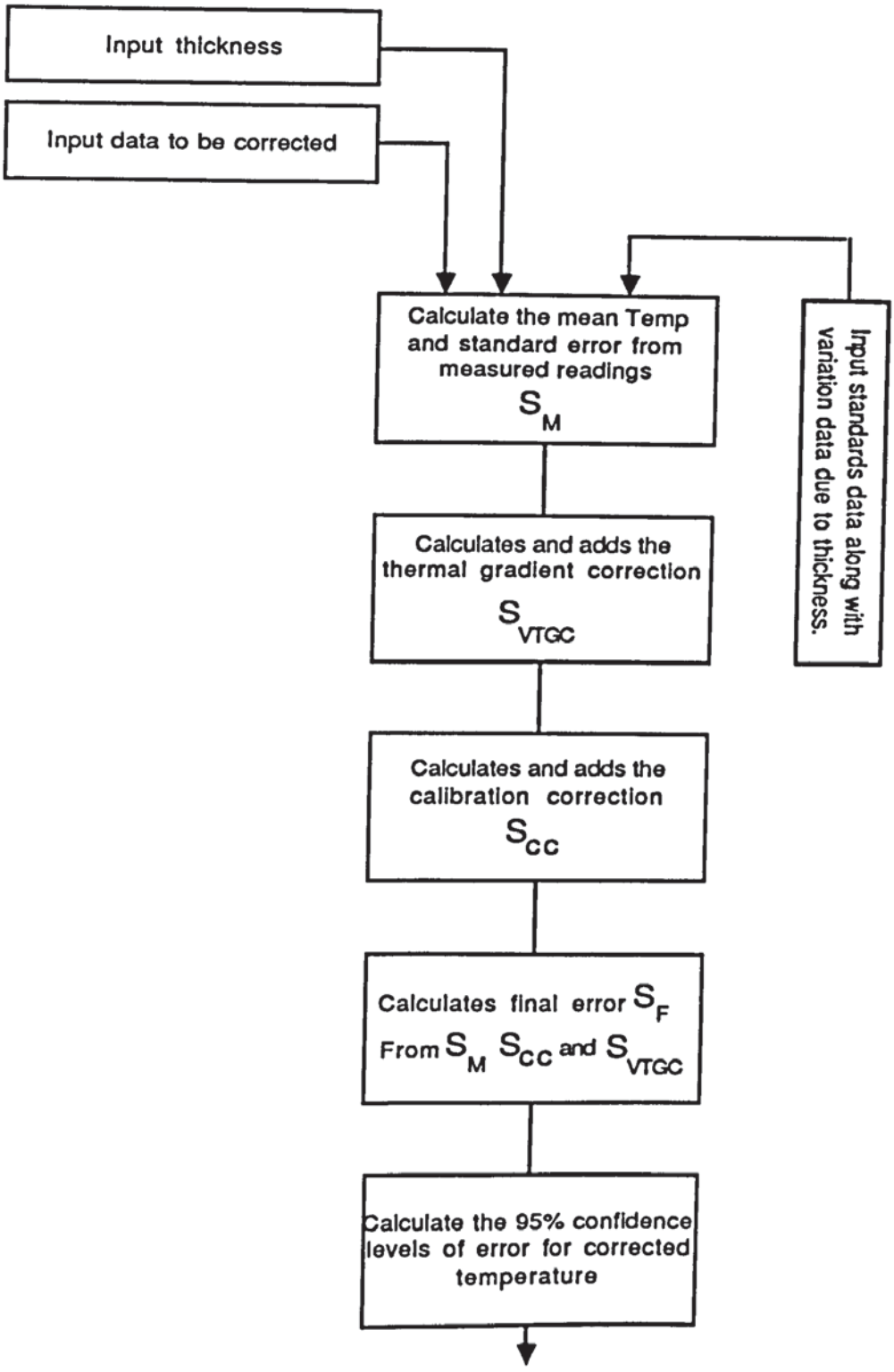

Figure A1.1

Schematic diagram of the program 'FLINCOR' used to correct the inclusion data. Full details of the program parameters and a listing is given in Robinson (1985).

APPENDIX 2

NH06 B1 Data Set 1: *Type-One* Sphalerite.

Zn	64.011	64.473	63.376	64.982	64.858	64.816	65.071
Cu	0.012	0.248	0.160	0.176	0.154	0.170	0.102
Fe	2.008	1.560	2.681	1.731	1.801	1.609	1.473
As	0.006	0.093	0.101	0.032	0.089	0.020	0.054
Cd	0.121	0.398	0.814	0.479	0.377	0.351	0.332
Sb	0.054	0.109	0.100	0.129	0.135	0.132	0.113
S	33.576	32.711	32.888	33.046	32.670	32.807	32.851
Total	99.788	99.593	100.12	100.576	100.083	99.906	99.998

Zn	65.452	65.134	65.438	64.891	64.549	64.165	64.159
Cu	0.122	0.256	0.100	0.144	0.164	0.215	0.166
Fe	1.558	1.390	1.320	1.568	1.637	1.893	2.188
As	0.056	0.060	0.084	0.106	0.037	0.107	0.090
Cd	0.397	0.278	0.164	0.378	0.518	0.556	0.566
Sb	0.111	0.162	0.129	0.153	0.141	0.120	0.111
S	32.889	32.898	32.738	33.149	32.821	32.812	32.965
Total	100.584	100.178	99.973	100.389	99.867	99.867	100.253

Zn	65.031	63.689	65.211	65.032	65.268	64.963	63.798
Cu	0.149	0.282	0.238	0.264	0.135	0.198	0.192
Fe	1.625	2.507	1.593	1.414	1.392	1.604	2.327
As	0.000	0.034	0.079	0.063	0.056	0.060	0.051
Cd	0.415	0.736	0.298	0.309	0.228	0.350	0.541
Sb	0.123	0.062	0.127	0.145	0.141	0.115	0.100
S	32.925	32.956	32.896	32.767	32.827	32.921	32.916
Total	100.267	100.265	100.443	99.994	100.047	100.210	99.925

Zn	63.794	63.088	63.553	64.516	64.637	64.637	64.818
Cu	0.140	0.169	0.203	0.209	0.240	0.209	0.170
Fe	2.088	2.738	2.631	1.480	1.681	1.480	1.505
As	0.128	0.121	0.059	0.044	0.043	0.044	0.019
Cd	0.515	0.665	0.656	0.318	0.432	0.318	0.367
Sb	0.116	0.078	0.081	0.132	0.100	0.132	0.154
S	33.091	32.871	32.839	32.898	32.908	32.898	32.963
Total	99.872	99.730	100.024	99.598	100.041	99.718	99.995

Zn	65.012	65.435	65.010	64.697	65.273	64.925	65.387
Cu	0.264	0.172	0.233	0.176	0.236	0.183	0.197
Fe	1.389	1.395	1.467	1.337	1.364	1.284	1.366
As	0.039	0.090	0.075	0.036	0.040	0.096	0.112
Cd	0.284	0.325	0.325	0.262	0.284	0.317	0.267
Sb	0.173	0.136	0.102	0.120	0.161	0.111	0.129
S	32.909	32.759	32.927	32.906	32.746	32.778	32.893
Total	100.071	100.311	100.139	99.534	100.104	99.694	100.351

Zn	62.991	63.685	65.266	65.503	64.229	65.045	63.573
Cu	0.201	0.126	0.090	0.176	0.180	0.216	0.185
Fe	2.529	2.645	1.663	1.536	1.814	1.601	2.299
As	0.019	0.012	0.023	0.068	0.034	0.048	0.033
Cd	0.664	0.480	0.239	0.241	0.454	0.435	0.579
Sb	0.063	0.079	0.097	0.108	0.104	0.094	0.087
S	32.991	32.957	32.914	32.880	32.798	32.369	32.909
Total	99.459	99.984	100.291	100.514	99.614	99.808	99.665

Zn	64.645	65.430	64.421	65.113	65.381	65.377	65.662
Cu	0.128	0.088	0.115	0.088	0.175	0.099	0.127
Fe	1.598	1.625	2.409	1.220	1.275	1.364	1.412
As	0.008	0.103	0.050	0.041	0.094	0.141	0.108
Cd	0.380	0.320	0.595	0.176	0.273	0.309	0.383
Sb	0.124	0.124	0.092	0.122	0.138	0.111	0.113
S	32.937	32.807	32.780	33.043	33.070	32.812	32.861
Total	99.819	100.497	100.461	99.803	100.406	100.213	100.666

Zn	65.264	65.711	65.369	65.604	65.002	65.726	65.622
Cu	0.129	0.115	0.090	0.153	0.098	0.202	0.171
Fe	1.322	0.790	0.826	0.684	0.728	0.738	0.777
As	0.052	0.076	0.056	0.086	0.092	0.090	0.084
Cd	0.285	0.159	0.160	0.156	0.179	0.191	0.228
Sb	0.100	0.089	0.077	0.117	0.099	0.141	0.148
S	32.830	32.753	32.817	32.787	32.969	32.944	32.878
Total	99.981	99.692	99.394	99.588	99.166	100.032	99.908

Zn	66.079	65.705	65.278	64.774	65.392	65.800	65.688
Cu	0.061	0.054	0.086	0.159	0.085	0.157	0.105
Fe	0.776	1.013	1.174	1.087	1.229	1.079	1.181
As	0.045	0.060	0.093	0.037	0.066	0.002	0.127
Cd	0.187	0.213	0.258	0.201	0.268	0.178	0.248
Sb	0.059	0.073	0.107	0.159	0.090	0.140	0.117
S	32.686	32.898	33.011	32.731	32.597	32.798	32.815
Total	99.893	100.017	100.007	99.148	99.728	100.155	100.280

Zn	64.774	65.202	64.991	64.651	65.631	65.587	65.270
Cu	0.132	0.124	0.104	0.110	0.136	0.107	0.138
Fe	1.300	1.318	1.397	1.592	1.456	1.242	1.129
As	0.071	0.019	0.019	0.053	0.080	0.058	0.088
Cd	0.285	0.358	0.379	0.408	0.355	0.336	0.181
Sb	0.101	0.105	0.114	0.117	0.110	0.122	0.138
S	32.681	32.774	32.918	32.628	32.814	33.193	32.407
Total	99.344	99.899	99.922	99.558	100.582	100.644	99.352

Zn	64.356
Cu	0.170
Fe	1.030
As	0.048
Cd	0.152
Sb	0.176
S	31.437
Total	97.370

Data Set NH06 B2 DATA SET 1 *Type-two* sphalerite

Zn	62.549	63.511	62.361	62.912	62.169	63.670	64.222
Cu	0.287	0.296	0.337	0.222	0.072	0.067	0.189
Fe	1.776	1.830	1.953	2.017	1.323	1.628	1.118
As	0.000	0.030	0.044	0.067	0.011	0.002	0.032
Cd	0.101	0.087	0.033	0.081	0.017	0.118	0.092
Sb	0.043	0.054	0.068	0.055	0.038	0.048	0.052
S	33.303	33.123	33.214	33.008	33.097	33.089	33.159
Total	98.060	98.931	98.010	98.362	96.726	98.622	98.865

Zn	64.295	62.141	61.336	61.597	62.920	59.933	61.268
Cu	0.081	0.055	0.100	0.087	0.305	0.041	0.106
Fe	1.957	3.036	4.948	4.593	3.030	5.472	5.285
As	0.026	0.008	0.023	0.022	0.049	0.000	0.016
Cd	0.120	0.198	0.210	0.168	0.168	0.235	0.188
Sb	0.052	0.068	0.075	0.085	0.082	0.044	0.052
S	33.134	33.251	32.741	33.179	33.110	33.303	33.326
Total	99.666	98.757	99.434	99.730	99.664	99.027	100.241

Zn	61.531	60.949	60.359	62.110	61.341	62.640	63.079
Cu	0.057	0.049	0.085	0.060	0.050	0.010	0.000
Fe	4.568	4.805	4.436	3.845	3.862	3.706	2.316
As	0.000	0.019	0.029	0.056	0.023	0.026	0.038
Cd	0.295	0.35	0.270	0.296	0.263	0.156	0.287
Sb	0.035	0.046	0.038	0.036	0.042	0.037	0.051
S	33.207	33.082	33.197	33.121	33.239	33.092	33.044
Total	99.692	99.302	98.415	99.525	98.820	99.667	98.815

Zn	62.791	63.622	60.427	60.344	59.821	63.056	60.383
Cu	0.031	0.000	0.025	0.019	0.000	0.016	0.013
Fe	2.122	2.081	4.052	4.393	4.557	3.084	4.561
As	0.046	0.002	0.055	0.042	0.061	0.011	0.057
Cd	0.110	0.086	0.220	0.175	0.270	0.115	0.180
Sb	0.046	0.050	0.046	0.044	0.030	0.036	0.055
S	33.185	33.244	33.099	33.270	33.297	33.261	32.983
Total	98.331	99.084	97.924	98.287	98.036	99.579	98.236

Zn	60.573	63.576
Cu	0.017	0.015
Fe	5.205	3.225
As	0.028	0.018
C	0.200	0.163
Sb	0.038	0.035
S	33.145	33.233
Total	99.205	100.265

NH06 B2 DATA SET 2: *Type-one* sphalerite.

Zn	64.180	64.316	64.178	64.954	63.515	64.501	63.960
Cu	0.160	0.237	0.008	0.091	0.036	0.097	0.058
Fe	2.098	2.005	2.292	1.773	2.363	1.800	2.347
As	0.026	0.060	0.022	0.083	0.011	0.112	0.000
Cd	0.138	0.077	0.222	0.101	0.194	0.101	0.217
Sb	0.083	0.079	0.040	0.049	0.047	0.051	0.049
S	32.872	32.968	32.280	32.889	32.923	32.894	32.876
Total	99.558	99.742	99.042	99.939	99.089	99.555	99.507
Zn	65.403	65.309	65.383	65.138	65.183	64.457	64.741
Cu	0.505	0.097	0.108	0.124	0.121	0.141	0.286
Fe	0.811	1.265	1.361	1.504	1.507	1.278	1.364
As	0.115	0.041	0.112	0.057	0.059	0.080	0.058
Cd	0.297	0.296	0.366	0.437	0.458	0.220	0.275
Sb	0.279	0.096	0.097	0.108	0.119	0.124	0.181
S	32.240	32.663	32.821	32.887	32.931	33.027	33.019
Total	99.653	99.767	100.248	100.254	100.37	99.327	99.926
Zn	64.531	64.944	63.676	64.729	62.376	64.005	62.891
Cu	0.166	0.254	0.341	0.116	0.162	0.242	0.145
Fe	1.600	1.394	1.380	1.480	2.664	1.808	3.099
As	0.041	0.058	0.035	0.042	0.048	0.071	0.000
Cd	0.394	0.244	0.220	0.260	0.688	0.335	0.695
Sb	0.134	0.191	0.179	0.057	0.104	0.133	0.032
S	32.874	32.969	31.405	33.110	32.862	33.122	32.977
Total	99.739	100.054	97.237	99.793	98.904	99.717	99.839
Zn	63.966	64.078	64.594	64.005	63.618	63.608	64.294
Cu	0.143	0.076	0.232	0.245	0.313	0.382	0.221
Fe	2.035	1.581	1.586	1.477	1.531	1.565	1.639
As	0.105	0.071	0.061	0.053	0.134	0.044	0.044
Cd	0.564	0.327	0.299	0.235	0.273	0.271	0.357
Sb	0.126	0.094	0.170	0.202	0.167	0.218	0.181
S	32.796	32.081	32.929	33.072	32.913	32.971	32.926
Total	99.735	99.308	99.871	99.289	98.949	99.062	99.662

Zn	63.822	63.961	64.202	63.645	63.649	63.325	63.056
Cu	0.137	0.073	0.072	0.119	0.341	0.174	0.145
Fe	1.747	1.652	1.624	1.827	1.653	1.951	1.961
As	0.081	0.074	0.078	0.008	0.052	0.063	0.078
Cd	0.360	0.409	0.324	0.301	0.314	0.411	0.346
Sb	0.104	0.085	0.080	0.139	0.217	0.124	0.126
S	33.066	32.907	32.798	32.742	32.928	32.981	33.029
Total	99.317	99.161	99.179	98.781	99.154	99.028	98.741

Zn	64.092	63.516	61.860	63.899	63.065	62.484	64.136
Cu	0.098	0.067	0.238	0.138	0.199	0.102	0.143
Fe	1.828	1.866	2.972	1.190	1.246	1.260	1.465
As	0.109	0.073	0.030	0.069	0.014	0.084	0.070
Cd	0.389	0.434	0.608	0.292	0.260	0.355	0.375
Sb	0.112	0.098	0.073	0.108	0.115	0.084	0.118
S	32.998	33.506	32.958	32.990	32.722	33.169	32.992
Total	99.626	99.560	98.739	98.688	97.621	97.537	99.298

Zn	63.571	64.078	64.493	64.668	64.952	65.006	65.163
Cu	0.157	0.148	0.090	0.114	0.190	0.147	0.228
Fe	1.622	1.310	1.410	1.406	1.355	1.310	1.320
As	0.085	0.044	0.000	0.049	0.036	0.029	0.011
Cd	0.352	0.234	0.244	0.284	0.260	0.264	0.281
Sb	0.101	0.131	0.123	0.109	0.148	0.133	0.153
S	33.056	32.860	32.687	32.575	32.779	32.705	32.706
Total	98.945	98.803	99.046	99.205	99.720	99.595	99.861

Zn	63.286	64.534	65.124	64.018	62.448	63.367	65.045
Cu	0.142	0.192	0.206	0.280	0.212	0.264	0.249
Fe	2.803	1.690	1.356	1.741	3.464	2.253	1.382
As	0.053	0.082	0.086	0.122	0.086	0.035	0.077
Cd	0.724	0.276	0.214	0.407	0.687	0.497	0.254
Sb	0.060	0.144	0.193	0.078	0.041	0.082	0.126
S	32.680	32.660	32.594	32.695	32.889	32.597	32.666
Total	99.748	99.579	99.773	99.346	99.827	99.095	99.798

Zn	64.891	64.834	64.889	63.223	64.135	65.310	64.630
Cu	0.199	0.168	0.208	0.140	0.210	0.178	0.159
Fe	1.236	1.403	1.340	1.190	1.326	1.256	1.499
As	0.065	0.026	0.055	0.293	0.103	0.051	0.004
Cd	0.205	0.323	0.344	0.344	0.291	0.213	0.344
Sb	0.094	0.147	0.146	0.096	0.161	0.164	0.144
S	32.752	32.638	32.619	30.264	32.411	32.695	32.394
Total	99.442	99.538	99.602	95.550	98.638	99.867	99.175

Zn	64.813	64.441	64.882
Cu	0.172	0.406	0.185
Fe	1.290	1.618	1.489
As	0.103	0.068	0.045
Cd	0.288	0.489	0.170
Sb	0.118	0.076	0.149
S	32.625	32.541	32.443
Total	99.409	99.638	99.365

REFERENCES

Akizuki, M. E., 1970. Slip structure of heated sphalerite. American Mineralogist. 55,1302-1312.

Akizuki, M. E., 1981. Investigation of phase transition of natural ZnS minerals by high resolution electron microscopy. American Mineralogist. 62, 1006-1012.

Allen, E. T., and Crenshaw, J. L., 1912. The sulfides of zinc, cadmium, and mercury; their crystalline forms and genetic conditions. American Journal Science. 34, 341-396.

Aragona, F. S., and Delavignette, P., 1966. Fautes de croissance dans la wurtzite. Journal de Physique. 27, Supplement C3, 121-127.

Baars, J., and Brandt, G., 1973. Structural phase transitions in ZnS. Journal Physics Chem. Solids. 34, 905-909.

Barber, D. J., 1970. Thin foils of non-metals made for electron microscopy by sputter etching. Journal Materials Science. 5, 1-8.

Barber, D. J., 1972. Review: sputter thinning for transmission electron microscopy. In. Proc Fifth European Congress on Electron Microscopy. University of Manchester.

Barker, C. E., and Halley, R. B., 1986. Fluid inclusion, stable isotope, and vitrinite reflectance evidence for the history of the Bone Springs Limestone, Southern Guadaloupe Mountains, Texas. In Roles of Organic Matter in Sediment Diagenesis. Ed. Gauter, D. L. S. E. P. M. Special Publication No. 38.

Barnes, H. L., and Czamanske, G. K., 1967. Solubilities and transport of ore minerals: Geochemistry of Hydrothermal Ore Deposits. 1st. edition. Ed. Barnes, H. L. Holt, Rinehart and Winston, New York. 334-381.

Barnes, H. L., 1983. Ore-depositing reactions in Mississippi Valley-type deposits. In. Int'l Conf. on Mississippi Valley-type

Lead-Zinc Deposits, proceedings volume. Ed. Kisvarsanyi, G. et al. University of Missouri-Rolla, 77-85.

Barton, P. B., 1967. Possible role of organic matter in the precipitation of the Mississippi Valley ores. In. Economic Geology Monograph 3: Genesis of Stratiform Lead-Zinc-Barite-Fluorite Deposits. 371-378.

Barton, P. B., 1978. Some ore textures involving sphalerite from the Furutobe mine, Akita Prefecture, Japan. Mining Geology. 28, 293-300.

Barton, P. B., 1982. Sphalerite: Raconteur for mineral deposits. Min. Soc. Bull. (London). 57, 3-4.

Barton, P. B., and Bethke, P. M., 1987. Chalcopyrite disease in sphalerite: Pathology and epidemiology. American Mineralogist. 72, 451-467.

Barton, P.B., Bethke, P. M., and Roedder, E., 1977. Environment of ore deposition in the Creede mining District, San Juan Mountains, Colorado: Part 3. Progress towards interpretation of the chemistry of the ore forming fluid for the OH vein. Economic Geology. 72, 1-24.

Barton, P. B., Bethke, P. M., and Toulmin, P., 1963. Equilibrium in ore deposits. Min. Soc. America. Special Paper 1, 171-185.

Barton, P. B., and Skinner, B. J., 1967. Sulfide mineral stabilities. In. Geochemistry of Hydrothermal Ore Deposits. 1st. Edition. Ed. Barnes, H. L., p 236-333. Holt, Rinehart and Winston.

Barton, P. B., and Toulmin, P., 1966. Phase relations involving sphalerite in the Fe-Zn-S system. Economic Geology. 61, 815-849.

Bell, R. L., and Cahn, R. W., 1957. The dynamics of twinning and the interrelation of slip and twinning in zinc crystals. Proc. Royal Society London. A239, 494-521.

Boldish, S. I., 1973. Relationship of the band gap to crystal chemical parameters. Unpuplished M. S. Thesis, Pennsylvania State Univ.

Bott, M. H. P., 1967. Geophysical investigations of northern Pennine basement rocks. Proc. Yorkshire Geological Society. 36, 139-168.

Bott, M. H. P., and Masson-Smith, D., 1953. Gravity measurements over the northern Pennines. Geol. Magazine. 90, 127-130 (with discussion by Holmes, A., Turner, J. S., Trotter, F. M., and the authors, 221-3, 299-300).

Bott, M. H. P., and Masson-Smith, D., 1957. The geological interpretation of a gravity survey of the Alston Block and the Durham Coalfield. Quarterly Journal Geological Society of London. 113, 93-117.

Bourcier, W. L., Eldridge, C. S., Barnes, H. L., and Ohmoto, H., 1984. The chalcopyrite disease in Kuroko ore: An experimental investigation. Geol. Soc. America Abstracts with Programs. 16, 452.

Brown, G. C., Ixer, R. A., Plant, J. A., and Webb, P. C., 1987. The geochemistry of granites beneath the North Pennines and their role in orefield mineralisation. Trans. Inst. Mining and Metallurgy (Sect. B : Applied Earth Sciences). 96, B65-B76.

Burruss, R. C., 1981. Hydrocarbon fluid inclusions in studies of sedimentary diagenesis. Min. Soc. Canada Short Course Handbook No. 6. 138-156.

Caless, J. R., 1983. Geology, Paragenesis, and Geochemistry of Sphalerite Mineralisation at the Young Mine, Mascot-Jefferson City Zinc District, East Tennessee. Unpuplished M. S. Thesis. Virginia Polytechnic Inst. State Univ. Blacksburg Virginia. 162p.

Champness, P. E., 1977. Transmission electron microscopy in earth science. Annual Review, Earth Planet. Sci. 5, 203-226.

Christie, J. M., and Ardell, A. J., 1976. Deformation structures in

minerals. In. Electron Microscopy in Mineralogy. Editor Wenk, H. R. Springer-Verlag, Berlin. 374-403.

Clark, A. H., and Sillitoe, R. H., 1970. Cuprian sphalerite and a probable copper-zinc sulfide., Cachiyuyo de Llampos, Copiapo, Chile. American Mineralogist. 55, 1021-1025.

Clark, B. R., and Kelly, W. C., 1973. Sulfide deformation studies: 1, experimental deformation of pyrrhotine and sphalerite to 2,000 bars and 500° C. Economic Geology. 68, 332-352.

Cotton, F. A., and Wilkinson, G., 1972. Advanced Inorganic Chemistry. Interscience Publishers, New York. 906-907.

Craig, J. R., and Kullerud, G., 1973. The Cu-Zn-S System. Mineralium Deposita. 8, 81-91.

Craig, J. R., Solberg, T. N., and Vaughan, D. J., 1983a. Growth characteristics of sphalerites in Appalachian zinc deposits. In. Int'l Conf. on Mississippi Valley-type Lead-Zinc Deposits, proceedings volume. Ed. Kisvarsanyi, G. et al. University of Missouri-Rolla, 317-327.

Craig, J. R., Solberg, T. N., and Vaughan, D. J., 1983b. Compositional variations in sphalerite ores of the East and Central Tennessee zinc deposits. In. Craig, J. R., ed., Tennessee Zinc Deposits. Blacksburg Virginia Polytechnic Inst. State Univ. Guidebook 9. 152-164.

Craig, J. R., and Vaughan, D. J., 1981. Ore Microscopy and Ore Petrography. Wiley, New York. 406p.

Craig, J. R., and Vaughan, D. J., 1986. Paragenetic studies of growth-banded sphalerites in Mississippi valley-type zinc deposits of the Appalachians. In Mineral Parageneses, Augustithis, S. S. et al., eds. Theophrastus Publications, Athens., 133-158.

Crawford, J., Fulweiler, R. E., and Miller, H. W., 1969. Mine geology of the New Jersey Company's Jefferson City Mine. In. Papers on the

Stratigraphy and Mine Geology of the Kingsport Formation Tennessee. Tennessee Divn. Geology Report. 23, 64-75.

Daniels, B. K., 1966. The phase changes of zinc sulfide and the stacking sequence of a new 66 polytype. Phil. Magazine. 14, 487-500.

DeWaal, S. A., and Johnson, J. A., 1981. Chemical heterogeneity of sphalerite in a base metal sulfide deposit. Economic Geology. 76, 694-705.

Dickinson, C., 1984. Oral Presentation at a General Meeting of the Mineralogical Society held at Burlington House London, on the 8th November,1984.

Dickinson, C., and Pattrick, R. A. D., 1986. Electron microscope investigation of sphalerite and sphalerite-chalcopyrite intergrowths. International Mineral Association. Abstracts with programmes. 89.

Dunham, K. C., 1934. Genesis of the north Pennine ore deposits. Quarterly Journal Geological Society of London. 90, 689-720.

Dunham, K. C., 1948. Geology of the Northern Pennine Orefield. Volume 1 Tyne to Stainmore. Mem. Geol. Survey U. K. H. M. S. O., London. 357p.

Dunham, K. C., in press. Mineralisation and Mining in the Dinantian and Namurian rocks of the northern Pennines.

Dunham, K. C., Dunham, A. C., Hodge, B. L., and Johnson, G. A., 1965. Granite beneath Visean sediments with mineralisation at Rookhope, northern Pennines. Quarterly Journal Geological Society of London. 121, 383-417.

Edwards, A. B., 1947. Textures of the ore minerals and their significance . Australian Institute of Mining and Metallurgy, Mellbourne. 185p.

Eldridge, C. S., Barton, P. B., and Ohmoto, H., 1983. Mineral textures

and their bearing on the formation of Kuroko orebodies. Economic Geology Monograph 5: The Kuroko and related volcanogenic massive sulfide deposits. 241-281.

Farkas-Jahnke, M., and Gacs, P., 1979. Changes in structure of ZnS crystals due to mechanical stresses. Kryst. und Tech., 14, 1475-1482.

Fehn, U., Cathles, L. M., and Holland, H. D., 1978. Hydrothermal convection and uranium deposits in abnormally radioactive plutons. Economic Geology. 73,1556-1566.

Fleet, M. E., 1975. Wurtzite: long period polytypes in dissordered 2H crystals. Science.190, 885-886.

Fleet, M. E., 1977a. The birefringence-structural state relation in natural zinc sulfides and its application to a schalenblende from Pribram. Canadian Mineralogist. 15, 303-308.

Fleet, M. E., 1977b. Structural transformations in natural ZnS. American Mineralogist. 62, 540-546.

Foley, N. K., 1980. Mineralogy and Geochemistry of the Austinville-Ivanhoe District, Wythe County, Virginia. M. S. thesis, Virginia Polytechnic Institute and State University, Blacksburg. 83p.

Foley, N. K., Sinha, A. K., and Craig, J. R., 1981. Isotopic composition of lead in the Austinville-Ivanhoe Pb-Zn district, Virginia. Economic Geology. 76, 2012-2017.

Frank, F. C., 1949. Sessile dislocations. Proc. Physical Society., Ser. A. 62, 202-203.

Frater, K. M., 1985. Mineralisation at the Golden Grove Cu-Zn deposit, Western Australia. 2 Deformation textures of the opaque minerals. Canadian Journal Earth Sciences. 22, 15-26.

Frey, F., Jagodzinski, H., and Steger, G., 1986. On the phase transformation zinc blende to wurtzite. Bull. Mineral. 109,

117-129.

Frondel, C., and Palache, C., 1950. Three new polymorphs of zinc sulfide. American Mineralogist. 35, 29-42.

Fulweiler, R. E., and McDougal, S. E., 1971. Bedded ore structures, Jefferson City mine, Jefferson City, Tennessee. Economic Geology. 66, 763-769.

Geilikman, M. B., 1982. Mechanisms of polytype stabilisation during the wurtzite-sphalerite transition. Physics and Chemistry of Minerals. 8, 2-7.

Gize, A., Barnes, H. L., and Hoering, T. G., 1981. The organic geochemistry of three M.V.T.-deposits. Geol. Soc. America Abstracts with Programs. 13, 459.

Gize, A., and Barnes, H. L., 1987. The organic geochemistry of two Mississippi Valley-type lead-zinc deposits. Economic Geology. 82, 457-470.

Grant, N. K., and Bliss, M. C., 1983. Strontium isotope and rare earth element variations in non-sulfide minerals from the Elmwood-Gordonsville mines, Central Tennessee. In. Int'l Conf. on Mississippi Valley-type Lead-Zinc Deposits, proceedings volume. Ed. Kisvarsanyi, G. et al. University of Missouri-Rolla, 206-210.

Green, H. W., 1976. Plasticity of olivines in peridotites. In. Electron Microscopy in Mineralogy. Editor Wenk, H. R. Springer-Verlag, Berlin. 443-464.

Haas, J. L., 1976. Physical properties of the coexisting phases and thermochemical properties of the H_2O component of boiling NaCl solutions (preliminary steam tables for NaCl solutions). U. S. Geol. Survey Bulliten. 1421-A. United States Dept. Interior, Washington.

Hagni, R. D., 1983. Minor elements in Mississippi Valley-type deposits. In. Unconventional Mineral Deposits. Editor, Shanks, W. Soc.

Mining Engineers, AIMME. 71-88.

Hatcher, R. D., and Odom, A. L., 1980. Timing of thrusting in southern Appalachians, U. S. A. - : Model for orogeny. Journal Geol. Soc. London. 137, 321-327.

Henry, D. K., Craig, J. R., and Gilbert, M. C., 1979. Ore mineralogy of the Great Gossan Lead, Virginia. Economic Geology. 74, 645-656.

Heuer, A. H., Firestone, R. F., Snow, J.D., Green, H. W., Howie, R. G., and Christie, J. M., 1971. An improved ion-thinning apparatus. Rev. Sci. Inst. 42, 1177-1184.

Hill, W. T., and Weddow, H., 1971. An early Middle Ordovician age for collapse breccias in the East Tennessee zinc deposits as indicated by compaction and porosity features. Economic Geology. 66, 725-734.

Hirsch, P. B., Howie, A., Nicholson, R. B., Pashley, D. W., and Wheelan, M. J., 1965. Electron Microscopy of thin crystals. Butterworths, London. 563p.

Holland, J. G., and Lambert, R. St. J., 1970. Weardale Granite, in Johnson, G. A. L., ed., Geology of Durham County. Newcastle History Society, 103-118.

Hollenbaugh, D. W., and Carlson, E. H., 1983. The occurence of wurtzite polytypes in Eastern Ohio. Canadian Mineralogist. 21, 697-703.

Hutchison, M. N., and Scott, S. D., 1981. Sphalerite geobarometry in the Cu-Fe-Zn-S system:. Economic Geology. 76,143-153.

Ineson, P. R., 1976. Ores of the northern Pennines, the Lake District and North Wales, in Wolf, K. L., ed., Handbook of stratabound and stratified ore deposits. Elsevier, Amsterdam. 5, 197-230.

Ixer R. A., 1986. The ore mineralogy and parageneses of the lead-zinc-fluorite-baryte orefields of the English Pennine and Mendip Hills. In Mineral Parageneses, Augustithis, S. S. et. al., eds. Theophrastus Publications, Athens., 179-210.

Ixer, R. A., and Stanley, C. J., 1987. A silver-nickel-cobalt mineral association at Tynebottom Mine, Garrigill, near Alston, Cumbria. Proc. Yorkshire Geol. Soc. 46, 133-139.

Ixer, R. A., Stanley, C. J., and Vaughan, D. J., 1979. Cobalt-, nickel-, and iron-bearing sulphanarsenides from the North of England. Mineralogical Magazine. 43, 389-395.

Ixer, R. A., Vaughan, D. J., Pattrick, R. A. D., and Alabaster, T., 1986. Mineralogical studies and their bearing on the genesis of massive sulfide deposits from the Semail Ophiolite complex, Oman. In Metallogeny of Basic and Ultrabasic Rocks. Institute of Mining and Metallurgy, London., 33-48.

Jahnke, M. F., 1986. Relationship between different types of stacking faults and the occurence of certain polytype stackings. Bull. Mineral. 109, 69-80.

Kay, D., 1965. Techniques for Electron Microscopy. 2nd Ed. Blackwells, Oxford.

Kojima, S., and Sugaki, A., 1984. Phase relations in the central portion of the Cu-Fe-Zn-S system between 800° and 500° C. Mineral Journal. 12, 15-28.

Kojima, S., and Sugaki, A., 1985. Phase relations in the Cu-Fe-Zn-S system between 500° and 300° C. under hydrothermal conditions. Economic Geology. 80, 158-171.

Komatsu, H., and Sunagawa, I., 1965. Surface structure of sphalerite crystals. American Mineralogist. 50, 1046-1057.

Koski, R. A., Clague, D. A., and Oudin, E., 1984. Mineralogy and chemistry of massive sulfide deposits from the Juan de Fuca Ridge. Geol. Soc. America Bulletin. 95, 930-945.

Krishna, P., and Sebastian, M. T., 1986. Mechanisms of phase transformations in polytypes. Bull. Mineral. 109, 99-116.

Kullerud, G., 1953. The FeS-ZnS system: a geological thermometer. Norsk. Geol. Tidsskr. 32, 61-147.

Kyle, J. R., 1976. Brecciation, Alteration, and Mineralisation in the Central Tennessee Zinc District. Economic Geology. 71,892-903.

Lawrence, L. J., 1973. Polymetamorphism of the sulfide ores of Broken Hill, New South Wales, Australia. Mineralium Deposita. 8, 211-236.

Lorimer, G. W., and Cliff, G., 1984. Quantitative X-ray microanalysis of thin specimens. In. Quantitative Electron Microscopy, proceedings of the 25th Scottish Summer School in physics. Editors Chapman, J. N., and Craven, A. J. The Scottish Summer School in Physics, Edinburgh. 305p.

Mardix, S., 1984a. The formation of macroscopic polytypic regions in ZnS crystals. Journal Applied Crystallography. 17, 328-330.

Mardix, S., 1984b. Polytypism in Zinc sulfide. Coll. Abstracts., International conference on crystal growth and characterisation of polytype structures. Marseille, 38-40.

Mardix, S., 1986. Crystallographic aspects of polytypism in ZnS. Bull. Mineral. 109, 131-142.

Mardix, S., and Kiflawi, I., 1970. ZnS crystals each containing polytypes of two families. Crystal Lattice Defects. 1, 129-134.

Mardix, S., Lang, A. R., and Blech, I., 1971. On giant screw dislocations in ZnS polytype crystals. Phil. Magazine. 24, 683-693.

Mardix, S., and Steinberger, I. T., 1970. Tilt and structure transformations in ZnS. Journal Applied Physics. 41, 5339-5341.

McConnell, J. D. C., 1977. Electron microscopy and electron diffraction. In. Physical Methods in Determinative Mineralogy. Ed. Zussman, J., Academic Press, London. 719p. 475-527.

McCormick, J. E., Evans, L. L., Palmer, R. A., and Rasnick, F. D., 1971. Environment of the zinc deposits of the Mascot-Jefferson City District, Tennessee. Economic Geology. 66, 757-762.

McKie, D., and McKie, C., 1974. Crystalline Solids. Nelson Publishers, London. 628p.

McKnight, E. T., and Fischer, R. P., 1970. Geology and ore deposits of the Picher Field, Oklahoma and Kansas. U.S.G.S. Prof. Paper 588, 165p.

McLimans, R. K., Barnes, H. L., and Ohmoto, H., 1980. Sphalerite stratigraphy of the Upper Mississippi Valley zinc-lead district, southwest Wisconsin. Economic Geology. 75, 351-362.

Nelkowski, H., and Pfutzenreuter, O., 1971. Kristallstruktur und Doppelbrechung Fehlgeordneter ZnS Einkristalle. Acta Crystallography. A27, 296-298.

Nord, G. L., Heuer, A. H., and Lally, J. S., 1976. Pigeonite exsolution from Augite. In. Electron Microscopy in Mineralogy. Editor Wenk, H. R. Springer-Verlag, Berlin. 220-227.

Ohle, E. L., 1985. Breccias in Mississippi Valley-type deposits. Economic Geology. 80, 1736-1752.

Ohmoto, H., Mizukami, M., Drummond, S. E., Eldridge., C. S., Pisutha-Arnold, V., and Lenagh, T. C., 1983. Chemical processes of Kuroko formation. Economic Geology Monograph 5: The Kuroko and Related Volcanogenic Massive Sulfide Deposits. 570-603.

Oudin, E., 1983. Hydrothermal sulfide deposits of the East Pacific Rise (21^0 N) Part 1: Descriptive Mineralogy. Marine Mining. 4, 39-72.

Palache, C., Berman, H., and Frondel, C., 1944. Dana's System of Mineralogy, 7 ed., John Wiley and Sons, New York.

Potter, R. W., and Brown, D. L., 1977. The volumetric properties of aqueous sodium chloride solutions from 0° to 500° C. at pressures up to 2000 bars based on a regression of available

data in the literature. U. S. Geol. Survey Bulletin. 1421-C. United States Dept. Interior, Washington.

Putnis, A., and McConnell, J. D. C., 1980. Principles of Mineral Behaviour. Blackwells, Oxford. 257p.

Ramdohr, P., 1980. The Ore Minerals and their Intergrowths. Permagon Press, Oxford. 1207p. 2nd edn., 2 Vols.

Reading, H. G., 1978. Sedimentary Environments and Facies. Blackwells, Oxford.

Reed, S. J. B., 1975. Electron Probe Microanalysis. Cambridge University Press, Cambridge.

Richards, S. M., 1966. Mineragraphy of fault-zone sulphides, Broken Hill, N. S. W., C. S. I. R. O., Tech. Pub. 5. 27p.

Robie, R. A., Hemingway, B. S., and Fisher, J. R., 1978. Thermodynamic properties of minerals and related substances at 298.15 K and 1 bar / 10^5 pascals pressure and at higher temperatures. Geological Survey Bulliten 1452. U. S. G. S.

Robinson, A. G., 1985. Calibration of the Linkam TH600 Heating-Cooling Stage for Fluid Inclusion Microthermometry. Unpublished report GCB/145/85. Geochemistry Branch Exploration and Production Division. B. P. Research Centre, Sunbury-on Thames.

Roedder, E.,1962. Ancient fluids in crystals. Scientific American. Oct. 1962, 38-47.

Roedder, E., 1968. The non-colloidal origins of "colloform" textures in sphalerite ores. Economic Geology. 63, 451-471.

Roedder, E., and Dwornik, E. J.,1968. Sphalerite colour banding: lack of correlation with iron content, Pine Point, North West Territories, Canada. American Mineralogist. 53, 1523-1529.

Roedder, E., 1971. Fluid inclusion evidence on the environment of

formation of mineral deposits of the southern Appalachian valley. Economic Geology. 66, 777-791.

Roedder, E., 1984. Fluid Inclusions. Reviews in Mineralogy, Volume 12. Series Editor Ribbe, P. H. Min. Soc. America, Blacksburg Virginia. 644p.

Sawkins, F. S., 1966. Ore genesis in the North Pennine Orefield in the light of fluid inclusion studies. Economic Geology. 61, 385-401.

Scott, S. D., 1968. Stoichiometry and phase changes in zinc sulfides. Ph. D. dissertation. The Pennsylvania State University.

Scott, S. D., and Barnes, H. L., 1971. Sphalerite geothermometry and geobarometry. Economic Geology. 66, 653-669.

Scott, S. D., and Barnes, H. L., 1972. Sphalerite-wurtzite equilibria and stoichiometry. Geochim. Cosmochim. Acta. 36, 1275-1295.

Scott, S. D., and Kissin, S. A., 1973. Sphalerite composition in the Zn-Fe-S system below 300 deg. C. Economic Geology. 68, 475-479.

Seal, R. R., Cooper, B. J., and Craig, J. R., 1985. Anisotropic sphalerite of the Elmwood-Gordonsville Deposits, Tennessee. Canadian Mineralogist. 23, 83-88.

Sebastian, M. T., and Krishna, P., 1984. Mechanisms of phase transformations in ZnS. Pramana. 23, 395-403.

Shanmugam, G., and Lash, G. G., 1982. Analogous tectonic evolution of the Ordovician foredeeps, southern and central Appalachians. Geology. 10, 562-566.

Shepherd, T., Rankin, A. H., and Alderton, D. H. M., 1985. Fluid Inclusion Studies. Blackie Publishers, London. 239p.

Shimazaki, H., 1980. Cooling history of orebody recorded in sphalerite: an example from the Tsumo Skarn deposit Japan. Jour. Fac. Sci. Univ. Tokyo. Series 2. 20, 61-76.

Smith, F. G., 1955. Structure of Zinc sulfide minerals. American Mineralogist. 40, 658-675.

Smith, J. V., 1974. Feldspar Minerals. Vol. 2 Chemical and Textural Properties. Springer-Verlag, Berlin. 690p.

Solomon, M., Rafter, T. A., and Dunham, K. C., 1971. Sulfur and oxygen isotope studies in the northern Pennines in relation to ore genesis. Trans. Inst. Mining Metall. Section B (Applied Earth Sciences). 80, B259-B275.

Spirakis, C. S., 1983. A possible precipitation mechanism for sulfide minerals in Mississippi Valley-type lead-zinc deposits. In. Int'l Conf. on Mississippi Valley-type Lead-Zinc Deposits, proceedings volume. Eds. Kisvarsanyi, G. et al. University of Missouri-Rolla, Rolla Missouri. 211-215.

Spry, A., 1969. Metamorphic Textures. Permagon Press, Oxford. 352p.

Steinberger, I. T., 1983. Polytypism in zinc sulfides. in Crystal Growth and Characterisation of Polytype Structures. Vol 7., Krishna, P., ed. Permagon Press, 7-54.

Sugaki, A., Kitakaze, A., and Kojima, S., 1987. Bulk composition of intimate intergrowths of chalcopyrite and sphalerite and their genetic implications. Mineral Deposita. 22, 26-32.

Taylor, M., Kelly, W. G., Kesler, S. E., McCormick, J. E., Rasnick, F. D, and Mellon, W. V., 1983a. Relationship of zinc mineralisation in East Tennessee to Appalachian orogenic events. In. Int'l Conf. on Mississippi Valley-type Lead-Zinc Deposits, proceedings volume. Ed. Kisvarsanyi, G. et al. University of Missouri-Rolla, 271-278.

Taylor, M., Kesler, S. E., Cloke, P. L., and Kelly, W. C., 1983b. Fluid inclusion evidence for fluid mixing, Mascot-Jefferson City zinc District, Tennessee. Economic Geology. 78, 1425-1439.

Urabe, L., 1974. Iron content of sphalerite coexisting with pyrite from

some Kuroko deposits. Mining Geology. Special Issue No 6, 373-384.

Vaughan, D. J., and Craig, J. R., 1978. Mineral Chemistry of Metal Sulfides. Cambridge University Press, Cambridge.

Vaughan, D. J., and Ixer, R. A., 1980. Studies of sulfide mineralogy of north Pennine ores and its contribution to genetic models. Transactions Institute Mining and Metallurgy (Section B: Applied Earth Sciences). 89, B99-B110.

Verma, A. R., 1956. A phase-contrast microscopic study of the surface structure of blende crystals. Mineralogical Magazine. 31, 136-144.

Wallace, W., 1861. The Laws which Regulate the Deposition of Lead-Ore in Veins. Illustrated by an Examination of the Geological Structure of the Mining District of Alston Moor. Stanford, London. 258p.

Webb, P. C., Tindle, A. G., Barritt, S. D., Brown, G. C., and Miller, J. F., 1985. Radiothermal granites of the United Kingdom: comparison of fractionation patterns and variation of heat production in selected granites. In. High heat production (H. H. P.) granites, hydrothermal fluids and ore genesis. Inst. Min. Metall. London. 409-424.

White, J. C., 1985. Editor; Short course in applications of electron microscopy in the earth sciences. Min. Soc Canada Short Course Handbook. Volume 11, 213p.

Wiggins, L. B., and Craig, J. R., 1980. Reconnaissance of the Cu-Fe-Zn-S system: Sphalerite phase relationships. Economic Geology. 75, 742-751.

Williams, D. B., 1984. Practical Analytical Electron Microscopy in Materials Science. Phillips Electronic Instruments, Inc. Electron Optical Publishing Group, New Jersey. 153p.

Young, B., Styles, M. T., and Berridge, N. G., 1985. Niccolite-magnetite

mineralisation from Upper Teesdale, North Pennines. Mineralogical Magazine. 49, 555-559.

Zussman, J., 1977. Physical Methods in Determinative Mineralogy. Academic Press, London. 720p. 2nd edn.